

**AN INVESTIGATION INTO  
ACCELERATION  
DETERMINATION FOR  
AIRBORNE GRAVIMETRY  
USING THE GLOBAL  
POSITIONING SYSTEM**

**D. R. PEYTON**

**October 1990**



**TECHNICAL REPORT  
NO. 149**

## PREFACE

In order to make our extensive series of technical reports more readily available, we have scanned the old master copies and produced electronic versions in Portable Document Format. The quality of the images varies depending on the quality of the originals. The images have not been converted to searchable text.

**AN INVESTIGATION INTO ACCELERATION  
DETERMINATION FOR AIRBORNE  
GRAVIMETRY USING THE GLOBAL  
POSITIONING SYSTEM**

Derrick R. Peyton

Department of Surveying Engineering  
University of New Brunswick  
P.O. Box 4400  
Fredericton, N.B.  
Canada  
E3B 5A3

October 1990

© D.R. Peyton, 1990

## PREFACE

This technical report is a reproduction of a thesis submitted in partial fulfillment of the requirements for the degree of Master of Science in Engineering in the Department of Surveying Engineering, June 1990. The research was supervised by Dr. David E. Wells, and funding was provided partially by a Natural Sciences and Engineering Research Council of Canada Strategic Grant and two Operating Grants held by Dr. Wells, and by an Energy, Mines and Resources Research Agreement held by Dr. A. Kleusberg.

As with any copyrighted material, permission to reprint or quote extensively from this report must be received from the author. The citation to this work should appear as follows:

Peyton, D.R. (1990). *An Investigation into Acceleration Determination for Airborne Gravimetry using the Global Positioning System*. M.Sc.E. thesis, Department of Surveying Engineering Technical Report No. 149, University of New Brunswick, Fredericton, New Brunswick, Canada, 140 pp.

## ABSTRACT

This thesis investigates the determination of acceleration using the NAVSTAR Global Positioning System (GPS) for airborne gravimetric applications. Particular attention is placed on the development and implementation of an observing model which will accurately measure accelerations using the second time derivative of the GPS carrier phase. This development follows from the work performed by Kleusberg et al [1989] and Kleusberg [1989].

The position and velocity requirements for airborne gravimetry have been met using GPS observing and processing techniques. However, the separation of the aircraft acceleration due to air pockets, wind gusts, etc., from the observed gravity still remains to be resolved to the 1 to 2 mGal accuracy requirements.

As a means towards determining accelerations to this accuracy level, this thesis develops a model in which the accelerations are obtained by utilizing the second time derivative of the GPS carrier phase. Carrier phase data was collected from pairs of GPS receivers located at fixed points. Three different types of GPS receivers available to the market today were used for data analysis. Spectral analysis techniques in determining acquired acceleration accuracy were applied to computed accelerations from these data sets. Low-pass filters were applied to the acceleration data in order to separate the high frequency receiver measurement noise from the low frequency acceleration data. The implications and handling of GPS data contaminated by selective availability is addressed. Results show that for carrier phase observations over a fixed baseline of less than 100 metres differential techniques can give accelerations which meet the 1 to 2 mGal accuracy requirements.

Recommendations for the continuation of this research are given as well.

## TABLE OF CONTENTS

	page
ABSTRACT .....	ii
TABLE OF CONTENTS.....	iii
LIST OF FIGURES .....	vi
LIST OF TABLES .....	viii
DEDICATION.....	ix
ACKNOWLEDGEMENTS.....	x
<b>CHAPTER 1: Scope of Thesis .....</b>	<b>1</b>
1.0 Introduction .....	1
1.1 Investigation of the Problem .....	2
1.2 The Use of GPS for Airborne Gravimetry .....	5
1.3 Methodology and Procedure .....	5
1.4 Thesis Contributions .....	6
1.5 Thesis Outline.....	7
<b>CHAPTER 2: Airborne Gravimetry :</b>	
<b>Accuracy Requirements and Techniques.....</b>	<b>10</b>
2.0 Introduction .....	10
2.1 Accuracy Requirements in Position .....	10
2.2 Accuracy Requirements in Velocity .....	10
2.3 Position and Velocity Determination Using GPS.....	11
2.4 Accuracy Requirements in Acceleration.....	11
2.4.1 Horizontal Accelerations .....	11
2.4.2 Vertical Accelerations.....	13
2.4.3 Evaluation of Aircraft Vertical Accelerations.....	13
2.5 Present Measurement Techniques - Results and Limitations .....	14
2.5.1 Horizontal Accelerations .....	14
2.5.2 Vertical Accelerations.....	15
2.6 Summary .....	17
<b>CHAPTER 3: The Global Positioning System.....</b>	<b>19</b>
3.0 Introduction .....	19
3.1 System Description.....	19
3.1.1 Signal Structure .....	20
3.2 GPS Observables.....	21
3.2.1 The Pseudo-range Observable.....	21
3.2.2 The Carrier Phase Observable .....	22
3.2.3 Measurement Noise .....	23
3.3 Biases and Errors.....	24
3.3.1 Satellite Orbital Errors .....	24
3.3.2 Satellite and Receiver Clock Biases .....	24
3.3.3 Atmospheric Effects .....	25
3.3.4 Differencing Techniques Using GPS Observables.....	26

3.3.5 Cycle Slips and Ambiguity Resolution .....	26
3.3.6 Antenna Errors .....	27
3.3.7 Selective Availability.....	29
3.4 Summary .....	29
<b>CHAPTER 4: Acceleration Determination</b>	
<b>Using Carrier Phase Observables.....</b>	<b>30</b>
4.0 Introduction .....	30
4.1 Accelerations Using the Carrier Phase Observable .....	30
4.2 Assessment of the Phase Observable.....	32
4.3 Technological Advances in Receiver and Antenna Design.....	32
4.4 Implications of a Full Satellite Constellation .....	34
4.5 Treatment of Biases and Errors .....	34
4.5.1 Satellite Orbital Errors .....	34
4.5.2 Satellite and Receiver Clock Biases.....	35
4.5.3 Atmospheric Effects .....	35
4.5.4 Cycle Slips.....	36
4.5.5 Antenna Errors .....	38
4.5.6 Selective Availability.....	38
4.6 Summary .....	38
<b>CHAPTER 5: Formation of the Least Squares Adjustment.....</b>	<b>40</b>
5.0 Introduction .....	40
5.1 Geometric Configuration of the 3 Epoch Observation Scheme .....	40
5.2 Formation of the Observation Equations.....	43
5.2.1 Velocity Averaging Over 3 Epochs .....	48
5.3 Satellite Orbital Velocities and Accelerations .....	50
5.4 Formation of the Normal Equations.....	50
5.5 Transformation of Position, Velocity and Acceleration .....	53
5.6 Summary .....	55
<b>CHAPTER 6: GPS Observations and Processing Results.....</b>	<b>57</b>
6.0 Introduction .....	57
6.1 TI 4100 Observations .....	57
6.1.1 TI 4100 Data Description.....	57
6.1.2 $\phi\lambda h$ Accelerations and Assessment of Results.....	58
6.2 Trimble 4000 SLD Observations .....	61
6.2.1 Trimble 4000 SLD Data Description.....	61
6.2.2 $\phi\lambda h$ Accelerations and Assessment of Results.....	62
6.3 Ashtech XII Observations .....	64
6.3.1 Ashtech XII Data Description.....	64
6.3.2 $\phi\lambda h$ Accelerations and Assessment of Results.....	65
6.4 Overview of Results.....	66
6.5 Summary .....	68
<b>CHAPTER 7: Spectral Analysis of Acceleration Data</b>	
<b>and Application of a Low-pass Filter .....</b>	<b>69</b>
7.0 Introduction .....	69
7.1 Spectral Decomposition of Acceleration Data .....	69

7.2 Application of a Low-pass Filter.....	73
7.2.1 Filter Description and Implementation.....	74
7.2.2 Spectral Decomposition of Filtered Acceleration Data .....	74
7.3 Summary .....	75
<b>CHAPTER 8: Implications of Selective Availability on Acceleration Determination.....</b>	<b>77</b>
8.0 Introduction .....	77
8.1 Implications of Selective Availability on Acceleration Determination .....	77
8.2 Handling Selective Availability when Determining Accelerations .....	79
8.3 Summary .....	81
<b>CHAPTER 9: Conclusions and Recommendations.....</b>	<b>82</b>
9.0 Overview of Thesis.....	82
9.1 Conclusions.....	83
9.2 Recommendation for Future Research .....	84
<b>REFERENCES .....</b>	<b>86</b>
<b>APPENDIX I</b> Sensitivity of Phase Acceleration to Errors in Position and Velocity using Propagation of Errors.....	92
<b>APPENDIX II</b> Phase Velocity and Acceleration Over Three Epochs.....	96
<b>APPENDIX III</b> Satellite Orbital Accelerations.....	98
<b>APPENDIX IV</b> Transformation of Position, Velocity, and Acceleration from the CT-System to the Geodetic Coordinate System .....	107
<b>APPENDIX V</b> Power Spectral Density Plots of Undifferenced Accelerations .....	110
<b>APPENDIX VI</b> Power Spectral Density Plots of Differenced Accelerations ..	122
<b>APPENDIX VII</b> Power Spectral Density Plots of Unfiltered and Filtered Accelerations.....	128
<b>APPENDIX VIII</b> Power Spectral Density Plots of GPS Accelerations Influenced by Selective Availability .....	134



## LIST OF FIGURES

	page
1.1	Areas of Insufficient Gravity Data within Canada..... 3
4.1	Methods in Determining Motion Using GPS Pseudo-range and Carrier Phase Measurements.....31
5.1	Geometric Configuration Between Satellite and Receiver in Determining Acceleration .....41
5.2	Receiver Acceleration by Differencing the GPS Carrier Phase in Time.....42
5.3	Design Matrix of Least Squares Adjustment .....52
6.1	Vertical Accelerations using Undifferenced TI 4100 Data.....58
6.2	Accelerations in Latitude using Undifferenced TI 4100 Data .....59
6.3	Accelerations in Longitude using Undifferenced TI 4100 Data.....60
6.4	Vertical Accelerations using Undifferenced Trimble 4000 SLD Data .....61
6.5	Accelerations in Latitude using Undifferenced Trimble 4000 SLD Data.....62
6.6	Accelerations in Longitude using Undifferenced Trimble 4000 SLD Data .....63
6.7	Vertical Accelerations using Undifferenced Ashtech XII Data.....64
6.8	Accelerations in Latitude using Undifferenced Ashtech XII Data .....65
6.9	Accelerations in Longitude using Undifferenced Ashtech XII Data.....66
8.1	Effect of Selective Availability on Vertical Position.....78
V.1	Power Spectral Density of TI 4100 Undifferenced Vertical Accelerations ..... 111
V.2	Power Spectral Density of TI 4100 Undifferenced Accelerations in Latitude..... 112
V.3	Power Spectral Density of TI 4100 Undifferenced Accelerations in Longitude .. 113
V.4	Power Spectral Density of Trimble 4000 SLD Undifferenced Vertical Accelerations ..... 114
V.5	Power Spectral Density of Trimble 4000 SLD Undifferenced Accelerations in Latitude..... 115
V.6	Power Spectral Density of Trimble 4000 SLD Undifferenced Accelerations in Longitude ..... 116
V.7	Power Spectral Density of Ashtech XII Undifferenced Vertical Accelerations ... 117
V.8	Power Spectral Density of Ashtech XII Undifferenced Accelerations in Latitude..... 118
V.9	Power Spectral Density of Ashtech XII Undifferenced Accelerations in Longitude ..... 119
V.10	Polar Plot of Satellite Sky Distribution for TI 4100 Data ..... 120
V.11	Polar Plot of Satellite Sky Distribution for Trimble 4000 SLD and Ashtech XII Data ..... 121
VI.1	Power Spectral Density of TI 4100 Differenced Vertical Accelerations..... 122
VI.2	Power Spectral Density of TI 4100 Differenced Horizontal Accelerations ..... 123
VI.3	Power Spectral Density of Trimble 4000 SLD Differenced Vertical Accelerations ..... 124
VI.4	Power Spectral Density of Trimble 4000 SLD Differenced Horizontal Accelerations..... 125
VI.5	Power Spectral Density of Ashtech XII Differenced Vertical Accelerations..... 126
VI.6	Power Spectral Density of Ashtech XII Differenced Horizontal Accelerations ... 127

VII.1	Power Spectral Density of Unfiltered Differenced TI 4100 Vertical Acceleration Data .....	128
VII.2	Power Spectral Density of Filtered Differenced TI 4100 Vertical Acceleration Data .....	129
VII.3	Power Spectral Density of Unfiltered Differenced TI 4100 Accelerations in Latitude.....	130
VII.4	Power Spectral Density of Filtered Differenced TI 4100 Accelerations in Latitude.....	131
VII.5	Power Spectral Density of Unfiltered Differenced TI 4100 Accelerations in Longitude .....	132
VII.6	Power Spectral Density of Filtered Differenced TI 4100 Accelerations in Longitude .....	133
VIII.1	Power Spectral Density of Undifferenced Vertical Accelerations Influenced by Selective Availability .....	135
VIII.2	Power Spectral Density of Undifferenced Accelerations in Latitude Influenced by Selective Availability .....	136
VIII.3	Power Spectral Density of Undifferenced Accelerations in Longitude Influenced by Selective Availability.....	137
VIII.4	Power Spectral Density of Differenced Vertical Accelerations Influenced by Selective Availability .....	138
VIII.5	Power Spectral Density of Differenced Horizontal Accelerations Influenced by Selective Availability .....	139
VIII.6	Polar Plot of Satellite Sky Distribution for Trimble 4000 SLD Data Set (Satellite 14 is Influenced by Selective Availability) .....	140

## LIST OF TABLES

	page
2.1 Aircraft Altitude Accuracies of Conventional Altimeter Systems.....	16
6.1 Summary of GPS Determined Accelerations.....	67
7.1 RMS Values of Undifferenced Accelerations within the Gravity Bandpass of 0.0083 Hz .....	70
7.2 Summary of Differenced GPS Determined Accelerations .....	71
7.3 RMS Values of Differenced Accelerations within the Gravity Bandpass of 0.0083 Hz .....	72
7.4 RMS Values of Differenced and Filtered Accelerations using TI 4100 Data Sets ..	76
8.1 Summary of GPS Determined Accelerations Influenced by Selective Availability.....	80
8.2 RMS Values of GPS Determined Accelerations Influenced by Selective Availability.....	80

## DEDICATION

This thesis is dedicated to Debbie and Jaime, whose love, patience, understanding, and support have inspired me to continue in times when quitting seemed so much easier. All my love to you guys, and now to Krista!

## ACKNOWLEDGEMENTS

In completing this thesis I would like to give thanks for the guidance and support provided by Dr. D.E. Wells and Dr. A. Kleusberg. Their suggestions and ideas have helped me tremendously in over coming the major hurdles in conducting this research.

The financial support for this research was provided by a Strategic Grant entitled "Applications of Differential GPS" made available by the Natural Sciences and Engineering Research Council (N.S.E.R.C.) of Canada. This grant was held by Dr. J. Tranquilla, Dr. D.E. Wells, Dr. A. Kleusberg, Dr. P. Vanicek, and Dr. R. Langley of the University of New Brunswick. Financial support was also made available from two other N.S.E.R.C. operating grants entitled "Global Positioning System Design: Online Tides" and "Integration of Hydrographic Systems" which were held by Dr. Wells. In addition, financial support was made available by Energy Mines and Resources (E.M.R) Research Agreement #50. This grant was held by Dr. A. Kleusberg and is entitled "On the Use of GPS for Airborne Gravimetry". Finally, Texas Instrument TI 4100 data used in this thesis was made available by the Geophysics Division of the Geological Surveys of Canada. The assistance provided by the above sources is greatly appreciated.

Finally, I would like to thank my fellow friends at the Surveying Engineering graduate school, especially Hasanuddin Abidin and Philip Rapatz, and Ken Doucet. The knowledge and advice I have obtained from these people has been invaluable to the completion of this thesis.

# CHAPTER ONE

## Scope of Thesis

### 1.0 Introduction

This thesis investigates the possible independent determination of aircraft accelerations utilizing the NAVSTAR Global Positioning System (GPS). These accelerations are subsequently applied as corrections to airborne gravity observations. Airborne gravity surveys are becoming a viable source in acquiring area mean gravity anomalies [Tapley et al., 1985]. Gravity measurements are used by geodesists to determine the geoid and the external gravity field of the earth. Exploration geophysicists measure gravity in order to detect gravity anomalies which give them some knowledge of the earth's subsurface composition. A major source of error in gravity data obtained from airborne gravimetry is the contamination of gravity accelerations with accelerations caused by aircraft motion [Telford et al., 1976]. In practice, these accelerations must be solved independently and subsequently removed from the gravity data.

The approach taken, after Kleusberg et al. [1989] and Kleusberg [1989], uses the second time derivative of the differential GPS carrier phase to extract the  $\phi\lambda h$  acceleration components of a moving antenna. Acceleration accuracy requirements for airborne gravimetry are in the range from 1 to 2 mGals. Consequently, accuracy levels of GPS derived platform accelerations, must meet or surpass these requirements in order for this technique to be useful.

The proposed method involves the formation of a simultaneous least squares adjustment of differential GPS pseudo-range and carrier phase observations to obtain the required accelerations. These accelerations are then subjected to a low-pass filter with a cut-off frequency of 0.0083 Hz. This cut-off frequency is used since it represents the

gravimeter integration interval of 120 seconds to which the observed gravity is subjected. Note, however, that the limits of the integral are from 0.001 Hz to the cut-off frequency of 0.0083 Hz. No signal below 0.001 Hz was considered because the power below this frequency contributes relatively little to the acceleration error [Bower et al., 1989]. The type of filter and its performance are covered in Chapter 7. A spectral analysis of the acceleration data is performed before and after filtering. Spectral analysis techniques allow for the verification of the acquired acceleration accuracy. More on the theory and implementation of these techniques is give in Chapter 7.

## **1.1 Investigation of the Problem**

Brozena [1988] and Wells [1988] show that airborne gravimetry is becoming a reliable technique in acquiring accurate gravity data. Three advantages of airborne gravity surveys are as follows:

- (1) In a marine environment, the cost of \$3.00 per kilometre of an airborne gravity survey is far less than the \$50.00 per kilometre for a ship based gravity survey [Bower and Halpenny 1987].
- (2) The maximum speed at which a ship can normally collect gravity data is 12 knots (approximately 22 km/hr) while an aircraft can collect gravity data at speeds of 190 knots (approximately 350 km/hr). This means an increase in production using airborne gravimetric techniques of 16 times that of ship based operations [Bower and Halpenny 1987].
- (3) The use of an aircraft will allow acquisition of gravity data in areas inaccessible by land based or marine based operations. Examples are the more remote regions of the north and south poles and in treacherous mountain terrain. Figure 1.1 is a contour map of geoidal undulations for Canada [Vanicek et al., 1986]. The figure shows several blank areas where no gravity data was available. These regions can be filled in with data obtained



Figure 1.1

Areas of Insufficient Gravity Data within Canada



using airborne gravimetry. Internationally, the continental shelf areas of the world are also candidates for airborne gravimetry since they lack gravity data because of economic and military pressure [Bower and Halpenny 1987]. Tapley et al. [1985] mentions that data coverage is substantially poorer in South America and Africa, and in many instances where data is available it is not necessarily at the desired accuracy of 1 to 2 mGal. Consequently, the implementation of airborne gravimetry which can collect data at this accuracy level would provide a fast and efficient means of acquiring a good gravity data base.

Airborne gravimetry data is commonly obtained using a gravimeter. Schwarz [1977] describes the gravimeter consisting of accelerometers which measure the resultant of gravitational and inertial forces. For observations at a fixed point on the earth the only major inertial force influencing the observation of the gravity field is the centrifugal force [Schwarz 1977]. In a dynamic environment, however, the gravimeter will measure the total acceleration of the moving platform.

According to Bell et al. [1988] the desired free air anomaly ( $A_{FAA}$ ) is obtained from the total acceleration measured by the gravimeter ( $A_{TOT}$ ) using the following equation:

$$A_{TOT} = A_{FAA} + A_{AIRCRAFT} + A_{EOTVOS} + A_{ELL} + A_{FAC} \quad (1.0)$$

where:

$A_{AIRCRAFT}$  = the acceleration resulting from the vertical and horizontal motion of the vehicle,

$A_{EOTVOS}$  = the acceleration caused by the movement of the platform across a rotating earth [see Bomford 1977],

$A_{ELL}$  = the gravity on the reference ellipsoid [see Vanicek and Krakiwsky 1986],

$A_{FAC}$  = the Free Air correction necessary to reduce the airborne measurements to the geoid [see Vanicek and Krakiwsky 1986].

Of most concern, and the problem investigated in this thesis, is the determination of the acceleration caused by the aircraft motion,  $A_{\text{AIRCRAFT}}$ . Details concerning the last three corrections of Equation (1.0) can be found in the referenced literature.

## 1.2 The Use of GPS for Airborne Gravimetry

Developments in determining platform velocities and accelerations using GPS have followed the methodology of taking the first and second time derivatives of the resultant  $\phi\lambda h$  coordinates. Brozena et al. [1989] show results using this technique. The route chosen in this thesis is not to solve directly for the aircraft position. Instead, the GPS carrier phase observation is differenced in time to solve for the aircraft accelerations.

The estimated error of the GPS carrier phase from data analysis plays an important role in the subsequent analysis of aircraft accelerations using the technique proposed here. Other factors include the GPS receiver update rate, satellite constellation, receiver antenna design and location, and satellite clock stability. These factors will be discussed later in this thesis. For now, it is sufficient to be aware of these errors and their propagation into the final solution.

The specifications for reconnaissance airborne gravimetry requires accuracies of 1 to 2 mGal in gravity with a spatial resolution of 5 km [Bower and Halpenny 1987, Goodacre 1987]. The success on how the GPS carrier phase observing technique can be used to measure aircraft accelerations depends on whether these specifications are met.

## 1.3 Methodology and Procedure

Based on the results of Kleusberg et al. [1989] the proposed method in evaluating GPS techniques for use in determining aircraft accelerations, is to perform an analysis of actual observed differential GPS data collected between two fixed points. Actual aircraft

accelerations would be obtained by placing one receiver at a known fixed point acting as a monitor station while the other receiver travelled with the aircraft. For evaluation purposes the data required for this thesis were from fixed receivers. If the acceleration is negligible then the second time derivative of the GPS carrier phase should show zero acceleration. The noise that remains from a time series of these accelerations should give a measure for the error in the acceleration. Kleusberg et al. [1989] conducted their tests on the noise of the GPS carrier phase data derived from forming linear combinations of the L1 and L2 measurements of two adjacent receivers.

This thesis performs similar tests on three sets of two adjacent receivers. One receiver played the role of the fixed station while the other played the role of the aircraft receiver. These sets consisted of Texas Instruments TI 4100, Trimble 4000 SLD and Ashtech XII GPS receivers. In this research, however, the  $\phi\lambda\dot{h}$  accelerations of the "moving" antenna with respect to the "fixed" antenna, are determined explicitly. This process involved developing an algorithm which would model all pertinent errors and biases.

The resultant time series of accelerations were subjected to spectral analysis techniques in order to determine the acquired acceleration accuracy. A low pass filter was applied to the acceleration time series in order to separate the high frequency receiver measurement noise from the low frequency acceleration data.

A further test was performed on GPS data which was influenced by selective availability (S/A). Details covering these results are provided in Chapter 8.

## 1.4 Thesis Contributions

Kleusberg et al. [1989] assessed the noise of the GPS carrier phase observable. They concluded that this technique could be used in acquiring aircraft acceleration with accuracies which would meet the 1 to 2 mGal specifications discussed earlier.

In working toward verifying these conclusions, this thesis makes the following contributions:

- (1) An observing and processing technique for determining fixed point accelerations in the geodetic coordinate system is presented. The technique involves a simultaneous parametric least squares adjustment of a combination of the GPS pseudo-range and carrier phase observables over three epochs. Development of the acceleration model involved deriving and implementing the GPS satellite XYZ accelerations. A low-pass filter was implemented such that it did not destroy the low frequency acceleration signal below the gravity band-pass as specified in airborne gravity surveys. This band-pass frequency level of 0.0083 Hz corresponds to a gravimeter integration interval of 120 seconds.
- (2) A comparison of the achievable  $\phi\lambda h$  accelerations and acceleration accuracies are assessed using three different GPS receivers which have been developed over the past decade. These are the Texas Instruments TI 4100, Trimble 4000 SLD and Ashtech XII GPS receivers. This assessment shows the result of advances made in receiver technology over the past few years with regards to carrier phase noise reduction, antenna design, and receiver processing time.
- (3) The implications of GPS selective availability are analyzed using contaminated data collected and assessed in this research.

## 1.5 Thesis Outline

Chapter 1 describes the potential of airborne gravimetry in acquiring gravity data. The technical implications of obtaining gravity data from a moving platform are briefly described. The motivation behind this thesis is given. Specifications governing the overall accuracy of the derived aircraft accelerations using GPS are given. The methodology and procedure of research in this thesis are discussed. The thesis contributions are listed as well as the outline of the thesis.

Chapter 2 reviews the accuracy requirements for airborne gravity surveys. These requirements include positioning, velocity and acceleration requirements. The present day accuracies achievable using GPS observing techniques are also given. Emphasis is placed on vertical acceleration determination. Present day techniques and accuracies of obtaining vertical accelerations using other altitude detection systems are described.

Chapter 3 describes the Global Positioning System. The observation equations of both the pseudo-range and carrier beat phase are introduced. Sources of error using GPS observing techniques for airborne gravimetry are discussed.

Chapter 4 introduces the concept of the second time derivative of the GPS carrier phase observable, and its use for the independent determination of the  $\phi\lambda h$  acceleration components of a moving platform. The GPS error sources mentioned in Chapter 3 are discussed in detail and methods of handling each of them are presented. Technological advances in GPS receiver and antenna design are discussed.

Chapter 5 develops the geometric configuration and the proposed observation scheme for determining aircraft accelerations. The observation equations for the parametric least squares adjustment are presented. Consideration is given to GPS satellite clock and orbital errors. The GPS satellite XYZ accelerations are derived from the broadcast orbital parameters. The least squares normal equations and the observation weight matrix are formulated.

Chapter 6 describes the three different data sets collected for this research. The  $\phi\lambda h$  accelerations determined from this data using the proposed methods are presented and assessed.

Chapter 7 briefly describes the purpose of applying spectral analysis techniques to the results of Chapter 6 in order to assess the accuracy of the acquired accelerations. The  $\phi\lambda h$  accelerations in each of the three data sets of Chapter 6 are subjected to a spectral analysis. The accuracy levels of each data set are presented and assessed. A low-pass

filter is described and implemented in order to reduce the high frequency noise of the acceleration data. The results of the the spectral analysis of the filtered accelerations are presented and discussed.

Chapter 8 defines the concept of selective availability and its implication on the GPS pseudo-range and carrier phase observables. Handling of S/A for airborne gravimetric applications is presented. Accelerations from GPS data influenced by S/A are computed and assessed.

Chapter 9 reviews the results obtained from this thesis and presents some conclusions. Recommendations for future research concerning acceleration determination for airborne gravimetry are discussed.

## CHAPTER TWO

### Airborne Gravimetry: Accuracy Requirements and Techniques

#### 2.0 Introduction

Chapter 2 reviews the accuracy requirements needed in airborne gravity surveys. Present day measurement techniques in aircraft acceleration determination are discussed. This discussion includes the results and limitations of these techniques. The utilization of the Global Positioning System is introduced as a method in determining aircraft accelerations for airborne gravimetry.

#### 2.1 Accuracy Requirements in Position

The position accuracy for airborne gravity surveys can be broken into two sets of components, namely, vertical and horizontal components.

Wells et al. [1986], and Vanicek and Krakiwsky [1986], stipulate that in order to achieve a 1 mgal correction accuracy for mid-latitude regions ( $45^{\circ}\text{N}$ ) an accuracy of 50 metres or better is required in the horizontal position. Wells et al. [1986], and Kleusberg et al. [1989] suggest that an accuracy of 3 metres or better is required in the vertical position for the same correction accuracy.

#### 2.2 Accuracy Requirements in Velocity

Velocity determination of a moving platform in a gravity survey is necessary in order to calculate the Eotvos correction. The Eotvos correction is the vertical component of the Coriolis acceleration. The Coriolis acceleration is a centrifugal acceleration experienced

by a moving platform as a result of passing over the surface of the earth and as a result of the rotating earth [ Bomford 1977; Telford et al., 1976].

Goodacre [1987] and Smit [1988] show that in order to achieve a 1 mGal correction accuracy at mid-latitudes the east-west velocity of a moving platform must be known to an accuracy of 0.1 metres per second.

## **2.3 Position and Velocity Determination Using GPS**

Results by Mader [1986], Cannon [1987], and Mader and Lucas [1988] show that the required position accuracy can be obtained using the combined GPS pseudo-range and carrier phase observables. Schwarz et al. [1987], and Brozena et al. [1989] suggest that the required kinematic velocity accuracy can also realistically be achieved using GPS techniques. Consequently, it is concluded that the accuracy requirements of position and velocity for airborne gravimetric applications can be obtained using GPS observing and processing methods.

The determination of platform accelerations, however, is still an ongoing problem in airborne gravimetry. Many authors view that the independent determination of aircraft acceleration is the most pressing problem in airborne gravimetry [eg. Tapley et al., 1985; Bell et al., 1986; Bower et al., 1989].

## **2.4 Accuracy Requirements in Acceleration**

The acceleration accuracy requirements for airborne gravimetry can also be divided into vertical and horizontal components.

### **2.4.1 Horizontal Accelerations**

Horizontal accelerations of an aircraft can result from course adjustments implemented to the aircraft during flying operations. These adjustments are necessary in



order to maintain a predetermined flight plan. Wind gusts acting on the aircraft are another source of horizontal accelerations. The horizontal acceleration corrections are applied to the gravimeter gyros, which in turn, are used to stabilize the gravimeter leveling system. The allowable (root mean square) rms in determining horizontal accelerations,  $A_{HOR}$ , can be found from [Brozena et al., 1986]:

$$A_{HOR}^2 = g_{obs\_err} 2g \frac{(\frac{\omega_0}{\omega})^4 + 1}{(\frac{\omega_0}{\omega})} \quad (2.1)$$

where,

$g_{obs\_err}$  = the gravity measurement error caused by table leveling errors,

designed to be 1 mgal or less (see Section 1.0),

$g$  = the acceleration of gravity (981 Gal),

$\omega_0$  = the circular frequency of the stable table based on horizontal

accelerations due to variations in heading of the aircraft such as wind gusts (4 minutes or 0.004167 Hz was found to be sufficient)

$\omega$  = the circular frequency of the horizontal acceleration which was specified in Chapter 1 as 120 seconds or 0.0083 Hz.

Letting  $\omega = 0.0083$  Hz then the rms of the horizontal acceleration must be known to within 6 Gal. The rms of 2.6 Gal obtained by Brozena et al. [1986] using accelerometers was under calm wind conditions. An rms of higher magnitude was expected under more turbulent conditions.

Bower and Halpenny [1987] suggest that the magnitude of horizontal acceleration experienced in aircraft motion for airborne gravimetry is not significant. Brozena et al.

[1986] suggests techniques which can reduce the effect of aircraft horizontal accelerations on gravity observations. These techniques involve switching off the gravimeter during times of major course corrections. This subsequently results in a loss of data for about one to two minutes during this time period.

## 2.4.2 Vertical Accelerations

Vertical accelerations of an aircraft are caused by wind gusts, unstable air conditions, and by natural oscillations of the aircraft. Filtered gravity measurements can be in error as much as 200 mgal as a result of aircraft vertical accelerations [Brozena et al., 1986].

Bower and Halpenny [1987] propose that a correction accuracy of 1 to 2 mGal is required for an aircraft altitude of 600 meters, and a spatial resolution of 5 kilometres. Gravimeter data under these conditions are subjected to a low-pass filter with a cut-off frequency of 0.0083 Hz (120 seconds).

## 2.4.3 Evaluation of Aircraft Vertical Accelerations

Bower and Halpenny [1987] evaluate the performance of a system used to measure platform acceleration by the rms height error within the aforementioned gravity bandpass of 0.0083 Hz. Thus, the acceleration correction to be applied to the observed gravity data is determined by twice differencing the measured altitude. In turn, the power spectral density (PSD) of the acceleration correction is then equal to the PSD of the altitude times the 4<sup>th</sup> power of the angular frequency ( $\omega^4$ ) [Bower et al., 1989]. Kleusberg [1989] relates the PSD of the platform vertical acceleration errors, PSD(f), to the platform acceleration measurement accuracy, rms, as follows:

$$\text{rms}^2 = \int_0^{f_0} \text{PSD}(f) df \quad (2.2)$$

where,

$f_0$  = the cut-off frequency of 0.0083 Hz,

PSD(f) = the power spectral density of the platform acceleration error within  $f_0$ .

Results given by Bower and Halpenny [1987] show that in order to meet the accuracy requirements stated above, the permissible rms error in height determination range from 0.7 cm to 1.5 cm. Their results depend on the behavior of the altitude error as a function of frequency within the gravity bandpass. An evaluation of the rms height acceleration error obtained in this thesis is given in Chapter 7.

## **2.5 Present Measurement Techniques - Results and Limitations**

Section 2.5 describes present techniques used in determining platform accelerations for airborne gravimetry. In addition, the performance and limitations of these techniques are reviewed.

### **2.5.1 Horizontal Accelerations**

The effect of horizontal accelerations on airborne gravity observations was discussed in Section (2.4.1). The method of handling these accelerations was to shut off the gravimeter until course corrections were completed. The method proposed in this thesis involves the constant measurement of horizontal accelerations using GPS observing techniques. Further discussion on these techniques are included in the subsequent chapters.

## 2.5.2 Vertical Accelerations

Aircraft vertical accelerations for airborne gravimetry have been determined using radar and pressure altimeters [Brozena et al., 1986], laser altimeters [Bower and Halpenny 1987], and most recently GPS [Brozena et al., 1989]. Vertical platform accelerations are determined from the second derivative of the altitude measurements [Kleusberg et al., 1990]. Details concerning the description and operation of these systems can be found in the above references.

Several disadvantages of the radar and pressure altimeters have been mentioned by Bell et al. [1986]. They state that the radar altimeter is limited in altitude, non-effective over ice or land, and expensive to install. The pressure altimeter, on the other hand, does not perform well over land unless calibration is available over nearby water bodies with known elevation. In addition, the pressure altimeter is limited in altitude and is susceptible to ice probing. Finally, Bell mentions that the aircraft pressure wake causes errors on the results from the pressure altimeter. [Bower and Halpenny 1987] suggest that the laser altimeter is weather dependent and specular reflection can occur over flat surfaces such as calm waters.

Results of tests for aircraft altitude accuracies using the above systems are given in Table 2.1. This information was obtained from Bell et al. [1986], Bower and Halpenny [1987], and Telford et al. [1976].

Residual undetermined vertical accelerations of an aircraft are traceable to uncorrected errors in measuring the altitude of the aircraft since, as mentioned above, the acceleration corrections to be applied to the gravimeter are determined by the second derivative of the altitude measurements [Bower et al., 1989]. The results displayed in Table 2.1 are based on flying over open water and not land. Flying over land causes additional error sources as discussed above. Bower and Halpenny [1987] conclude from

their analysis of the above systems that airborne gravimetry under the specifications listed in Section 2.4.2 is just feasible over sea and not feasible over land.

Table 2.1  
Aircraft Altitude Accuracies of Conventional Altimeter Systems

Altimeter	Altitude Accuracy
Radar	< 2 cm
Pressure	< 20 cm
Laser	< 2 cm

The above conclusions were also based on results of vertical accelerations as derived from GPS observation techniques. However, information provided at the time indicated that the spectrum of GPS phase measurements was white Bower et al. [1989]. Results by Georgiadou and Kleusberg [1988] show that the low-frequency part of the GPS phase measurement spectrum can be contaminated by multipath interference. Further details concerning their analysis is given in Chapter 4. Latter tests by Kremer et al. [1989] indicate that Selective Availability may have some effect on acceleration determination using GPS. More on Selective Availability will be given in Chapter 8. Bell et al. [1986] lists the following advantages of using GPS for airborne gravimetric surveys:

- 1) GPS equipment is becoming inexpensive and easy to install,
- 2) GPS results are not limited by altitude,
- 3) GPS can operate over land, sea, or ice,
- 4) GPS can operate in an all weather environment, and

5) GPS is not affected by isobars or areas of varying pressure as with an altimeter.

Some results of vertical accelerations using GPS observing techniques have already been presented. Brozena et al. [1989] was able to obtain 2 mGal accuracies in vertical accelerations with spatial resolution of 20 kilometres at flight speeds of 360 km/hr. A radar altimeter was used as the reference system for this analysis. One of the main limitations in acquiring more accurate data was the influence of cycle slips in the GPS phase observations. The integration of GPS with an Inertial Navigation System (INS) can be implemented to help resolve the cycle slip problem [Schwarz et al., 1987; Kleusberg 1988]. An alternative to handling cycle slips for acceleration purposes is given in Chapter 4.

## 2.6 Summary

This chapter has reviewed the accuracy requirements needed in airborne gravimetric surveys with regards to aircraft position, velocity, and horizontal and vertical acceleration. A review of literature shows that the position and velocity requirements can be obtained using GPS observing techniques.

The most stringent of the acceleration requirements was determined to be the vertical component. Specifications indicate that a 1 to 2 mGal correction accuracy is required for airborne gravity surveys. It was found that the magnitude of horizontal accelerations experienced in aircraft motion for airborne gravimetry was not significant. Present day techniques in acquiring vertical accelerations include radar, pressure, and laser altimeters, and GPS observing methods. All four methods have limitations and produce results which do not make them feasible for airborne gravimetric surveys with the above specifications. However, the Global Positioning System was described as being a favourable system in obtaining vertical accelerations and that many of its limitations could be overcome.

Initial results from GPS campaigns in airborne gravimetric applications show that GPS was not able to meet the 1 to 2 mGal requirements stated above. However, recent research by Kleusberg et al. [1989], and as discussed by Bower et al. [1989], indicate that GPS can achieve these accuracy requirements. Further details of these studies are covered in Chapter 4.

In order to obtain a better understanding of the concepts which will be proposed in future chapters, it first becomes necessary to introduce the Global Positioning System and the biases and errors which are associated with the system.

## CHAPTER THREE

### The Global Positioning System

#### 3.0 Introduction

This chapter introduces the Global Positioning System (GPS). It gives a brief review of the basic concepts and characteristics of GPS as well as the fundamental equations which describe the observables in the system. The remainder of the chapter gives a brief review of the errors and biases of the GPS observables.

#### 3.1 System Description

The Global Positioning System is a navigation and positioning system which utilizes radio frequency signals transmitted from orbiting satellites. The system has been under development for more than a decade by the United States Department of Defense and is predicted to be fully operational by the middle of the 1990s. Once operational, GPS is designed to have a constellation consisting of 24 satellites, three of which are spares. The so called Primary 21 Satellite Constellation [Green et al., 1988] is to have an approximate altitude of 20,000 kilometres and are to be configured into six orbital planes with four satellites per plane. The equally spaced orbital planes are inclined to the earth's equatorial plane by 55 degrees. The design of the constellation is such that at least four satellites will be visible above the horizon from any place on the earth at virtually all times [Wells and Kleusberg 1989].

The overall operation of the system is under the control of the US Department of Defense. A network of ground control stations track the orbiting satellites. These control stations determine precise orbital and clock parameters of each satellite and transmit this information back to the satellite. The information is then sent to the GPS receiver in a



coded message as a broadcast ephemeris [Quek 1988]. Using this ephemeris and clock data, and the signal transmitted by the satellite, a receiver position can be computed. In addition to solving for the three positional coordinates of the receiver, the receiver time offset from some reference time must also be determined. Details concerning the solution for these unknowns can be obtained from Wells et al. [1986]. For now it suffices to say that observations from at least four satellites are needed to compute a unique solution for the receiver position. Fewer satellites can be observed if one or more of these four unknown parameters listed above is constrained in some way [Lachapelle et al., 1987].

### 3.1.1 Signal Structure

Each of the GPS satellites contains a very high precision oscillator such as a rubidium or a cesium frequency standard. This standard has a fundamental frequency of 10.23 MHz, used to generate two L-band frequencies [Spilker 1978]:

$$L1 = 1575.42 \text{ MHz} = 154 \times 10.23 \text{ MHz}$$

$$L2 = 1227.60 \text{ MHz} = 120 \times 10.23 \text{ MHz}$$

The L2 signal is modulated with a precise code, called the P-code, and a satellite navigation message. The L1 signal is modulated with a P-code, satellite message, and a less accurate coarse acquisition code called a C/A-code. The P-code is emitted at a frequency of 10.23 MHz and has a repetition period of 237 days. The C/A code is emitted at a frequency of 1.023 MHz and repeats itself every millisecond.

The satellite message is emitted at a frequency of 50 Hz and contains the information concerning the satellite health, and the orbital and clock parameters.

## 3.2 GPS Observables

The fundamental observables used in the Global Positioning System are the pseudo-range and carrier phase observable. The following sections give a brief description of these observables

### 3.2.1 The Pseudo-range Observable

Wells et al. [1986] defines the pseudo-range as the time shift required to line up a replica of the GPS code generated within the receiver with the incoming received code from the satellite. The time shift is converted to metres by multiplying by the speed of light. This time shift is the measure of the difference between the transmission time at the satellite and reception time at the receiver [Wells 1985]. Note that these two time frames do not coincide and thus give a bias which must be determined.

The mathematical model for the pseudo-range observation between the receiver  $j$ , and the satellite at  $k$ , at time  $t$  is given as follows [Wells and Kleusberg 1989]:

$$P_j^k(t) = \rho_j^k(t) + c[dt^k(t) - dT_j(t)] + d_{ion}(t) + d_{trop}(t) + \epsilon(t) \quad (3.1)$$

where,

$P_j^k(t)$  = the observed pseudo-range in metres between satellite  $k$  and receiver  $j$  at time  $t$ ,

$$\rho_j^k(t) = \sqrt{(X^k - X_j)^2 + (Y^k - Y_j)^2 + (Z^k - Z_j)^2}$$

$X^k, Y^k, Z^k$  = represent the satellite coordinates as given by the ephemeris,

$X_j, Y_j, Z_j$  = the unknown receiver coordinates,

$c$  = the speed of light in a vacuum,

$dt^k(t)$  = the satellite clock offset from GPS time at time  $t$ ,

$dT_j(t)$	= the receiver clock offset from GPS time at time $t$ ,
$d_{ion}(t)$	= the atmospheric correction due to the effect of ionospheric refraction at time $t$ ,
$d_{trop}(t)$	= the atmospheric correction due to the effect of tropospheric refraction at time $t$ ,
$\epsilon(t)$	= the remaining unmodelled errors (eg. receiver noise, multipath,etc.).

### 3.2.2 The Carrier Phase Observable

Wells et al. [1986] defines the carrier beat phase as the difference between the incoming Doppler-shifted satellite carrier signal and the GPS receiver generated reference signal. The receiver generated signal is considered to be of nominally constant frequency.

Like the pseudo-range observable, the time of reception of the signal and the time of transmission of the signal are biased with respect to GPS time. In addition, the propagation of the carrier wave is affected by atmospheric conditions. Keeping these items in mind, the carrier phase observation is modelled as follows [Kleusberg et al., 1989]:

$$-\lambda\phi_j^k(t) = \rho_j^k(t) + c[dt^k(t) + dT_j(t)] - d_{ion}(t) + d_{trop}(t) + \lambda N_j^k + \epsilon(t) \quad (3.2)$$

where,

$\lambda$	= the wavelength of the carrier phase signal in metres,
$\phi_j^k(t)$	= the observed phase measurement in cycles between satellite $k$ and receiver $j$ at time $t$ . Note that the integer count of cycles since lock-on is buried in this quantity,
$\rho_j^k(t)$	= as Equation 3.1 above,
$c$	= the speed of light in a vacuum (metres per second),

$dt^k(t)$	= the satellite clock offset from GPS time at time $t$ ,
$dT_j(t)$	= the receiver clock offset from GPS time at time $t$ ,
$d_{ion}(t)$	= the atmospheric correction due to the effect of ionospheric refraction at time $t$ ,
$d_{trop}(t)$	= the atmospheric correction due to the effect of tropospheric refraction at time $t$ ,
$N_j^k$	= the carrier phase integer cycle ambiguity between receiver $j$ and satellite $k$ ,
$\epsilon(t)$	= the remaining unmodelled errors (eg. receiver noise, multipath,etc.).

The next section discusses the errors and biases which are associated with the above GPS observables and their implications with respect to acceleration determination.

### 3.2.3 Measurement Noise

Apart from the errors and biases, which are discussed below, the measurement noise of a GPS observable depends on several factors [Wells and Kleusberg 1989]. These include the type of measurement, the measuring technique, the mode of operation, and the receiver design. Evans et al. [1985] gives the Texas Instrument TI 4100 GPS receiver noise levels of 60 centimetres and 2 millimetres for the pseudo-range and carrier phase measurements respectively. Development in receiver technology has provided lower noise levels. Ashjaee et al. [1988] report 1 millimetre level signal resolution on the carrier phase obtained by the Ashtech XII receivers. Alison et al. [1988] claim the same accuracy with the Trimble 4000SLD. Srinivasan et al. [1989] claim decimetre level noise for the pseudo-range measurement of the Rogue GPS receiver. More on GPS technological advances are given in Chapter 4. Wells and Kleusberg [1989] suggest that codeless receivers have a higher noise level due to the lower signal to noise level. The data collected for this research

is from code correlating receivers only. Consequently, all discussion will pertain to these types of receivers.

### **3.3 Biases and Errors**

Associated with each of the observables mentioned above are biases and errors which originate from the satellite, the receiver, and the atmospheric conditions of the propagating signal.

#### **3.3.1 Satellite Orbital Errors**

The  $\rho_j^k$  term of equations (3.1) and (3.2) contains the satellite coordinates which are derived from the satellite ephemeris. Errors in the ephemeris can propagate into errors in receiver position, velocity, and acceleration. Satellite position errors from the broadcast ephemeris are approximately 20 metres [Wells and Kleusberg 1989]. More accurate satellite positions can be obtained from the precise ephemerides which are available from various sources [Robinson 1988, Remondi and Hoffman-Wellenhof 1989]. Depending on their magnitude, satellite ephemeris errors can be reduced by differencing techniques which are discussed in Section 3.4.4. The size of the satellite ephemeris errors and their effect on acceleration determination is discussed in Chapter 4.

#### **3.3.2 Satellite and Receiver Clock Biases**

As previously mentioned the satellite and receiver clock times are with respect to the GPS time frame. The satellite clock offset is closely monitored by the ground control network. This time offset, along with the frequency offset, and frequency drift, are transmitted via the broadcast ephemeris to the GPS receiver. These biases are in the form of coefficients of a second order polynomial as given below [Van Dierendonck et al., 1978]:

$$dt = a_0 + a_1(t - t_0) + a_2(t - t_0)^2 \quad (3.3)$$

where,

- dt = the correction to be applied to the satellite transmission time,
- a<sub>0</sub> = the satellite clock time offset,
- a<sub>1</sub> = the satellite clock frequency offset,
- a<sub>2</sub> = the satellite clock frequency drift,
- t<sub>0</sub> = the satellite clock reference epoch,
- t = the time of signal transmission from the satellite.

Equation 3.3 is a model for clock behavior, based on historical tracking data. The accuracy with which this model agrees with the actual clock behavior depends on the stability of the clocks. Section 3.1.1 mentioned that the GPS satellites have highly stable atomic frequency standards to control their timing. These types of clocks have a frequency offset accuracy which is usually better than 10<sup>-11</sup> and a frequency drift accuracy of better than 10<sup>-14</sup> per second [King et al., 1985].

The GPS receivers are normally equipped with less stable frequency standards such as a quartz crystal clock. Consequently, the unknown bias of the receiver clock from GPS time must be solved for when determining position. Two other options in handling the unknown receiver clock offset are to use differencing techniques or to solve directly for the coefficients expressed in Equation 3.3. A discussion on differencing as it applies to this thesis is given in Section 3.3.4.

### 3.3.3 Atmospheric Affects

The ionosphere is defined as that portion of the atmosphere which contains ionized particles dense enough to have a measurable effect on the propagation of a radio wave passing through it [Heroux, 1988]. It extends from about 50 kilometres to about 1000 km

above the earth [Wells and Kleusberg, 1989]. The ionospheric effect on the GPS signal is frequency dependent. Wells et al. [1986] gives a typical observation error of 30 metres at the zenith due to ionospheric affects on the signal. If dual frequency receivers are used, meaning the receiver observes both the L1 and the L2 signals, then the ionospheric effect on the GPS range can be measured directly [Goad 1985]. For single frequency observations the ionospheric effect can be estimated using modelling equations [Lachapelle and Wade 1982] or reduced using differencing techniques.

The troposphere is defined as the non-ionized portion of the lower atmosphere [Hopfield 1971]. This area extends from the surface of the earth to about 50 kilometres. Like the ionosphere, the troposphere effects the propagation of the GPS signal. This affect can be as much as 10 metres along the horizon on the measured GPS range. The tropospheric effect is not frequency dependent and is most severe on signals observed near the horizon [Wells and Kleusberg 1989].

### **3.3.4 Differencing Techniques Using GPS Observables**

Previous sections have mentioned that clock and atmospheric biases as well as satellite orbital errors can be significantly reduced, if not eliminated, using differencing techniques. Differencing between GPS observables involves forming certain linear combinations of equations (3.1) and (3.2). The method can entail differencing between receivers, and/or between satellites, and/or between measurement epochs. By applying these differencing techniques, the common errors in the GPS observable can be eliminated. More details on differencing can be found in Wells et al. [1986].

### **3.3.5 Cycle Slips and Ambiguity Resolution**

Cycle slips are of most concern when dealing with high accuracy positioning using the GPS carrier phase. Kleusberg [1987] defines a cycle slip as a discontinuity in the time

series of a carrier phase as measured in the GPS receiver. The cycle ambiguity term of Equation 3.2 accounts for an unknown integer number  $N$  cycles of length  $\lambda$  in the carrier phase measurements. The ambiguity term is in general an arbitrary unknown number which changes if the receiver loses lock to the tracked signal [Wells and Kleusberg, 1989]. The two terms are related in that causes of cycle slips include blockage of the signal to the receiver, receiver power failure, and low signal strength. The implication of cycle slips in the phase data means that the cycle ambiguity term of equation (3.2) becomes more difficult to calculate. If this ambiguity term is not solved for than the subsequent range, after a cycle slip, will show an apparent jump. The magnitude of this jump will be equivalent to the size of the cycle slip scaled into metres. Thus, a cycle slip results in having to solve for an extra unknown ambiguity term.

The existence of cycle slips can be significant if accelerations in airborne gravimetry are based on phase measurements. Jumps in range measurements can obviously lead to jumps in accelerations which, in turn, can suggest false aircraft movements. This topic is further discussed in Chapter 4. For now, it suffices to say that the detection and handling of cycle slips must be assessed in order to meet airborne gravimetry accuracy requirements.

### 3.3.6 Antenna Errors

Some of the unmodelled errors of equations (3.1) and (3.2) are related to the receiver antenna and the environment in which it is located. These errors consist of multipath, imaging, and phase centre location and variation.

Multipath occurs when the received GPS signal is contaminated with one or more constituents of the same signal [Georgiadou and Kleusberg 1988]. This contamination is a result of the incoming signal being reflected by a nearby surface and being indistinguishable from the correct transmitted signal. Multipath can occur at the satellite or at the receiver. However, Young et al. [1985] shows that satellite multipath can be



insignificant when differencing between receivers spanning a baseline of a few tens of metres or more.

Multipath at the receiver cannot be reduced by differencing. The effect of multipath at the receiver is highly dependent upon the reflective environment about the antenna. In addition, receiver multipath also depends on the antenna amplitude response. An antenna which has a response pattern that allows for the observation of satellites below the horizontal are susceptible to multipath signals originating from a reflective surface below the antenna [Tranquilla 1986]. Georgiadou and Kleusberg [1988] show that multipath can cause cyclic errors larger than the receiver noise level. These periods can range from less than a few minutes to more than an hour. Evans [1986] shows that multipath effects on pseudo-range measurements can be as much as 10 metres.

The phase centre of a transmitting antenna is defined as the apparent source of radiation of the antenna [Wells et al., 1986]. However, due to manufacturing errors, the phase centre is not necessarily the point which a receiving antenna, such as a GPS antenna, uses as a reference point in its position determination. The actual phase centre location is a function of the observing angle to the satellite from the antenna [Tranquilla 1986]. The phase centre will vary in time as the satellites move across the sky. These variations are due to the non-spherical phase pattern of the antenna.

Imaging occurs when another conducting material situated near an antenna interferes with the radiation characteristics of the antenna. The phase centre of an antenna can be measured [Tranquilla 1986]. However, the source of radiation due to imaging is site dependent and thus, would be difficult to measure in practical applications.

Form the above discussion it is evident that these antenna errors can have some influence on the determination of accelerations for airborne gravimetry. Especially when dealing with the low frequency part of the spectrum as described in Chapter 2. Bower and Halpenny [1987] suggested that the error spectrum of the GPS phase measurement was

white. However, Georgiadou and Kleusberg [1988] point out that the GPS phase observable is not necessarily white noise, but instead can be significantly influenced by effects described above.

### **3.3.7 Selective Availability**

Selective availability (S/A) means the intentional degradation of the transmitted information from the GPS satellite in order to limit the positioning capabilities of the user. This degradation can be implemented in the form of erroneous satellite ephemeris or dithering of the satellite clock. The position accuracy available to unauthorized users is suggested to be limited to 100 metres [Zachmann 1989]. Wells and Kleusberg [1989] suggest that differencing methods can reduce the effect of dithering. At the same time they suggest that further research is needed to fully understand the implications of selective availability.

S/A, like the other error sources, can limit the acceleration accuracy obtainable from GPS measurements. Any dithering of the satellite clock or use of an erroneous satellite ephemeris will result in the computation of false accelerations in a moving vehicle. Selective availability, as it pertains to acceleration determination is covered in Chapter 8.

## **3.4 Summary**

This chapter has introduced the operational concepts of the Global Positioning System and has described the GPS signal characteristics. In addition, the pseudo-range and carrier phase observations have been introduced along with the errors and biases associated with these observables. It was noted that these errors can limit the accuracy of acceleration determination for airborne gravimetric applications. Consequently, these errors should be modelled or eliminated depending on the type of error and the data processing technique used.

## CHAPTER FOUR

### Acceleration Determination using Carrier Phase Observables

#### 4.0 Introduction

This chapter introduces the concept of using GPS carrier phase measurements to determine accelerations. An assessment of the phase observable errors is given. The impact of technological advances in receiver and antenna design is discussed. Implementation of a full satellite constellation and its affect on acceleration determination is given. Finally, the treatment of the various error sources discussed in Chapter 3 is proposed.

#### 4.1 Accelerations Using the Carrier Phase Observable

A standard techniques for determining accelerations has been to determine vehicle coordinates and then to take the first and second time derivatives to obtain velocity and acceleration respectively [Brozena et al., 1988].

An alternative for determining accelerations, and the one chosen in this thesis, is to monitor the movement of the antenna in the direction of the satellite. The use of the pseudo-range measurement is not adequate for determining accelerations because of its inherent noise level (see Section 3.2.3). Kleusberg et al [1989] explains that the computation of accelerations involves two successive numerical differentiations of the measured range. Consequently, each differentiation will tend to increase the high frequency, noise like measurement errors. However, the low noise level of the carrier

phase makes this an attractive measurement for this technique. Taking the first and second

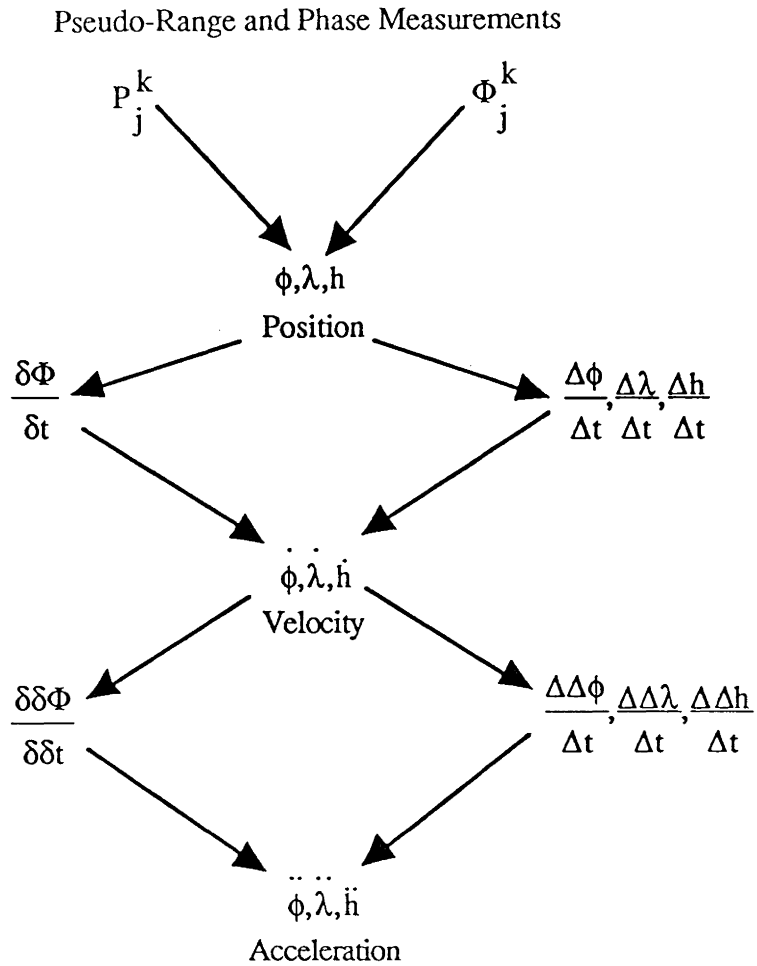


Figure 4.1

Methods in Determining Motion Using GPS Pseudo-Range and Carrier Phase Measurements

time derivatives of the carrier phase will give the antenna velocity and acceleration values, in the direction of the satellite. Combining several simultaneous such values to different satellites allows the determination of velocity and acceleration components.

Figure 4.1 depicts the relationship between the two methods described above.

## 4.2 Assessment of the Phase Observable

The measurement noise of equation (3.2) can be separated from the GPS phase observable using a linear combination of phase measurements from two adjacent dual frequency receivers [Georgiadou and Kleusberg 1988]. Assessment of the measurement errors associated with the GPS phase observable was performed by Kleusberg et al. [1989] using the above technique. Their results indicate that GPS phase data is not necessarily a white noise sequence. Low frequency cyclic variations, such as those due to multipath, can exist in the data. They conclude that these low frequency cyclic variations are responsible for the main GPS error at the gravity cut-off frequency of 0.0083 Hz used in airborne gravimetry. Consequently, it is antenna performance (multipath), and not receiver noise, that limits the accuracy at which accelerations in this band can be determined. Propagation of phase errors into the acceleration accuracies, in the frequency domain, using the proposed differencing technique has been assessed by Kleusberg [1989]. His analysis shows that the low frequency acceleration noise, such as aircraft motion and signal multipath, will be suppressed, while the high frequency receiver measurement noise will be amplified. Referring to equation (2.2), it will be shown later that this propagation of errors becomes significant when evaluating the low frequency part of the acceleration spectrum below 0.0083 Hz.

## 4.3 Technological Advances in Receiver and Antenna Design

Results by Kleusberg et al. [1989] were based on data collected using a Texas Instrument TI 4100 GPS receiver. Improvements in receiver design since the development of the TI 4100 are,

- a) Multichannel receivers which provide a separate channel for each incoming satellite signal. A multichannel receiver may have a signal to noise advantage over other types of

receivers, such as multiplex or sequencing receivers [Maher 1986; Lachapelle et al., 1987]. This is due to the fact that multichannel receivers allow for continuous tracking and more frequent sampling of the satellite signal.

- b) Rapid development of microprocessor capabilities has lead to faster sampling rates within the receiver [McDonald 1988].
- c) Advanced circuit integration and hardware design has allowed receivers to measure the phase of the carrier to better than 1 millimetre [Ashjaee et al., 1988].
- d) Improved antenna design results in the phase centre of the antenna being theoretically well defined [Lachapelle et al., 1987].

The above advancements in technology enhance the capability of GPS to measure aircraft accelerations to the 1 to 2 mGal accuracy level. The use of multichannel receivers permits the continuous simultaneous tracking of the carrier phase to as many as 12 satellites [McDonald 1988]. With more satellites being tracked, there is a better chance to detect any cycle slips which may have occurred during the observing session [Goad 1985]. The higher signal to noise ratio of the multichannel receiver enables the receiver to have continuous tracking of the satellite signal with a narrower bandwidth [Ashjaee 1986]. Consequently, this reduction in the signal to noise ratio reduces the chance of loss of lock to the signal and thus, a loss of data.

Also, the capability of a faster sampling rate will allow for finer resolution of aircraft movement.

As mentioned in the previous section, multipath effects have a significant contribution on the low frequency part of the phase measurement error within the gravity passband of 0.0083 Hz. Improvements in antenna design can lead to reductions in the power spectrum of these low frequency signals. In turn, this reduces the acceleration error within the same passband.

## 4.4 Implications of a Full Satellite Constellation

In addition to the above technological advancements, the satellite constellation will play a significant role in determining accelerations. The availability of extra satellites allows for redundancy in the acceleration solution as well as flexibility in project planning when certain satellites are not available.

## 4.5 Treatment of Biases and Errors

The treatment of the biases and errors discussed in Chapter 3 must be addressed in order to formulate an observation model for acceleration determination.

### 4.5.1 Satellite Orbital Errors

The accuracy of the satellite ephemeris is important in justifying if the satellite position, velocity, and acceleration can be considered known when developing the model for acceleration determination for a receiver. Kleusberg et al. [1985] assessed the influence of the orbital errors on kinematic applications by analyzing the temporal variations in the errors of the predicted ephemeris using a pseudo-range residual plot of a fixed point. His results showed that the slope of the long period variations of the residual plot was the error in satellite to receiver range. It was shown that this error did not exceed  $\pm 0.3$  cm/sec. In addition, the change in slope of the long period variations is a measure of the acceleration error contributed by the satellite ephemeris. Using the results from the above reference, the change in slope is in the order of magnitude of  $10^{-4}$  mm/sec<sup>2</sup> which is less than 0.01 mGal. Consequently, the broadcast ephemeris data will be considered errorless in developing the acceleration model.

## 4.5.2 Satellite and Receiver Clock Biases

Equation 3.3 gave the second order polynomial used in modelling the satellite clock error. Section 3.3.2 gave the satellite clock frequency offset accuracy as  $10^{-11}$  and the frequency drift as  $10^{-14}$  per second. Of most concern for acceleration determination is the effect of the frequency drift on the phase acceleration. As mentioned in Section 3.3.2 the satellite clock errors can be reduced by differencing between two receivers observing at the same time, one receiver being positioned at a known point, while the other receiver being mounted on the moving platform. The remaining clock satellite clock errors can be considered negligible using this differencing technique.

The receiver clock is less accurate than the satellite clock. Consequently, the receiver time offset, frequency offset, and frequency drift should be solved for at each epoch using the measured ranges.

## 4.5.3 Atmospheric Effects

When dealing with the atmospheric biases on the GPS observable, differencing has its limitations. Kleusberg [1986] stipulates that differencing between dual frequency receivers with a baseline length of 40 kilometres can result in ionospheric induced errors far above the receiver noise. Shorter baselines of approximately ten kilometres, however, show no significant effects. The data collected for this research was over baselines of less than 50 metres with an elevation difference of not more than 5 metres. For very short baselines like this one, the atmospheric conditions along the path of the propagating signal from the satellite to each receiver is practically the same. Consequently, differencing techniques will reduce, if not eliminate, the atmospheric effects on the phase observations. It should be noted that baselines of a few tens of metres do not exist in airborne gravimetry. It is the intention here to eliminate as many biases as possible in order to verify whether GPS gives useful accelerations at all under ideal conditions.



Heroux [1988] indicates that the ionosphere at high latitudes can cause severe amplitude and phase variations to the point where signal strength is decreased and cycle slips can occur on single frequency receivers. It was further stipulated that the only way to guarantee that GPS data from northern regions was not adversely affected by the ionosphere is to observe with dual frequency receivers. The application of this recommendation to airborne gravimetry has yet to be studied. Heroux's study suggests that when using single frequency receivers, the ionosphere will have a significant effect on GPS determined accelerations for airborne gravimetric surveys in the northern regions.

Wells and Kleusberg [1989] suggest that the spatial coherence of tropospheric conditions is limited and that differencing over baselines of a short distance (eg. few kilometres) is not likely to successfully eliminate tropospheric effects. Chapter 1 gave certain regions where airborne gravimetry would cover large areas. Consequently, tropospheric influences on GPS satellite signals would have to be estimated using measured temperature and pressure data. For airborne gravimetry these measurements would probably need to be measured on the fly.

On very short baselines, like the tens of metres used in this thesis, differencing between receivers will avoid any differential atmospheric delays [Geogiadou and Kleusberg 1988]. Consequently, it is expected that the tropospheric effect will be practically eliminated using the differencing between receivers.

#### **4.5.4 Cycle Slips**

Cycle slips have been considered as one of the major causes for limiting the accuracy at which accelerations can be determined [Brozena et al., 1989]. Following the approach taken in this thesis, whereby accelerations are determined by taking the second time derivative of the carrier phase observable, cycle slips can have less effect on the overall acceleration determination. This advantage is explained as follows. Chapter two

stated that the cut-off frequency for the gravity data was 0.0083 Hz (120 seconds) for airborne gravimetry. The aircraft acceleration correction applied to this gravity value is equal to the mean of the observed aircraft acceleration over the same time period [Kleusberg 1989]. With a GPS receiver sampling rate of one second, the total number of aircraft acceleration determinations which can be obtained over this time period is 118. Each cycle slip introduced to the phase data will decrease the total number of acceleration measurements within the passband by three. This will have a negligible effect on the final result representing the 120 second time period. Thus, the proposal in this thesis for handling cycle slips is simply to detect and reject them. The total acceleration correction applied to gravity over the 120 second period is then determined from the measurements which remain.

As implied in the above discussion, the magnitude of the cycle slip does not have to be determined. However, detection of the cycle slip is important. A description of methods for detecting cycle slips in kinematic applications, and their success, can be found in Mader and Lucas [1989] and Goad [1985].

The data collected for this thesis consisted of GPS pseudo-range and carrier phase observations on fixed points. Collecting data at a stationary point was necessary in order to assess the measured error in acceleration using the GPS carrier phase. Therefore, all computed accelerations should theoretically be zero. Any data which is contaminated with cycle slips would give a sudden rise in acceleration above the normal level. In this way cycle slip and other erroneous data was checked against a tolerance level and subsequently rejected. This technique may not be practical for actual airborne gravimetry applications. Methods to detect and reject cycle slips which may be useful in airborne gravimetry are described in Mader and Lucas [1989], and Goad [1985].

#### **4.5.5 Antenna Errors**

The existence of multipath and imaging in the receiver antenna are functions of the environment in which the data is collected. Thus, the reduction of multipath effects on the acceleration determination can be obtained by positioning the GPS receiver antenna in an area which minimizes the possibility of multipath or imaging. Antenna phase centre and phase variations are functions of the antenna design. The reduction of these errors depends on the type of antenna used. Antenna design can also play a role in reducing multipath effects.

#### **4.5.6 Selective Availability**

Dithering of the satellite clock or contaminating the satellite ephemeris with false information will cause subsequent changes in the apparent position, velocity, and acceleration of a receiver. Assuming that selective availability is common to two receivers observing during the same time period, then the effects of selective availability can be eliminated by differencing between receivers. The effects of selective availability and the implementation of differencing techniques in handling it are covered in Chapter 8.

### **4.6 Summary**

This chapter has introduced the concept of determining acceleration using the GPS carrier phase measurement.

The accuracy with which accelerations can be resolved was shown to have been, in part, dependent on the technological advancements in GPS receiver and antenna design. Developments in this technology were itemized as they pertain to acceleration determination. In addition, the implication of a full satellite constellation on determining accelerations was discussed.

The treatment of biases and errors introduced in Chapter 3 were assessed. Methods of treating these errors in the present research were proposed. Implications of these errors for airborne gravity surveys were also addressed.

Thus, the tools provided in this chapter have paved the way for the development of the least squares adjustment model which is presented in the next chapter.

## CHAPTER FIVE

### Formation of the Least Squares Adjustment

#### 5.0 Introduction

The procedure used to determine acceleration in this research is to first determine the accelerations of each receiver and then difference between receivers to eliminate systematic errors. Chapter 5 begins with the development of the geometric configuration and the subsequent observation scheme for determining aircraft accelerations using a single frequency GPS measurement technique. The observation equations for a parametric least squares adjustment are then formulated. In this formulation, consideration is given to the development of the equations which describe the satellite orbital position, velocity, and acceleration. Next, the phase velocity and acceleration values are formulated. A weighting scheme is developed in the event of unequally spaced data. The least squares normal equations are then addressed with emphasis placed on the elements of the design matrix of the unknown receiver parameters and on the covariance matrix of the observables. Next, the equations for the transformation of accelerations from the conventional terrestrial (CT) coordinate to the geodetic coordinate system are developed. Finally, differences between receivers are performed.

#### 5.1 Geometric Configuration of the 3 Epoch Observation Scheme

This thesis proposes to determine acceleration by modelling the second time derivative of the GPS carrier phase observable. Initially, the single frequency receiver measurement technique is addressed. Once accelerations are determined, differential corrections are applied. The overall geometric configuration for this observation scheme is

illustrated in Figure 5.1. For simplicity, Figure 5.1 has only one satellite range representing the observing scenario. Real observation sessions would involve ranges from several satellites.

The satellite in Figure 5.1 is in constant motion through its orbit about the earth. The objective in modelling the receiver acceleration is to relate the receiver motion to the satellite motion in the same coordinate and time frame. Results shown in Chapter 4 indicate that the satellite motion can be considered known for acceleration determination. The satellite coordinates, velocities, and accelerations can be derived from the orbital parameters provided in the broadcast ephemeris.

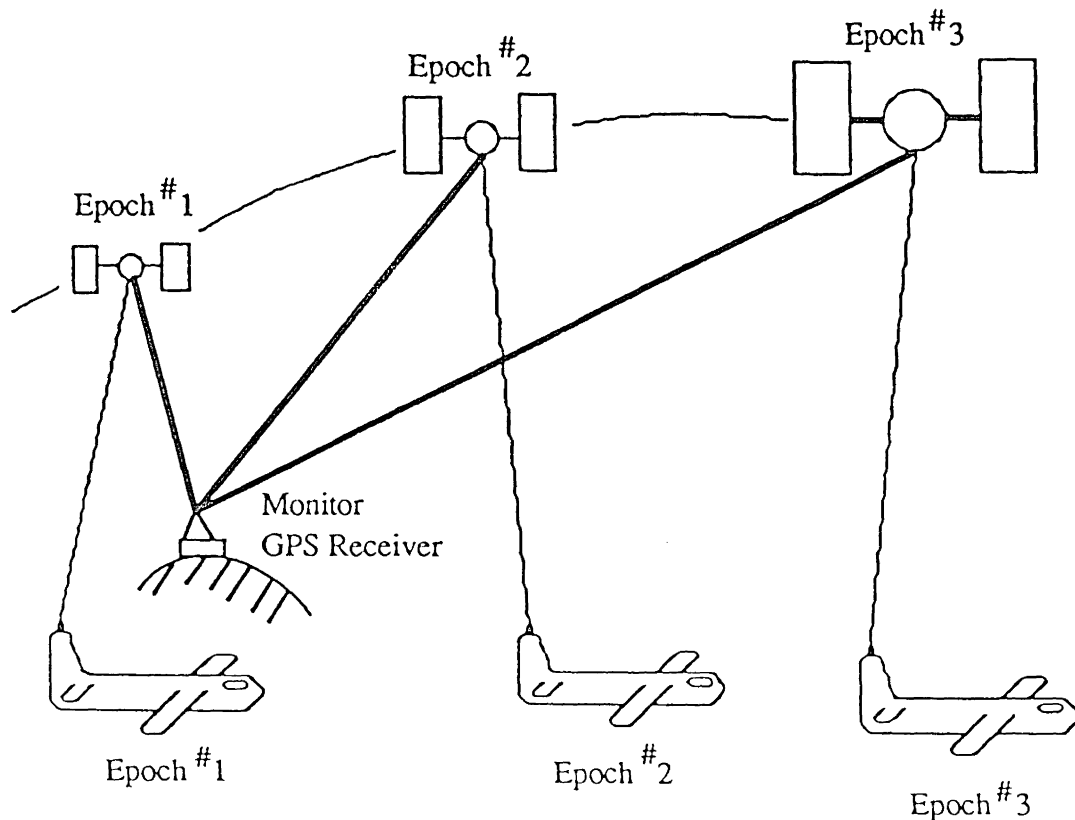


Figure 5.1

Geometric Configuration Between Satellite and Receiver in Determining Acceleration

Note that the phase measurement is sampled at each epoch over a three epoch time interval. The relative change in the receiver position from epoch to epoch is all that is needed to measure the receiver velocity and acceleration. Consequently, to measure the velocity of the receiver, phase observations for two epochs are required. To measure the receiver acceleration, which is the change in velocity over time, phase observations for three epochs are required. This three epoch observation scheme can be used to determine receiver accelerations over a series of observations epochs.

Figure 5.2 shows a typical scenario of an aircraft moving along in time observing phase measurements from a single satellite at epochs 1,2,3,4,.....,n.

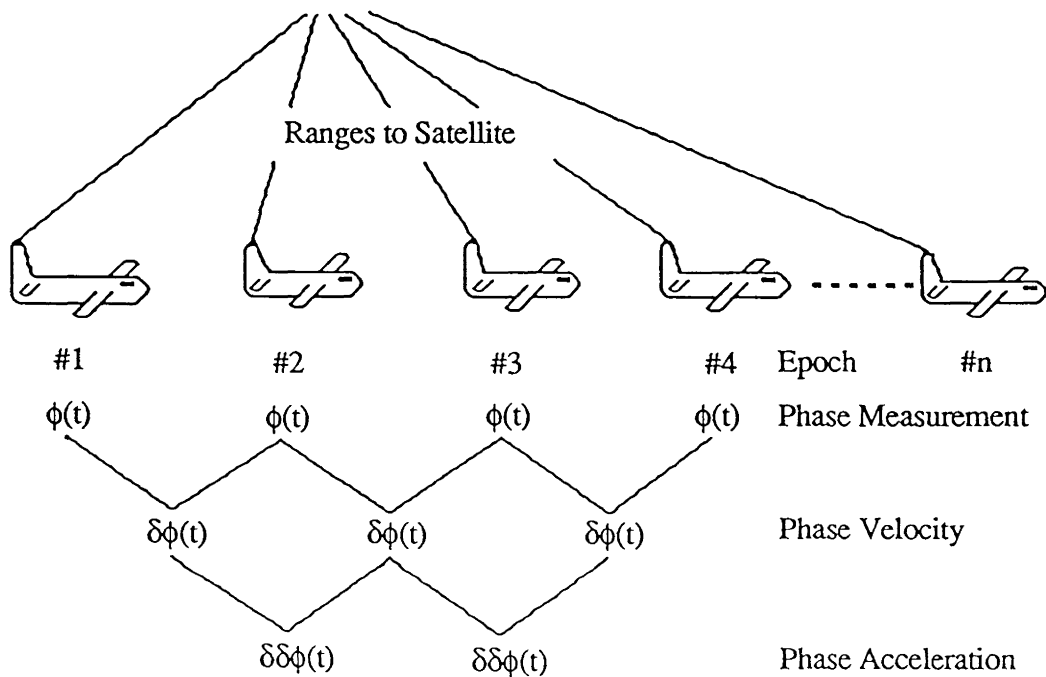


Figure 5.2

Receiver Acceleration by Differencing the GPS Carrier Phase in Time

The velocity of the receiver in the direction of the satellite from epoch #1 to epoch #2 is determined by differencing the carrier phase measurement over the time period between the two epochs. The velocity of the receiver in the direction of the same satellite from epoch #2 to epoch #3 is determined in the same manner. Consequently, the acceleration of the receiver from epoch #1 to epoch #3 is determined by differencing the velocity estimates over the time period of the velocity change. In order to give some spatial resolution this acceleration is referenced with respect to the location of epoch #2. The acceleration for epoch #3 is then computed from phase measurements obtained at epochs #2, #3, and #4. In this manner, the accelerations for the remaining epochs can be determined up to epoch n-1. Note that only the moving receiver is shown in Figure 5.2. The approach taken in this thesis is to difference the computed accelerations between the moving and monitor receivers.

## 5.2 Formation of the Observation Equations

The velocity value determined above is formed by differencing equation (3.2) over time. The time derivative for a satellite k and a receiver j is given as follows:

$$\delta\phi = \frac{\partial\phi}{\partial t} = \frac{1}{\rho_j^k} \left\{ (X^k - X_j)(\dot{X}^k - \dot{X}_j) + (Y^k - Y_j)(\dot{Y}^k - \dot{Y}_j) + (Z^k - Z_j)(\dot{Z}^k - \dot{Z}_j) \right\} + \dots$$

$$\dots + c(\dot{dt}^k + \dot{dT}_j) - \dot{d}_{ion} + \dot{d}_{trop} + \dot{\epsilon} \quad (5.1)$$

where,

- $\delta\phi$  = the first time derivative of the phase observable (the Doppler observation),
- $\rho_j^k$  = the geometric range from the satellite to the receiver,
- $X^k Y^k Z^k$  = the position of the satellite in the CT-system,



$\dot{X}^k \dot{Y}^k \dot{Z}^k$	= the velocity of the satellite in the CT-system,
$X_j Y_j Z_j$	= the position of the receiver in the CT-system,
$\dot{X}_j \dot{Y}_j \dot{Z}_j$	= the velocity of the receiver in the CT-system,
$c$	= the speed of light in a vacuum,
$\dot{t}^k$	= the satellite clock frequency offset,
$\dot{T}_j$	= the receiver clock frequency offset,
$\dot{d}_{ion}$	= the time derivative of the ionospheric delay of the propagating signal,
$\dot{d}_{trop}$	= the time derivative of the tropospheric delay of the propagating signal,
$\dot{\epsilon}$	= the time derivative of the unmodelled measurement errors,
CT	= the Conventional Terrestrial coordinate system.

The time dependence given in equation (3.1) is not included in equation (5.1) since, according to Section 5.1, the velocity of the receiver is based on phase measurements over two epochs. For now, the timetag for the velocity value will be referenced to the mid-time of the two phase measurements.

The acceleration value is formed by differencing equation (5.1) over time. This second time derivative for a satellite  $k$  and receiver  $j$  is given as follows:

$$\begin{aligned}
\delta\delta\phi = \frac{\partial^2\phi}{\partial t^2} = \frac{1}{\rho_j^k} & \left[ \{ (X^k - X_j)(\ddot{X}^k - \ddot{X}_j) + (\dot{X}^k - \dot{X}_j)^2 \} + \{ (Y^k - Y_j)(\ddot{Y}^k - \ddot{Y}_j) + (\dot{Y}^k - \dot{Y}_j)^2 \} + \dots \right. \\
& \left. \dots + \{ (Z^k - Z_j)(\ddot{Z}^k - \ddot{Z}_j) + (\dot{Z}^k - \dot{Z}_j)^2 \} \right] - \dots \\
& \dots - \frac{1}{(\rho_j^k)^3} \left[ (X^k - X_j)(\dot{X}^k - \dot{X}_j) + (Y^k - Y_j)(\dot{Y}^k - \dot{Y}_j) + (Z^k - Z_j)(\dot{Z}^k - \dot{Z}_j) \right]^2 + \dots \\
& \dots + c(\dot{dt}^k + \dot{dT}_j) - \ddot{d}_{ion} + \ddot{d}_{trop} + \ddot{\varepsilon}
\end{aligned} \tag{5.2}$$

where,

$\delta\delta\phi_k$	= the second time derivative of the phase observable,
$\rho_j$	= the geometric range from the satellite to the receiver,
$X^k Y^k Z^k$	= the position of the satellite in the CT-system,
$\dot{X}^k \dot{Y}^k \dot{Z}^k$	= the velocity of the satellite in the CT-system,
$\ddot{X}^k \ddot{Y}^k \ddot{Z}^k$	= the acceleration of the satellite in the CT-system,
$X_j Y_j Z_j$	= the position of the receiver in the CT-system,
$\dot{X}_j \dot{Y}_j \dot{Z}_j$	= the velocity of the receiver in the CT-system,
$\ddot{X}_j \ddot{Y}_j \ddot{Z}_j$	= the acceleration of the receiver in the CT-system,
$c$	= the speed of light in a vacuum,
$\dot{dt}^k$	= the satellite clock frequency drift,
$\dot{dT}_j$	= the receiver clock frequency drift,
$\ddot{d}_{ion}$	= the second time derivative of the ionospheric delay of the propagating GPS signal,
$\ddot{d}_{trop}$	= the second time derivative of the tropospheric delay of the propagating GPS signal,
$\ddot{\varepsilon}$	= the second time derivative of the unmodelled measurement errors.
CT	= the Conventional Terrestrial coordinate system.

Section 5.1 showed that the acceleration was based on the phase measurements over three epochs. Consequently, the timetag for the acceleration will be referenced to the middle epoch.

The sensitivity of the phase acceleration to an error in position can be determined by error propagation. Assuming all other variables of equation (5.2) are known, the error in acceleration due to an error in position is given as follows:

$$\sigma_{\delta\delta\phi}^2 = \left(\frac{\partial\delta\delta\phi}{\partial X_j}\right)^2 \sigma_{X_j}^2 + \left(\frac{\partial\delta\delta\phi}{\partial Y_j}\right)^2 \sigma_{Y_j}^2 + \left(\frac{\partial\delta\delta\phi}{\partial Z_j}\right)^2 \sigma_{Z_j}^2 \quad (5.3)$$

where,

$\sigma_{\delta\delta\phi}^2$  = the error in the phase acceleration in the direction of the satellite,  
 $\sigma_{X_j}^2 \sigma_{Y_j}^2 \sigma_{Z_j}^2$  = the error in the receiver position with respect to the CT-system,  
 $\left(\frac{\partial\delta\delta\phi}{\partial X, Y, Z_j}\right)^2$  = the Jacobian of the transformation from the receiver X,Y,Z coordinates with respect to the CT- system to the geodetic coordinate system.

Appendix I gives an example illustrating the effect of an error in receiver position on the determined acceleration of the receiver in the direction of the satellite. Satellite parameters for the example were obtained from GPS data collected for this research. The result shows that an error of 100 metres has no significant effect on the receiver acceleration as determined by equation (5.2). Wells et al. [1986] stipulates that an accuracy of 50 metres or better is realizable using the GPS pseudo-range observable. This implies that the pseudo-range observation can be used to determine the position of the receiver in equations (5.1) and (5.2). Thus, to complete the set of observation equations the pseudo-range equation is expressed once again as follows:

$$P_j^k = \rho_j^k + c[dt^k - dT_j] + d_{ion} + d_{trop} + \varepsilon \quad (5.4)$$

The variables of equation (5.4) were defined in equation (3.1). The time of the pseudo-range observation has been omitted in order to present the equation in the same manner as equations (5.1) and (5.2).

Also provided in Appendix I is the sensitivity of the phase acceleration to an error in velocity of 1 m/sec. The results show that if the velocity is determined by pseudo-range observations, variations of several mGals would be experienced in the subsequent accelerations. Consequently, because of its low noise level characteristics, the carrier phase was used to determine velocity in the acceleration model.

Performing differences between receivers, in order to eliminate the satellite clock errors and reduce atmospheric effects to negligible values, gives the following set of equations:

$$\Delta P_j^k(t) = \Delta \rho_j^k(t) + c\Delta dT_j(t) + \Delta \varepsilon(t) \quad (5.5)$$

$$\Delta \delta \phi_j^k(t) = \Delta \delta \rho_j^k(t) - c\Delta \delta dT_j(t) + \Delta \delta \varepsilon_j^k(t) \quad (5.6)$$

$$\Delta \delta \delta \phi_j^k(t) = \Delta \delta \delta \rho_j^k(t) - c\Delta \delta \delta dT_j(t) + \Delta \delta \delta \varepsilon_j^k(t) \quad (5.7)$$

The unknown parameters in the above equations are the three receiver coordinate differences, the three receiver velocities and accelerations, and the three receiver clock parameters. These clock parameters are the time offset, the clock frequency offset and frequency drift. A minimum of four satellites is needed to solve for these twelve

unknowns. The observations from these four satellites and three epochs are the four pseudo-ranges, the four first time derivatives in the phase measurements, and the four second time derivatives in the phase measurements derived from three subsequent phase measurements. The total number of observations equates to twelve. Three additional observations are obtained for each extra satellite observed. The procedure used is to first determine the accelerations of each receiver and then difference between receivers to eliminate systematic errors.

In summary, the acceleration model is described by the three epoch observation scheme where the receiver accelerations are related to the GPS observables as follows:

$$\ddot{\mathbf{R}} = f\{P, \delta\phi, \delta\delta\phi\} \quad (5.5)$$

where,

- $\ddot{\mathbf{R}}$  = the XYZ acceleration of the receiver with respect to the CT-coordinate system,
- $P$  = the GPS pseudo-range observable,
- $\delta\phi$  = the GPS phase observable differenced over time (the Doppler observation),
- $\delta\delta\phi$  = the second time derivative of the GPS phase observable.

Note, that the time of  $\ddot{\mathbf{R}}$  represents the middle epoch of the three epochs required in determining the receiver acceleration.

### 5.2.1 Velocity Averaging Over Three Epochs

The three epoch observing scheme introduces two velocities which have to be related to the acceleration which is related to the middle reference time. In the case of an

equal time interval between epochs the velocity is simply the average of the velocity before and after the reference time. However, the situation often occurs where the time interval between observations is not a constant but can change as much as 100 milliseconds. Such data were experienced with the Trimble 4000 SLD GPS receiver.

Recognizing that the time intervals used to compute the receiver velocity can be different, weighting of the data becomes necessary. The weighting technique applied here assumes that more information on the aircraft movement can be gained from the shortest time interval used to determine the velocity. Given a three epoch observation scheme, where the three epochs are represented by  $t_1$ ,  $t_2$ , and  $t_3$ , and their corresponding phase measurements are  $\phi_1$ ,  $\phi_2$ , and  $\phi_3$ , then the velocity of the receiver in the direction of the satellite for the centre epoch,  $\dot{\phi}$ , is given as follows:

$$\dot{\phi} = \frac{\phi_1 - \phi_2}{(t_1 - t_2) \left(1 - \frac{t_1 - t_2}{t_3 - t_2}\right)} + \frac{\phi_3 - \phi_2}{(t_3 - t_2) \left(1 - \frac{t_3 - t_2}{t_1 - t_2}\right)} \quad (5.5)$$

The corresponding acceleration of the receiver,  $\ddot{\phi}$ , in the direction of the satellite for the centre epoch is given as follows:

$$\ddot{\phi} = \frac{\phi_3 - \phi_2}{(t_3 - t_2) \left(\frac{t_3 - t_1}{2}\right)} + \frac{\phi_1 - \phi_2}{(t_1 - t_2) \left(\frac{t_1 - t_3}{2}\right)} \quad (5.6)$$

The complete derivations of equations (5.5) and (5.6) are presented in Appendix II.

### 5.3 Satellite Orbital Velocities and Accelerations

Recall that Equations 5.1 and 5.2 include the satellite velocities and accelerations. The accelerations of a satellite can be determined from the parameters which describe the orbital motion of the satellite. Values for these parameters are given in the broadcast ephemeris. Note, these values describe the satellite orbit for a period of approximately one hour [Wells et al., 1986]. New ephemeris parameter values are used every hour. A description of the satellite orbital parameters can be found in Quek [1989].

The final form of the satellite coordinates used in the observation equations is given with respect to the Conventional Terrestrial coordinate system [Kleusberg 1987]. The satellite coordinates determined from the broadcast ephemeris are with respect to an Earth Centred Space Fixed (ECSF) reference frame. Consequently, the satellite coordinates must undergo a transformation in order to express them in the CT coordinate system. The computation of the satellite coordinates from the orbital parameters of the broadcast ephemeris is given in Wells et al. [1986]. The computation of the satellite velocities in the ECSF coordinate system is accomplished by taking the time derivative of the satellite coordinates. This means taking the first time derivative of the orbital parameters expressed in the broadcast ephemeris. Satellite accelerations are subsequently derived by taking the second time derivative of the satellite coordinates. Thus, this means taking the second time derivatives of the orbital parameters described by the broadcast ephemeris. A summary of the formula representing the satellite accelerations as derived from the satellite ephemeris is given in Appendix III.

### 5.4 Formation of the Normal Equations

The general form of the linearized approximation of the observable  $l$ , which is a function of the unknown parameters  $x$  is given as follows [Wells and Krakiwsky 1971]:

$$l = l^0 + r = f(x^0) + \left. \frac{\partial f}{\partial x} \right|_{x=x^0} (x - x^0) \quad (5.9)$$

where,

$x^0$  = the a priori estimates of  $x$ ,

$x - x^0$  = the corrections to the initial estimate of  $x$ ,

$l^0$  = the observed values of  $l$ ,

$r$  = the residuals on  $l$ ,

$\frac{\partial f}{\partial x}$  = the first order design matrix for  $x$ .

Denoting the design matrix  $\frac{\partial f}{\partial x}$  by  $A$ , the misclosures  $f(x^0) - l^0 = \omega$ , and the corrections  $x - x^0$  by  $\delta$ , equation (5.9) can be written in the well known form:

$$A\delta + \omega = r \quad (5.10)$$

The normal equations result from the minimization of the sums of the squares of the weighted residuals (ie. minimization  $r^T C_1^{-1} r$ ).  $C_1^{-1}$  represents the covariance of the observed quantities. For a parametric least squares adjustment, where the observables are expressed as functions of the unknown parameters, the least squares normal equations are given as follows [Wells and Krakiwsky 1971]:

$$N\delta = b$$

and, the solution to the normal equations is given as,

$$\hat{\delta} = N^{-1}b$$

or,

$$\hat{\delta} = (A^T C_1^{-1} A)^{-1} A^T C_1^{-1} \omega \quad (5.11)$$



The design matrix, A, for the equations (5.6, 5.7, and 5.8) will consist of the partial derivatives of the observations with respect to each of the 12 unknown quantities given in Section 5.3. This will be a hyper-triangular matrix consisting of design matrices representing each type of observation necessary in acquiring the receiver acceleration. Figure 5.3 illustrates this design matrix.

$$\begin{bmatrix} \frac{\partial P}{\partial_{X,Y,Z,T}} & 0 & 0 \\ \frac{\partial \delta\phi}{\partial_{X,Y,Z,T}} & \frac{\partial \delta\phi}{\partial_{\dot{X},\dot{Y},\dot{Z},\dot{T}}} & 0 \\ \frac{\partial \delta\delta\phi}{\partial_{X,Y,Z,T}} & \frac{\partial \delta\delta\phi}{\partial_{\dot{X},\dot{Y},\dot{Z},\dot{T}}} & \frac{\partial \delta\delta\phi}{\partial_{\ddot{X},\ddot{Y},\ddot{Z},\ddot{T}}} \end{bmatrix}$$

Figure 5.3

#### Design Matrix of Least Squares Adjustment

The variances applied to the measurement noise of the pseudo-range and carrier phase observables were obtained from error analyses performed by other authors [Milliken and Zoller 1980; Evans et al., 1985; Langley 1986; Ashjaee et al., 1988]. The TI 4100 was estimated to have a P-code pseudo-range error of 2 metres and a carrier phase error of 2 millimetres. Modern receivers such as the Ashtech XII and Trimble 4000 SLD receivers were estimated to have a C/A code pseudo-range error of 1 metre and a phase measurement error of 1 millimetre. Propagating the phase measurement error using equations (5.5) and (5.6) gives the Doppler observable a measurement error of 8 millimetres for the TI 4100 and 4 millimetres for the other two receivers. The  $\delta\delta\phi$  observable subsequently has

measurement error of 8 millimetres for the TI 4100 and 4 millimetres for the other two receivers.

Note here that the correlation between the pseudo-range and the phase measurements is assumed to be zero. In addition, the physical correlation between phase measurements was not considered. This subsequently creates a diagonal weight matrix of the observables containing their corresponding measurement errors given above. The off-diagonal elements are zeros.

Following the procedure of the least squares process, the estimated correction vector  $\hat{\delta}$ , is applied to the initial estimates of the unknown parameters. The process is iterated until the unknown parameters converge to a level where further iterations are of no significance.

## 5.5 Transformation of Position, Velocity and Acceleration

Letting X represent the XYZ cartesian coordinates of the receiver and U represent the  $\phi\lambda h$  geodetic coordinate of the same point, then the transformation from U to X is given by [Krakiwsky and Wells 1971]:

$$X = J U \quad (5.12)$$

The matrix J represents the Jacobian of the transformation from U to X and is given as follows [Krakiwsky et al., 1977]:

$$J = \begin{bmatrix} -(M+h) \sin\phi \cos\lambda & -(N+h) \cos\phi \sin\lambda & \cos\phi \cos\lambda \\ -(M+h) \sin\phi \sin\lambda & (N+h) \cos\phi \cos\lambda & \cos\phi \sin\lambda \\ (M+h) \cos\phi & 0 & \sin\phi \end{bmatrix} \quad (5.13)$$

The error propagation for these three dimensional coordinate systems involves the transformation of the covariance matrix of the cartesian coordinates,  $C_{XYZ}$ , into the geodetic covariance matrix,  $C_{\phi\lambda h}$ . Using the law of propagation of errors this transformation is given as follows [Wells and Krakiwsky 1971]:

$$C_{\phi\lambda h} = J^{-1} C_{XYZ} (J^{-1})^T \quad (5.14)$$

In this thesis it becomes necessary to transform the velocities and accelerations, and their associated errors from the cartesian coordinate to the geodetic coordinate system. Appendix IV gives the derivation of these transformations.

In summary, the geodetic velocities are expressed as follows:

$$\dot{U} = J^{-1} \dot{X} \quad (5.15)$$

where,

- $\dot{U}$  = the velocities of the receiver in the geodetic coordinate system,
- $J^{-1}$  = the Jacobian matrix for the transformation (equation 5.13),
- $\dot{X}$  = the velocities of the receiver in the cartesian coordinate system.

The propagation of the cartesian velocity errors,  $\Sigma_{\dot{X}}$ , to the geodetic velocity errors,  $\Sigma_{\dot{U}}$ , is represented by:

$$\Sigma_{\dot{U}} = J^{-1} \Sigma_{\dot{X}} (J^{-1})^T \quad (5.16)$$

The time derivative of equation (5.15) gives the accelerations in the geodetic coordinate system as follows:

$$\ddot{U} = \dot{J}^{-1} \ddot{X} + J^{-1} \dot{\ddot{X}} \quad (5.17)$$

where,

- $\ddot{U}$  = the accelerations of the receiver in the geodetic coordinate system,  
 $\dot{J}^{-1}$  = the time derivative of Jacobian matrix for the transformation (see Appendix IV),  
 $\ddot{X}$  = the accelerations of the receiver in the average terrestrial coordinate system.

The corresponding propagation of acceleration errors from the cartesian coordinate system to the geodetic coordinate system is given as:

$$\Sigma_{\ddot{U}} = J^{-1} \Sigma_{\ddot{X}} (J^{-1})^T + \dot{J}^{-1} \Sigma_{\dot{\ddot{X}}} (\dot{J}^{-1})^T + \dot{J}^{-1} \Sigma_{\ddot{X}\dot{X}} (J^{-1})^T + J^{-1} \Sigma_{\dot{\ddot{X}}\dot{X}} (\dot{J}^{-1})^T \quad (5.18)$$

where,

- $\Sigma_{\ddot{U}}$  = the covariance matrix of the receiver accelerations in the geodetic coordinate system,  
 $\Sigma_{\ddot{X}}$  = the covariance matrix of the receiver accelerations in the cartesian coordinate system,  
 $\Sigma_{\ddot{X}\dot{X}}, \Sigma_{\dot{\ddot{X}}\dot{X}}$  = the correlation matrices between the receiver velocities and accelerations in the cartesian coordinate system.

## 5.6 Summary

The method used in this chapter to determine accelerations using single frequency GPS carrier phase observing techniques was to first determine the accelerations of each receiver and then difference between receivers to eliminate systematic errors. This chapter

has developed the least squares adjustment model for determining these accelerations. The model has been based on a three epoch observation scheme. The observations consisted of pseudo-range and carrier phase observations. The phase measurement was differenced in time to give the receiver accelerations. The pseudo-range observations were used to determine the receiver position in the adjustment. Although the pseudo-range position is not as smooth as the carrier phase determined position, it was shown that the apparent noise in the pseudo-range position from epoch to epoch had no significant effect on the determination of the receiver acceleration in the direction of the satellite.

In formulating the observation equations the satellite accelerations were derived using the orbital parameters described by the broadcast ephemeris. In addition, a weighting scheme was designed to handle data where the three epoch observing scheme had unequal spaced time intervals. Finally the transformation of the coordinates, velocities, and accelerations from the cartesian coordinate system to the geodetic coordinate system was developed.

The next step towards evaluating the possible acceleration accuracy achievable from GPS measurements is to test the model presented here using observed GPS data. The next chapter performs this test and comments on the results.

## CHAPTER SIX

### GPS Observations and Processing Results

#### 6.0 Introduction

Chapter 6 applies the theory for determining accelerations presented in this thesis to observed GPS data. Three GPS data sets were collected. Each set consisted of pseudo-range and carrier phase measurements at two fixed points situated within 50 metres of each other. The data sets are described and accelerations are determined. The results are assessed as they pertain to this thesis.

#### 6.1 TI 4100 Observations

The first set of data was collected using two Texas Instrument TI 4100 GPS Receivers. The TI 4100 is a C/A-code plus P-code, L1/L2 single channel multiplexing receiver. It records dual frequency pseudo-range and carrier phase measurements as well as the navigation message. More details concerning this receiver can be found in Ward [1984].

##### 6.1.1 TI 4100 Data Description

The TI 4100 data was collected on December 16, 1987, in Ottawa, Canada (approximately  $45.1^{\circ}\text{N}$ ,  $76.1^{\circ}\text{W}$ ). The two receivers were spaced less than 50 metres apart. The sampling interval for both receivers was two seconds. The receivers recorded the L1/L2 P-code pseudo-range and carrier phase measurements. The time length of the observing session was approximately 40 minutes. The receivers at both ends of the baselines were held fixed. Consequently, the theoretical accelerations of the receivers should be zero. The accelerations were determined from pseudo-range and phase

observations from four satellites. Only the L2 carrier phase was utilized. It was found that the ionospheric correction obtained from using dual frequency observations was insignificant when determining accelerations. The PDOP value for the observing session centred about 4. A polar plot giving the sky distribution of the satellites during the time period of observing is given in Appendix V.

### 6.1.2 $\phi\lambda h$ Accelerations and Assessment of Results

Figure 6.1 shows the time series of undifferenced vertical accelerations for each receiver. The mean value for each plot shows that the acceleration value does not exceed

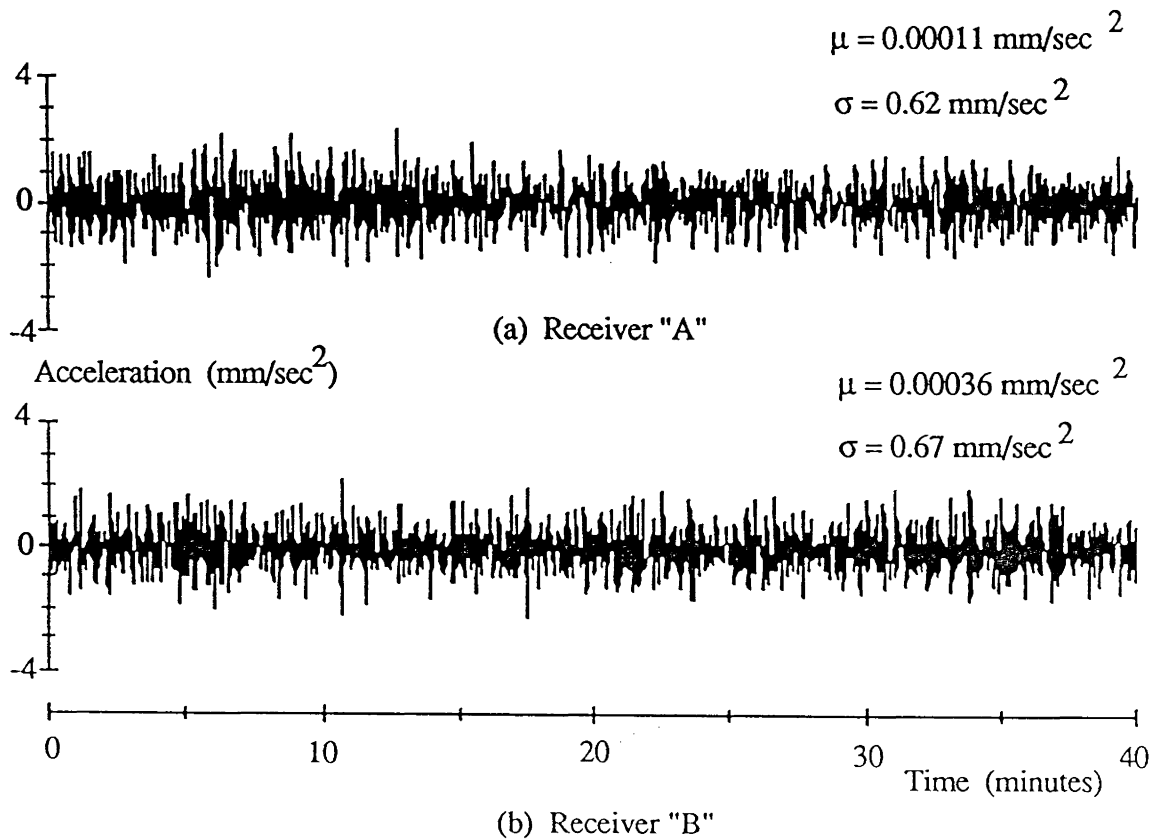


Figure 6.1 Vertical Accelerations Using Undifferenced TI 4100 Data

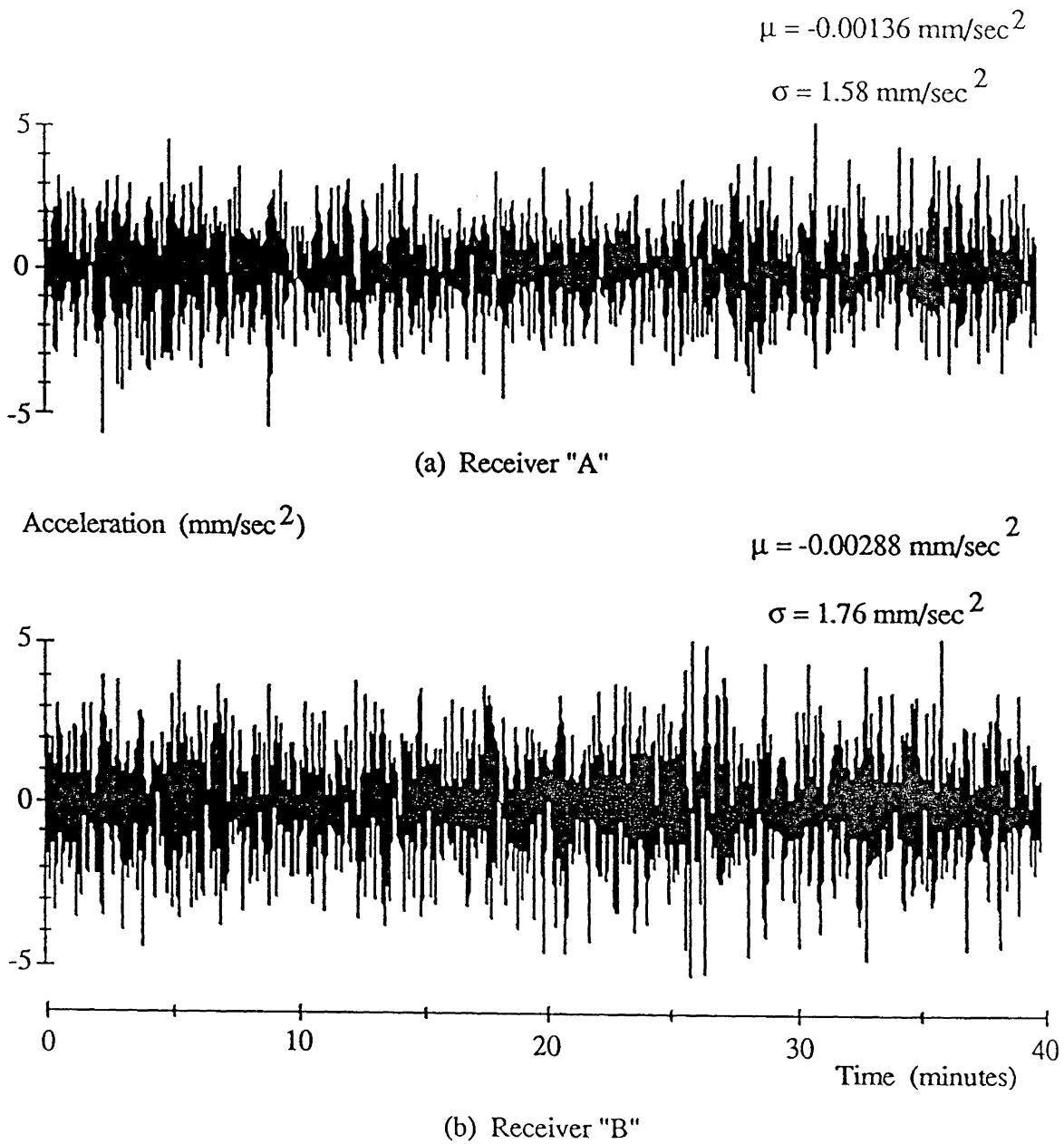


Figure 6.2 Accelerations in Latitude Using Undifferenced TI 4100 Data

$0.00036 \text{ mm/sec}^2$  which equates to less than  $0.1 \text{ mGal}$ . This indicates that no apparent bias is present in the data and testifies to the validity of the theory presented here. The



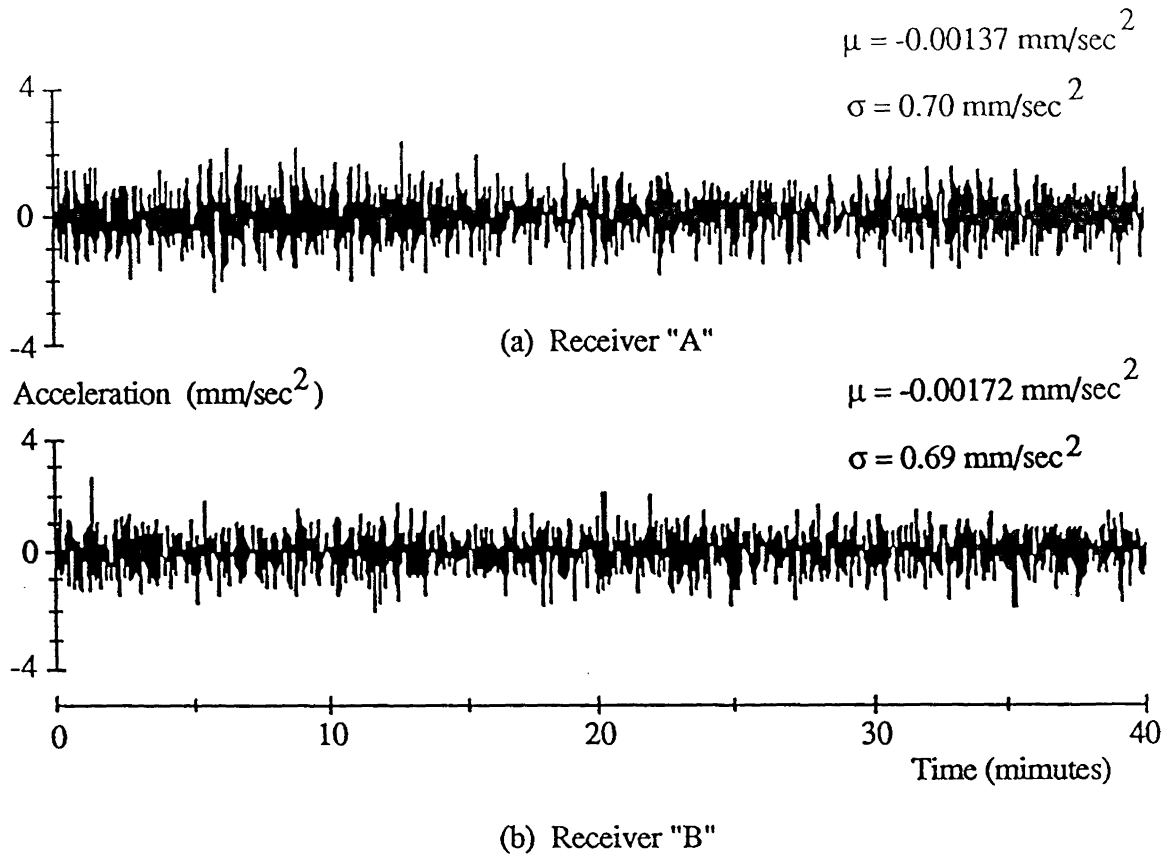


Figure 6.3 Accelerations in Longitude Using Undifferenced TI 4100 Data

standard deviation about zero of each time series shows a magnitude ranging from 0.62 mm/sec<sup>2</sup> to 0.67 mm/sec<sup>2</sup> which corresponds to 62 mGal and 67 mGal respectively.

Figure 6.2 and 6.3 show the time series of horizontal accelerations for each receiver. The mean value in the latitude does not exceed 0.00288 mm/sec<sup>2</sup> while the mean value in the longitude does not exceed 0.00172 mm/sec<sup>2</sup>. These accelerations are also less than 0.1 mGal which also indicates that no apparent bias is in the horizontal components of the acceleration data. The standard deviations of the horizontal accelerations do not exceed 1.76 mm/sec<sup>2</sup> and 0.70 mm/sec<sup>2</sup> for the latitude and longitude components respectively. The polar plots of the satellite sky distribution during the observing session are given in Appendix V. The plots show the majority of the satellites situated in the northern part of

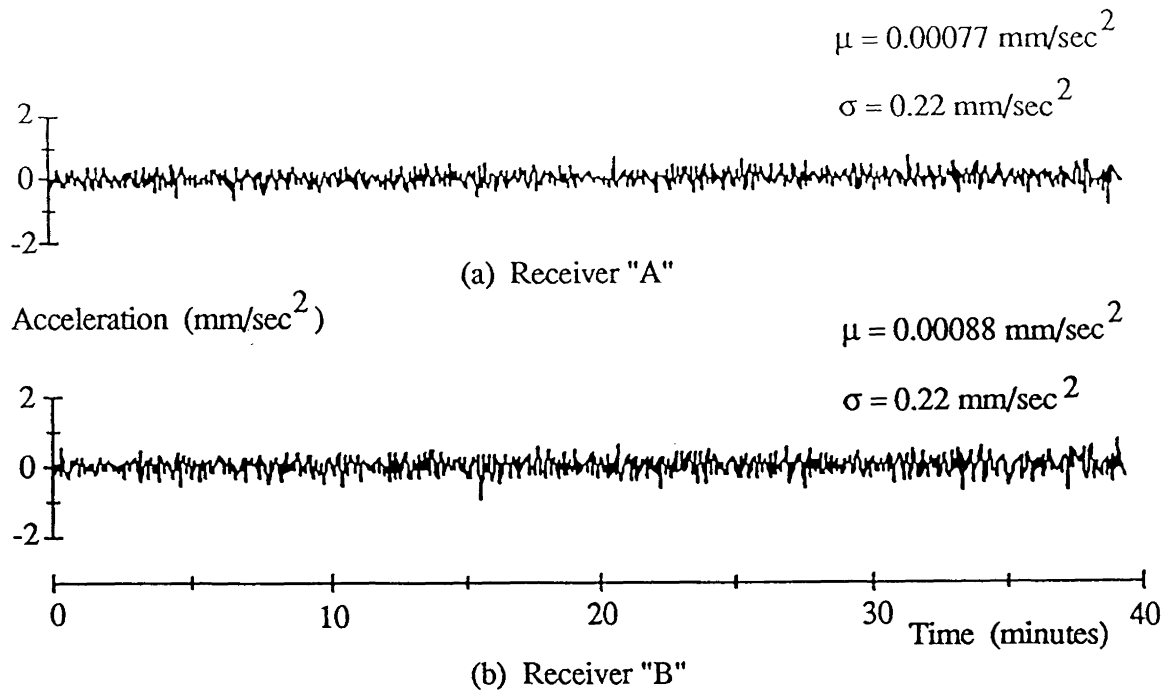


Figure 6.4 Vertical Accelerations Using Undifferenced Trimble 4000 SLD Data

the sky. Thus, the difference in the noise levels of the horizontal components could be a result in the geometric configuration of the satellites.

## 6.2 Trimble 4000 SLD Observations

The second set of data was collected using two Trimble 4000 SLD receivers. This receiver is a C/A-code, L1/L2 multichannel receiver. The receiver can observe five satellites on both L1 and L2 frequencies or ten satellites on just the L1 frequency. More details concerning the Trimble 4000 SLD receiver can be found in Alison et al. [1988].

### 6.2.1 Trimble 4000 SLD Data Description

The Trimble data was collected on May 27, 1989, in Fredericton, Canada (approximately  $45.9^{\circ}\text{N}$ ,  $66.6^{\circ}\text{W}$ ). The receivers were situated within 50 metres of each other. The sampling interval for the observing session was four seconds. The observing

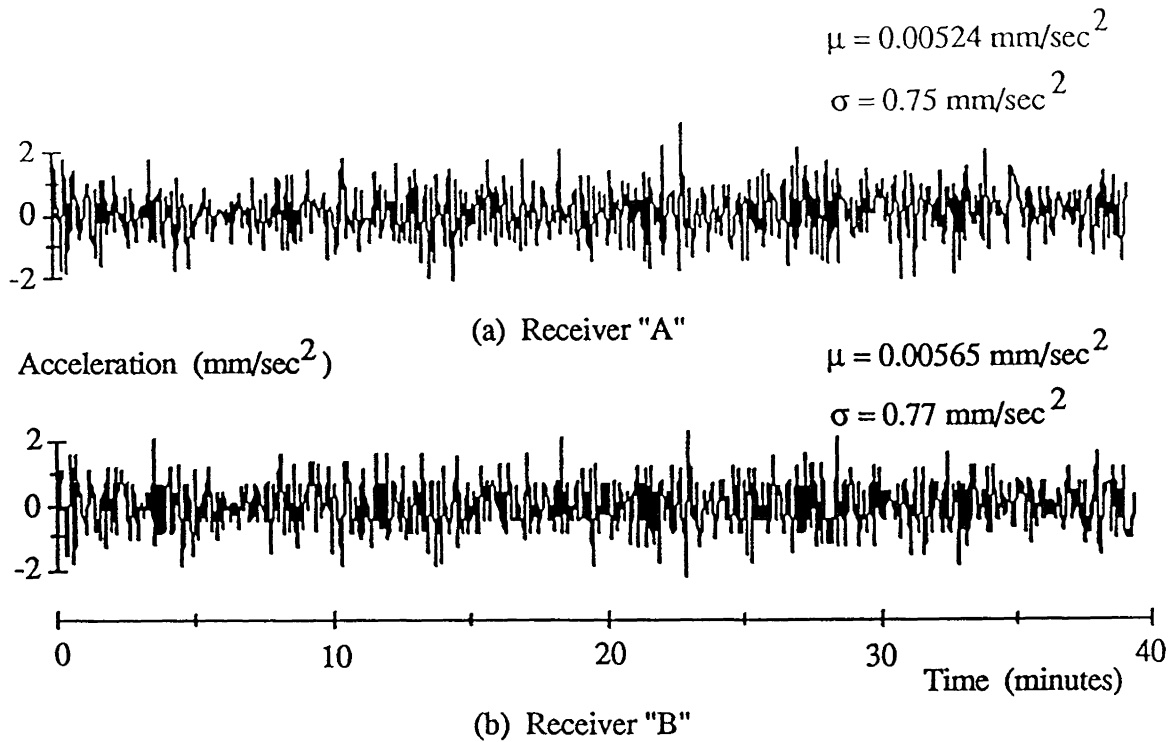


Figure 6.5 Accelerations in Latitude Using Undifferenced Trimble 4000 SLD Data

session was for approximately 40 minutes. The receivers at both ends of the baselines were held fixed and recorded the L1 signal only. Acceleration results were based on recording pseudo-range and carrier phase measurements from six satellites. The PDOP for the observing session centred about 3. A polar plot of the satellite sky distribution for the observing session is given in Appendix V.

### 6.2.2 $\phi\lambda h$ Accelerations and Assessment of Results

Figure 6.4 shows the vertical accelerations as computed using observed pseudo-range and carrier phase data from the Trimble 4000 SLD.

The mean value does not exceed  $0.00088 \text{ mm/sec}^2$ . This compares quite well with the sub-mGal vertical acceleration determined using the TI 4100. This further confirms the validity of the procedure used here in determining acceleration. The standard deviation of

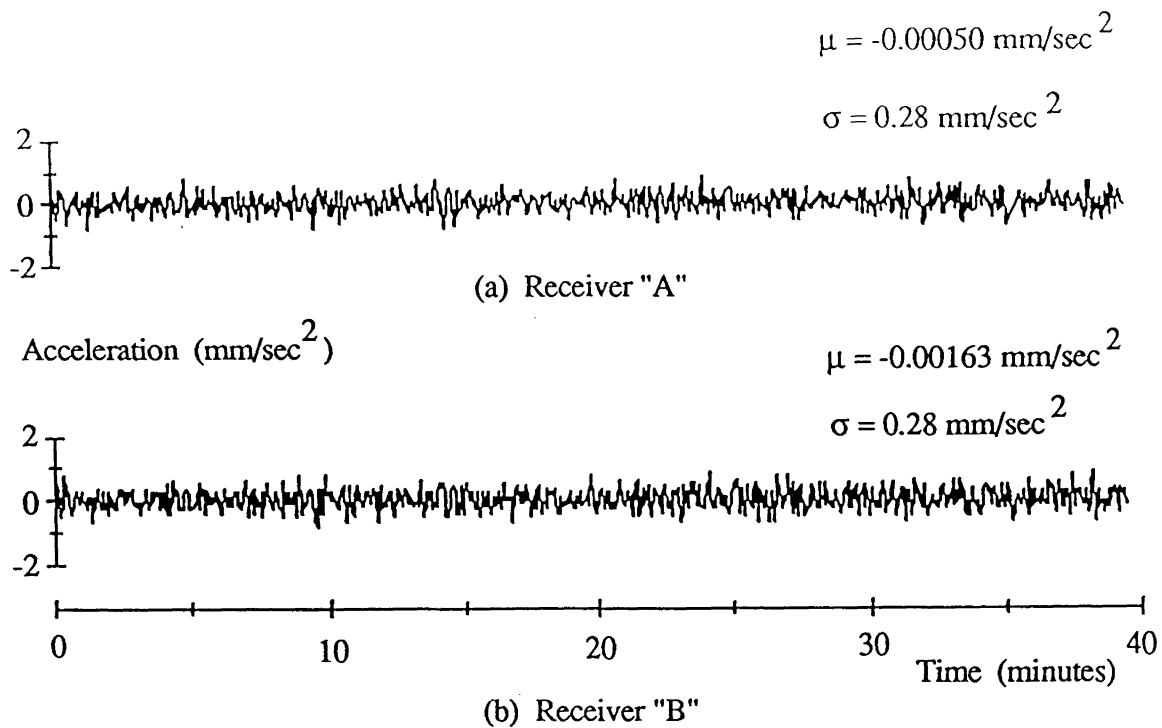


Figure 6.6 Accelerations in Longitude Using Undifferenced Trimble 4000 SLD Data

the vertical accelerations using the Trimble data does not exceed  $0.22 \text{ mm/sec}^2$ . The noise level between the two vertical acceleration time series is noticeably different. This gives a clear indication of the advances in receiver technology (eg. multichannel receivers) and the implementation of extra satellites towards a full constellation.

Figure 6.5 and 6.6 show the horizontal accelerations in the latitude and longitude directions. The mean accelerations do not exceed  $0.00565 \text{ mm/sec}^2$  and  $0.00163 \text{ mm/sec}^2$  for latitude and longitude respectively. The standard deviations of these time series are no larger than  $0.77 \text{ mm/sec}^2$  and  $0.28 \text{ mm/sec}^2$  for the latitude and longitude respectively. These are much smaller than the error associated with the TI 4100. This may reflect the level of accuracy which has been gained over the past decade as a result of the technological advances mentioned earlier.

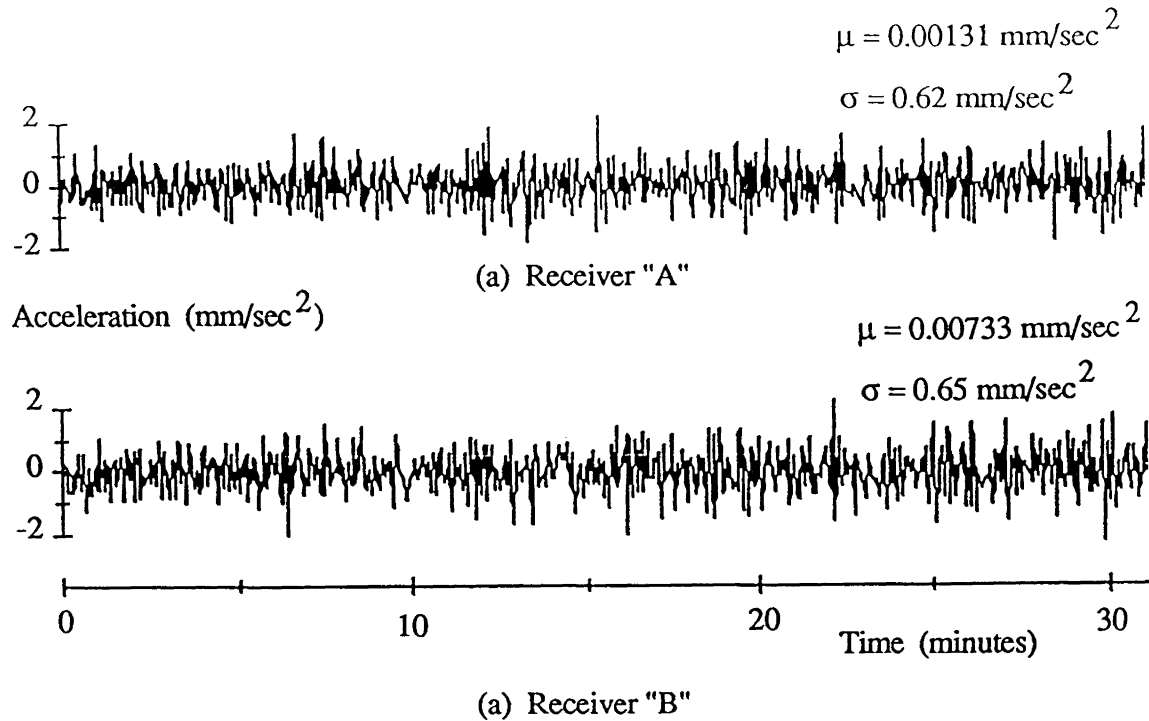


Figure 6.7 Vertical Accelerations Using Undifferenced Ashtech XII Data

### 6.3 Ashtech XII Observations

The final set of GPS data was collected using the Ashtech XII GPS receiver. This receiver is a multichannel C/A-code tracking receiver which presently operates using the L1 frequency. The receiver can simultaneously track up to 12 satellites on 12 separate channels. More details concerning this receiver can be obtained from Ashjaee et al. [1988].

#### 6.3.1 Ashtech XII Data Description

The Ashtech data was collected in Fredericton, Canada in September 1989. The two receivers were placed approximately 10 metres apart and were held fixed for the duration of the observing session. Pseudo-range and carrier phase data from as many as seven satellites were observed at a two second sampling interval. The PDOP value for the observing session centred about 3. A polar plot giving the satellite sky distribution for the

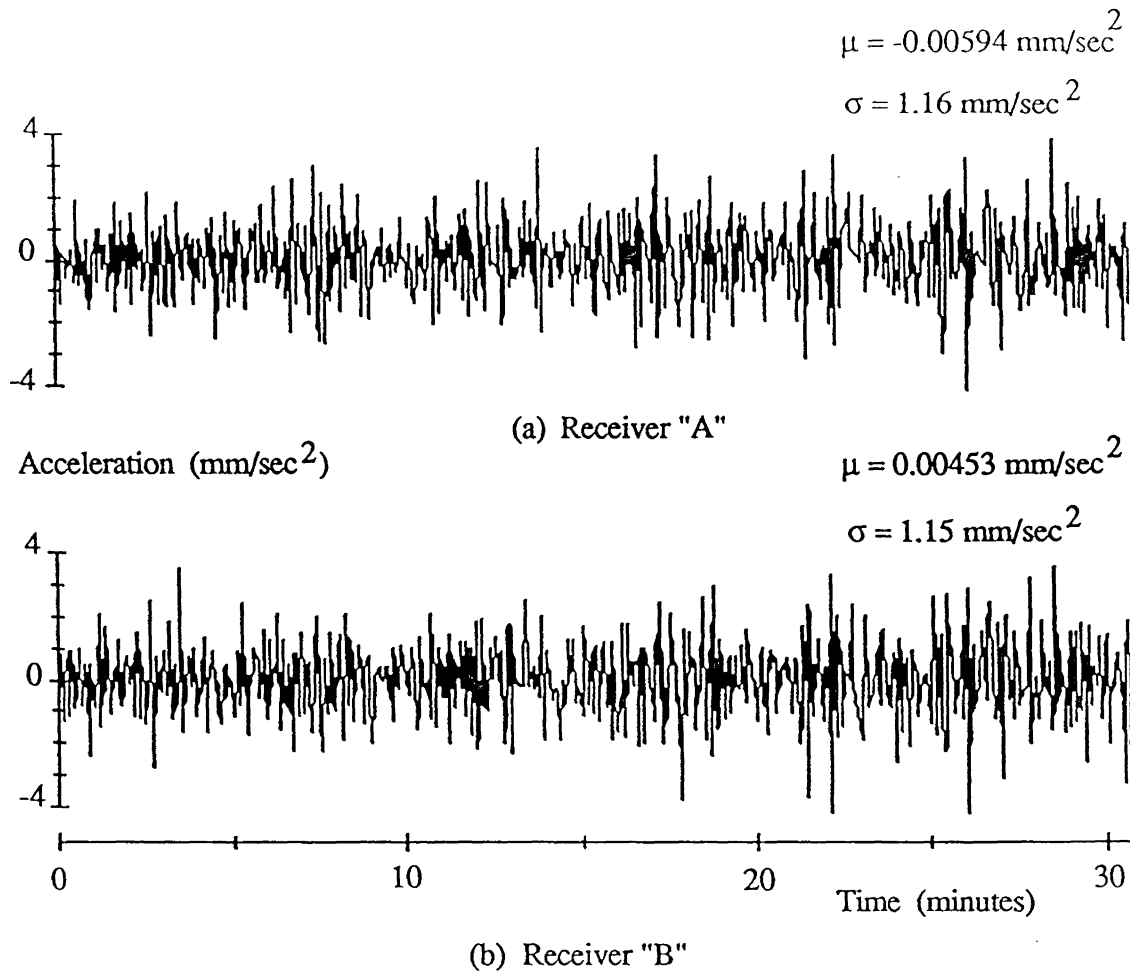


Figure 6.8 Accelerations in Latitude Using Undifferenced Ashtech XII Data

time period during observing is given in Appendix V. It should be noted that Selective Availability was believed to be in operation at this time.

### 6.3.2 $\phi\lambda h$ Accelerations and Assessment of Results

Figure 6.7 shows the vertical accelerations of both receivers as computed here. The mean accelerations and standard deviations do not exceed  $0.00733 \text{ mm/sec}^2$  and  $0.65 \text{ mm/sec}^2$  respectively. This is similar to the result obtained with the Trimble 4000 SLD. Figure 6.8 and 6.9 show the horizontal accelerations as determined using the Ashtech

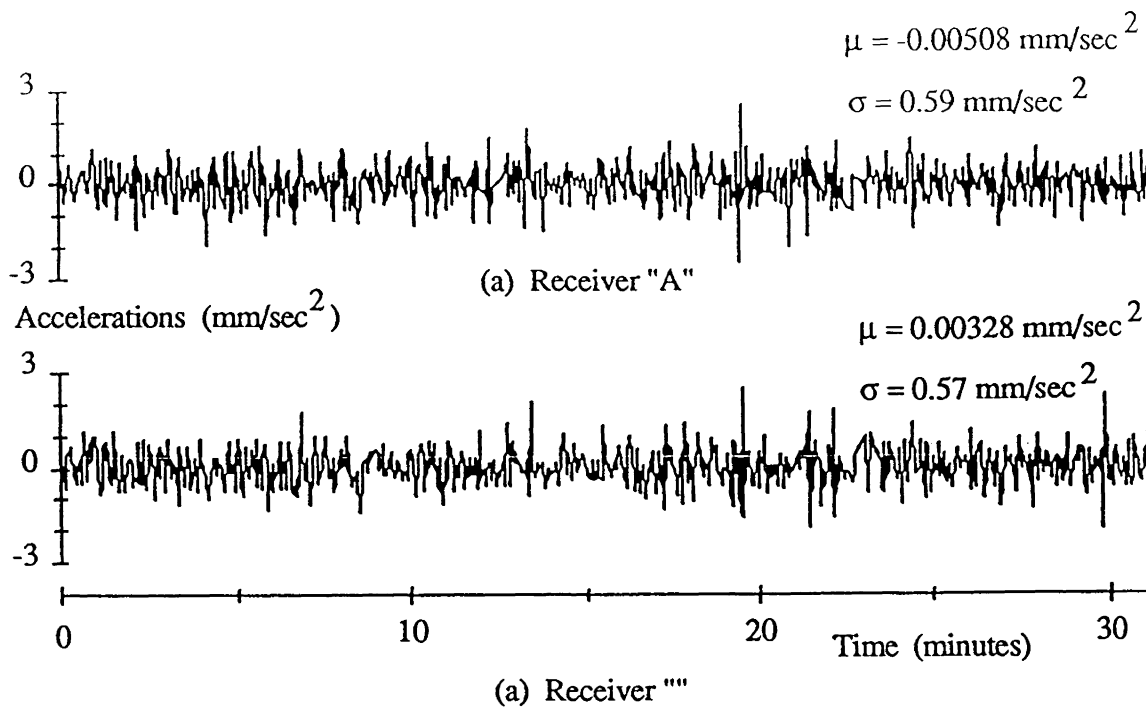


Figure 6.9 Accelerations in Longitude Using Undifferenced Ashtech XII Data

receivers. The mean and standard deviations of the horizontal and vertical accelerations are of the same order of magnitude as the previously displayed results of the TI 4100 and the Trimble 4000 SLD data sets.

## 6.4 Overview of Results

Table 6.1 gives a summary of the acceleration results. A direct comparison among the three types of data sets indicates that the TI 4100 mean accelerations are smaller than the Trimble results which are then smaller than the Ashtech XII mean values. The noise level of the accelerations among the three types of data sets show that the TI 4100 and Ashtech XII results are relatively equivalent. However, the Trimble 4000 SLD results are only half as noisy as the other two receivers.

Table 6.1  
 Summary of Undifferenced GPS Determined Acceleration  
 (mm/sec<sup>2</sup>)

Receiver	$\mu_{\phi}^{\ddot{}}$	$\sigma_{\phi}^{\ddot{}}$	$\mu_{\lambda}^{\ddot{}}$	$\sigma_{\lambda}^{\ddot{}}$	$\mu_{h}^{\ddot{}}$	$\sigma_{h}^{\ddot{}}$
TI 4100						
"A"	-0.00136	1.58	-0.00137	0.70	0.00011	0.62
"B"	-0.00288	1.76	-0.00172	0.69	0.00036	0.67
Trimble 4000 SLD						
"A"	0.00524	0.75	-0.00050	0.28	0.00077	0.22
"B"	0.00565	0.77	-0.00163	0.28	0.00088	0.22
Ashtech XII						
"A"	-0.00594	1.16	-0.00508	0.59	-0.00131	0.62
"B"	0.00453	1.15	0.00328	0.57	0.00733	0.65

A closer look at the results show that the signature and magnitude of the mean acceleration values of the TI 4100 and the Trimble results are similar for data sets from both receivers. In comparison, the Ashtech results show a larger difference between the mean acceleration values of data sets from both receivers. The noise level, however, remains the same. A reason for this unusual higher noise level could not be resolved at this time. It is believed that Selective Availability, which has shown to be in effect at this time [Kremer et al 1989], could be the cause of this irregularity.

The similar mean acceleration values between each data set are expected since it was assumed that the antenna of each like receiver were electronically identical and were placed in an environment where multipath and imaging have been minimized. The noticeable difference in mean acceleration in the Ashtech results can possibly be due to antenna



differences or the influence of imaging and/or multipath. Also, as mentioned above, Selective Availability could have contributed to these results. On the other hand, the non-zero means given in Table 6.1 can be attributable to the unmodelled accelerations which originate from antenna variations which are not common in each GPS antenna.

A spectral decomposition of the data was performed in order to give some insight into the relationship between these data sets. This is part of the analysis which is presented in the next chapter.

## 6.5 Summary

This chapter has shown computed accelerations from fixed points using the observing and processing techniques described in this thesis. The results show that the acceleration of a fixed point can be resolved to less than 1 mGal. The advances in receiver technology and the implementation of extra satellites towards a full constellation were shown to give lower noise levels in accelerations. An exception, however, was with the Ashtech XII data set where unusual higher noise levels were experienced. No firm conclusion on why this resulted could be reached. Several factors were believed possible. These factors included the antenna, the antenna environment, or Selective Availability.

The standard deviations of the accelerations given by all three data sets were in the order of tens of mGal/sec<sup>2</sup>. These values are similar to those given by Kleusberg et al. [1989], and are unacceptable for airborne gravimetric applications. However, as mentioned earlier, the gravity cut-off frequency was 0.0083 Hz. This implies that only noise with frequencies less than 0.0083 Hz will contaminate the gravity measurements. The process of assessing the GPS determined accelerations within the passband involves a spectral decomposition of the time series of acceleration data. This subject is the topic of the next chapter.

## CHAPTER SEVEN

# Spectral Analysis of Acceleration Data and Application of a Low-pass Filter

### 7.0 Introduction

Chapter 7 continues the analysis of the acceleration data in order to obtain an accuracy level at which the GPS determined accelerations have been computed. The chapter begins with a spectral decomposition of the acceleration data to determine the power spectrum of the signals which exist in the acceleration time series. This analysis is performed for each data set obtained in Chapter 6. An assessment of the results is given. A low-pass filter is then applied to the acceleration in order to filter out the high frequency noise within the gravity bandpass. Finally, a discussion is given on the implication of Selective Availability when determining accelerations.

### 7.1 Spectral Decomposition of Acceleration Data

The link between the Fourier spectrum and the covariance matrix is the Fourier transformation [Abidin 1989]. In turn, this relates the Power Spectral Density (PSD) function to the covariance function. This relationship was expressed in Chapter 2 and is again written as follows:

$$\text{rms} = \sqrt{\int_0^{f_0} \text{PSD}(f) df} \quad (7.1)$$

Consequently, in order to assess the acceleration error within the gravity bandpass cut-off frequency of 0.0083 Hz a spectral decomposition of the acceleration time series was performed.

The PSD plots of the vertical and horizontal accelerations obtained from Chapter 6 are illustrated in Appendix V. In general, all plots show an increasing power in the high frequency part of the spectrum. This is attributed to the measurement white noise being amplified as a result of the numerical differentiation of the carrier phase [Kleusberg et al., 1989]. A lower powered signal exists within the bandpass of 0.0083 Hz. Table 7.1 gives the corresponding rms values of the acceleration data using equation (7.1).

Table 7.1  
Rms Values of Undifferenced Accelerations  
within the  
Gravity Bandpass of 0.0083 Hz

Receiver	Acceleration Accuracies (mGal)		
	$\ddot{\phi}$	$\ddot{\lambda}$	$\ddot{h}$
TI 4100			
"A"	7	4	2
"B"	7	4	2
Trimble 4000 SLD			
"A"	10	4	3
"B"	9	4	3
Ashtech XII			
"A"	6	5	3
"B"	5	4	4

The limits of the integral are from 0.001 Hz to the cut-off frequency of 0.0083 Hz. No signal below 0.001 Hz was considered because the power below this frequency contributes relatively little to the acceleration error [Bower et al., 1989]. The results show that the vertical accelerations over the passband have an rms value ranging from 2 to 4 mGal. These accuracy levels are outside of the acceptable accuracy range of the 1 to 2 mGal accuracy requirement of airborne gravimetry.

A closer look at the PSD plots of Appendix V reveals that the low frequency part of the acceleration spectrum have similar power spectral densities. Assuming no common multipath effects exist between the two receivers, then this low frequency signal may be attributable to atmospheric conditions, common receiver and antenna electrical characteristics, and satellite clock errors. In order to reduce these effects, the acceleration values were differenced between receivers. Table 7.2 gives the mean and standard deviation of each data set after differencing between receivers. The sub-mGal mean results show that no biases have been introduced in the differencing process.

Table 7.2

Summary of Differenced GPS Determined Accelerations (mm/sec<sup>2</sup>)

Receiver	$\mu_{\phi}^{\ddot{\cdot}}$	$\sigma_{\phi}^{\ddot{\cdot}}$	$\mu_{\lambda}^{\ddot{\cdot}}$	$\sigma_{\lambda}^{\ddot{\cdot}}$	$\mu_h^{\ddot{\cdot}}$	$\sigma_h^{\ddot{\cdot}}$
TI 4100	0.00313	1.89	0.00060	0.68	0.00016	0.53
Trimble 4000 SLD	-0.00041	0.40	0.00113	0.22	-0.00010	0.16
Ashtech XII	-0.00512	0.81	-0.00835	0.60	-0.00864	0.50

The PSD plots which result from this differencing are shown in Appendix VI. Table 7.3 summarizes the acceleration accuracies obtained by implementing equation (7.1). The differencing results presented in Table 7.3 reflect the direct differencing of the mean values given in Table 6.1.

The PSD plots show that the high frequency noise of the phase measurements still remains. However, the low frequency signal has decreased in power by an order of magnitude. Exceptions exist, however, for the latitude component of the Trimble receiver and all three acceleration components of the Ashtech receiver.

Table 7.3  
Rms Values of Differenced Accelerations  
within the  
Gravity Passband of 0.0083 Hz

Receiver	Acceleration Accuracies (mGal)		
	$\ddot{\phi}$	$\ddot{\lambda}$	$\ddot{h}$
TI 4100	0.4	0.1	0.2
Trimble 4000 SLD	2	0.5	0.4
Ashtech XII	5	3	3

It is believed that the discrepancy in the Trimble latitude acceleration data is a result of multipath effects. One of the two Trimble antennas was situated within 10 metres of a large wall, while the other was located in a wide open space. The effect of multipath on the acceleration time series would cause a different power in the low frequency part of the spectrum. The difference in the power of the two acceleration time series is quite dominant

in the lower part of the acceleration spectrum. A separate data set in a multipath free environment to resolve this discrepancy was not obtained at the time of observing.

The Ashtech data set was collected in a farm field away from any obstructions which may cause multipath or imaging. If the two antenna are not electronically identical, that is, the phase centre and phase variations of each antenna are different, then the acceleration time series could show a different power spectrum in the low frequency band [Tranquilla 1989]. Such differences exist in the power spectrum of the Ashtech acceleration data. Consequently, the difference in the acceleration power spectrum of the data set is believed to result from the electronic differences between the two Ashtech antenna.

With respect to the TI 4100 and Trimble data sets the rms values of the vertical acceleration data within the gravity bandpass range from 0.2 mGal to 0.4 mGal, which are within the 1 to 2 mGal accuracy level for airborne gravimetry. The results also compare favourably with results predicted by Kleusberg et al. [1989]. The rms values, for the same two receivers, of the horizontal acceleration data within the gravity bandpass of 0.0083 Hz range from 0.1 mGal to 0.5 mGal, which is well within the 6 Gal horizontal accuracy requirement level for airborne gravimetry.

## 7.2 Application of a Low-Pass Filter

The corrected gravity value for the gravity passband is given as follows:

$$g_{cor} = g_{obs} - (\ddot{h} - \ddot{h}_{high}) \quad (7.2)$$

where,

- $g_{cor}$  = gravity corrected for receiver vertical accelerations,
- $g_{obs}$  = the observed gravity as a result of low-pass filtering over the passband with cut-off frequency of 0.0083 Hz,

- $\ddot{h}$  = the measured receiver acceleration,  
 $\ddot{h}_{\text{high}}$  = the high frequency part of the measured receiver acceleration  
outside the gravity bandpass.

As shown in Chapter 6, the low and high frequency signals are embedded within the same data set. In order to separate these low and high frequency signals the acceleration data needs to be subjected to a low pass filter.

### 7.2.1 Filter Description and Implementation

The ideal low-pass filter has a transfer function,  $H(\omega)$ , given as follows:

$$H(\omega) = \begin{cases} 1 & \text{if } 0 \leq \omega \leq \omega_c \\ 0 & \text{if } \omega_c < \omega \leq \infty \end{cases}$$

where,

- $H(\omega)$  = the transfer function,  
 $\omega$  = the frequency of the signal,  
 $\omega_c$  = the cut-off frequency.

The above filter can be implemented by fixing the range of the impulse response function and then find the filter whose transfer function best approximates  $H(\omega)$  in the least squares sense. Details concerning the design of this filter can be found in Bloomfield [1976]. This implementation of this filter to the data collected for this thesis is described below.

### 7.2.2 Spectral Decomposition of Filtered Acceleration Data

A symmetric non-recursive least squares low-pass filter was applied to the TI 4100 acceleration data obtained for this thesis. Only the TI 4100 data was used in order to test

the ability of the low-pass filter. In summary, the filter had a 65, and a 33, term least squares approximation to the cut-off frequency of 0.0083 Hz. The transfer function had a transition band of width  $4\pi/2NS+1$  surrounding the cut-off frequency of 0.0083 Hz. The value of  $2NS+1$  represents the number of terms in the least squares approximation. Appendix VII shows the spectral decomposition of the filtered vertical and horizontal acceleration from the TI 4100 data set. The plots show that the low frequency signal still remains while much of the high frequency signal has been removed. Some distortion in the low frequency part of the spectrum has resulted. The distortion is more pronounced as the transition band about the cut-off frequency is narrowed.

Another practical aspect of the filtered data is if the signal maintains its phase value after filtering has been applied. Otnes and Enochson [1978] state that when using a symmetric nonrecursive filter, such as the one used here, there is zero shift in phase of the filtered signal. However, the trade-off when implementing these filter types is a shortening of the data set. The magnitude of this reduction is equivalent to one half the span of the filter. Consequently, the data set in the above analysis, recognizing the filter spanning  $64+1$  terms, will be reduced by 32 epochs at each end. Consequently, in order to compensate for this reduction, 64 extra observations would be required. In terms of airborne gravimetric applications, this means that the collection of data would have to start 32 epochs earlier in order to obtain the same spatial coverage as the unfiltered data.

Using equation (7.1), and adding on the error contribution due to receiver measurement noise, the total rms errors in acceleration are given in Table 7.4. The results are still within the acceleration accuracy requirements for airborne gravimetry.

### 7.3 Summary

This chapter has applied spectral analysis techniques in order to obtain a measure of the accuracy of the acceleration data determined using GPS measurements. The results



have shown that a strong correlation exists between corresponding data sets. This correlation can be attributed to the satellite clock error and atmospheric conditions. Differencing between receivers was shown to reduce the acceleration error by an order of magnitude. The remaining error was within the acceptable limits of the 1 to 2 mGal accuracy requirements of airborne gravimetry. It was shown however, that these accuracies cannot be reached if the electronic characteristics of the receiver antennas are not identical.

Table 7.4  
Rms Values of Differenced and Filtered Accelerations  
using TI 4100 Data Sets

Number of Terms	Rms (mGal)		
	$\ddot{\phi}$	$\ddot{\lambda}$	$\ddot{h}$
33	0.7	0.2	0.3
65	0.2	0.1	0.2

A low-pass filter was implemented on the acceleration data in order to reduce the contribution of the high frequency receiver measurement noise to the total acceleration error within the gravity bandpass. The total acceleration error was still within the 1 to 2 mGal accuracy level.

The final chapter in this thesis investigates the implications of Selective Availability on acceleration determination using GPS observing and processing techniques.

## CHAPTER EIGHT

### Implications of Selective Availability on Acceleration Determination

#### 8.0 Introduction

Chapter 8 presents acceleration data which is thought to be contaminated by selective availability. The chapter investigates the implications of this type of selective availability (S/A) on acceleration determination using the GPS observing and processing techniques presented in this thesis. Differencing techniques of the acceleration data are then applied in order to see if the effect of S/A experienced here can be reduced if not eliminated. Analysis of the data follows along the same approach as that taken in the previous chapter

#### 8.1 Implications of Selective Availability on Acceleration Determination

Section 4.5.6 defined selective availability as the intentional contamination of the GPS signal such as dithering the satellite clock or changing the satellite broadcast ephemeris. Part of the observing session for the Trimble 4000 SLD data involved observing phase and pseudo range data from satellite PRN#14. Satellite 14 is part of the Block II satellites which are presently being launched into orbit. In addition, these satellites have been programmed to transmit signals which have been influenced by S/A [Kremer et al., 1989].

Figure 8.1 shows the computed height position as a result of including satellite 14 in the observation session. The height positions were computed with pseudo-range observations. The plot shows the characteristic high frequency noise from pseudo-range

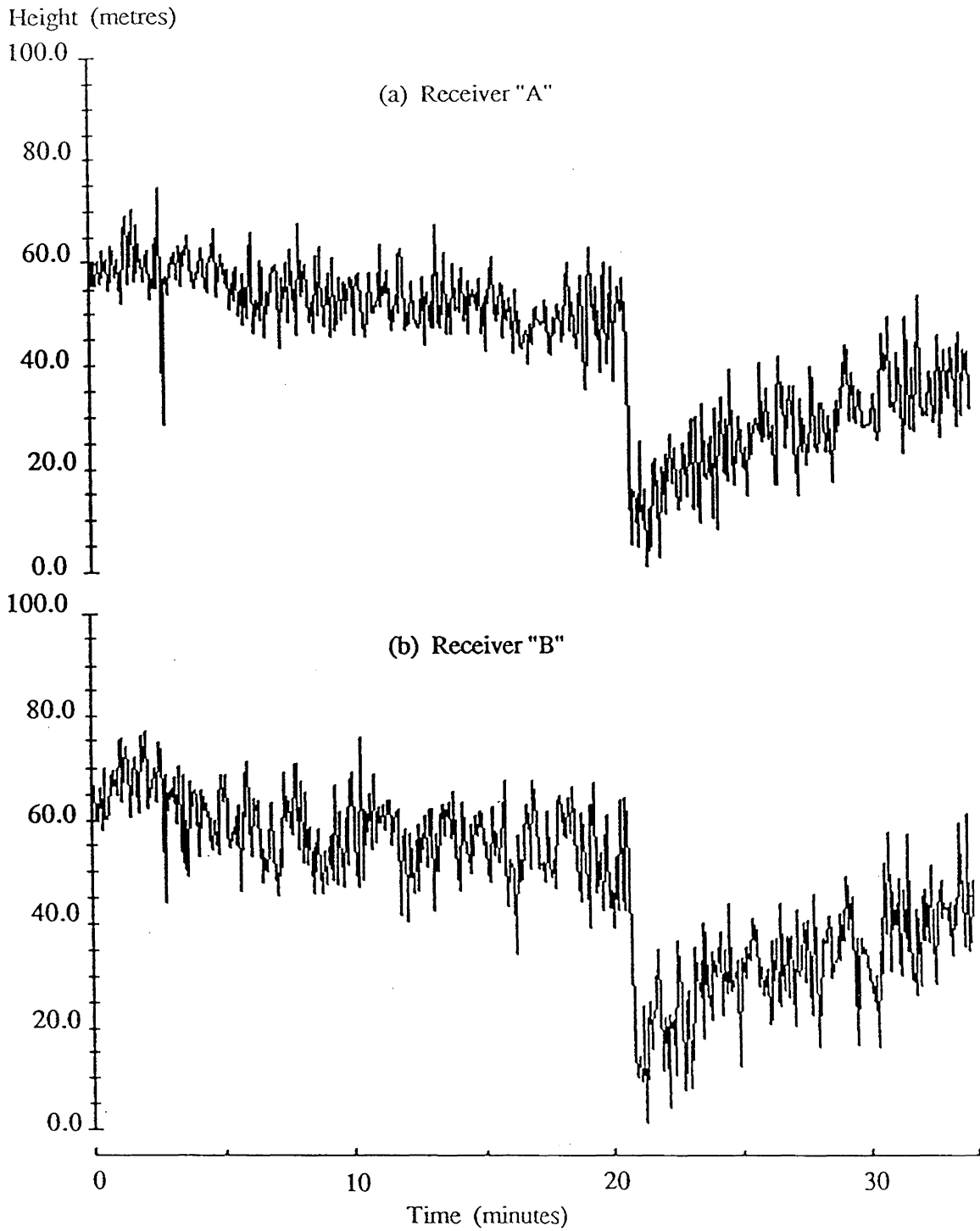


Figure 8.1

Effect of Selective Availability on Vertical Position

positioning. However, a large uncharacteristic jump of approximately 60 metres simultaneously occurs in both receivers near the 20 minute time period.

Analysis of the data set showed that both the pseudo-range and the carrier phase data of satellite 14 experienced a large change in magnitude. The change occurred within the sampling rate of four seconds. Results without using satellite 14 show the same characteristics as in Figure 8.1 only without the large jump. Figure 8.1 does not resemble the characteristic effects of S/A as shown by Kremer et al. [1989]. However, as only one ephemeris record was used throughout the observing session, it is believed that the contamination of the signal was a result of the dithering of the satellite clock, and thus is believed to be some form of selective availability.

## **8.2 Handling Selective Availability when Determining Accelerations**

Figure 8.1 shows that the height position, after the apparent jump, tends to gradually recover towards the value it would normally have had if the signal had not been distorted. This movement, or settling, occurs similarly in both receivers. This appears to be the settling of the satellite clock after dithering. Consequently, assuming the settling is common in both receivers, the effect should be removed by differencing between receivers. The apparent jump in acceleration, which occurs at the time of selective availability, can be treated for airborne gravimetry in much the same manner as cycle slips. That is, disregard the acceleration resulting from S/A in the averaging process over the gravity passband of two minutes.

In order to test this approach the accelerations for the above data set were computed using the contaminated data of satellite 14. Table 8.1 gives the results of this test. The table shows that the mean values of the acceleration data sets are still sub-mGal.

Table 8.1

Summary of GPS Determined Accelerations Influenced by Selective Availability  
(mm/sec<sup>2</sup>)

Receiver	$\ddot{\phi}$	$\sigma_{\ddot{\phi}}$	$\ddot{\lambda}$	$\sigma_{\ddot{\lambda}}$	$\ddot{h}$	$\sigma_{\ddot{h}}$
Trimble 4000 SLD						
"A"	0.00575	0.61	-0.00241	0.27	-0.00002	0.21
"B"	0.00266	0.61	-0.00034	0.28	-0.00004	0.23
Differenced	0.00308	0.33	-0.00207	0.21	0.00002	0.15

Table 8.2

Rms Values of GPS Determined Accelerations  
Influenced by Selective Availability

Receiver	$\ddot{\phi}$ (mGal)	$\ddot{\lambda}$ (mGal)	$\ddot{h}$ (mGal)
Trimble 4000 SLD			
"A"	6	4	3
"B"	8	4	3
Differenced	3	0.6	0.7

Appendix VIII shows the power spectral density plots of S/A contaminated accelerations determined from both receivers. The low frequency part of the spectrum for all three acceleration components show similar results. An exception once again exists in the latitude component where it is believed multipath may be influencing the results.

Appendix VIII also shows the PSD results after differencing between the two receivers.

Table 8.2 gives the rms values of accelerations within the gravity passband of 0.0083 Hz. This table reveals that by applying the differencing technique the rms values of the GPS determined acceleration within the passband of 0.0083 Hz are well within the accuracy specifications required for airborne gravimetry. Another aspect of Table 8.1 and Table 8.2 is that the height accelerations show slightly better results when compared with those of Table 6.1 and Table 7.2. The reason for these results was not completely ascertained. However, a look at the satellite polar plot shows that there is a better geometric configuration with the addition of satellite 14 into the observation scheme.

### **8.3 Summary**

This chapter has shown the effect of what is thought to be a form of selective availability on GPS pseudo-range positioning. A jump of 60 metres in height was experienced with the Trimble 4000 SLD data set presented in previous chapters. The suggested handling of selective availability in determining aircraft accelerations for airborne gravimetry was to ignore the apparent large acceleration resulting at the time of S/A, and to difference between receivers to eliminate the systematic settling of the satellite clock after S/A has been implemented. Analysis of the acceleration data using power spectral density techniques showed that the acceleration accuracy requirements for airborne gravimetry can be met when handling S/A in the manner described above.

In retrospect, if we consider the poorer than expected performance of the Ashtech receiver, it could be viable to suggest that selective availability, in some other form (eg. Kremer et al [1989]), contaminated the Ashtech data.

## CHAPTER NINE

### Conclusions and Recommendations

#### 9.0 Overview of Thesis

This thesis has investigated the determination of acceleration for airborne gravimetry using the NAVSTAR Global Positioning System. It was shown from a review of the literature that vehicle position and velocity accuracy requirements for airborne gravimetry can already be met using the GPS observing and processing techniques. However, the separation of the vehicle acceleration from the gravity measurements was shown as one of the major problems presently facing airborne gravimetric surveys. The capabilities of conventional techniques such as radar, pressure, and laser altimeters can not meet the vertical acceleration requirements of 1 to 2 mGals. This accuracy measure was based on filtered gravity data over a passband of 0.0083 Hz (2 minutes).

This thesis has developed and implemented a technique whereby the vertical and horizontal accelerations of a GPS receiver can be determined by using the pseudo-range and carrier phase observations. This development follows from the work performed by Kleusberg et al. [1989] and Kleusberg [1989]. The theory behind this technique was to utilize the second time derivative of the carrier phase to determine the acceleration of a moving receiver. The three cartesian component accelerations were then transformed to give accelerations in the geodetic coordinate system. A three epoch observing and weighting scheme was developed in order to formulate the mathematical model describing the receiver acceleration.

Static data sets of GPS pseudo-range and carrier phase observations were collected from three different types of GPS receivers. These were the TI 4100, the Trimble 4000 SLD, and the Ashtech XII receivers. Each data set consisted of observations from two

receivers which were situated within 50 metres of each other. Spectral analysis techniques were applied to the computed accelerations in order to determine the acceleration accuracy within the gravity passband of 0.0083 Hz.

A non-recursive low-pass filter was applied to the data in order to separate the low frequency signal of the acceleration from the high frequency receiver noise signal. The results of this filtering were presented.

Finally, the height position from a data set which was thought to be contaminated with selective availability was presented. In addition, the accelerations of this data set as processed using the technique developed above were presented.

## **9.1 Conclusions**

Several conclusions have been formed as a result of the research that was conducted in writing this thesis.

- (1) With respect to a static data set, the application of the GPS pseudo-range and carrier phase observations can be used to determine antenna accelerations which meet the airborne gravimetric acceleration requirements of 1 to 2 mGals (Chapter 5,6 and 7).
- (2) Multipath effects on the carrier phase signal may limit the achievable acceleration accuracy (Section 7.1).
- (3) The electrical quality of the GPS receiving antenna may limit the accuracy at which accelerations can be determined (Section 7.1).
- (4) The acceleration accuracy obtained by processing data from a single GPS receiver does not meet the 1 to 2 mGal requirements of airborne gravimetry. The signal in the low frequency part of the acceleration spectrum showed a high power. The power spectral density plots of adjacent acceleration data sets revealed that this high powered signal is common in both time series. Consequently, differencing the accelerations between



receivers reduced the power. The accuracy of the differenced accelerations were well within the required specifications (Chapter 6 and 7).

(5) The application of a non-recursive low-pass filter to the acceleration data can separate the high frequency receiver noise from the low frequency acceleration values. This filtering does not change the phase of the acceleration signal within the gravity passband. However, by narrowing the transition band of the filter some distortion occurs to the characteristics of the low frequency acceleration signal (Chapter 7).

(6) Selective Availability can cause apparent jumps in acceleration values within the sampling rate of the signal. In the case of satellite clock dithering, the behaviour of the receiver's apparent position, and subsequent acceleration, is common in adjacent receivers observing over the same time period. Consequently, this settling effect can be eliminated by differencing accelerations between receivers (Chapter 8).

(7) The apparent acceleration jumps caused by cycle slips and selective availability can be handled by omitting them in the averaging process over the gravity passband of 120 seconds. With a high sampling rate this would have little effect on the overall mean value. However, it should be noted that the type of selective availability experienced in this thesis does not resemble that found by other authors [Kremer et al., 1989]. Consequently, the method of handling selective availability, as discussed in this thesis, refers only to the data collected here (Chapter 8).

## **9.2 Recommendations**

This thesis has investigated the use of GPS observing and processing techniques towards determining aircraft accelerations for airborne gravimetry. The data collected for this research was static data from three different GPS receivers. The following recommendations are presented as a basis for future research involving this topic:

- (1) The collection and processing of a test data set is essential in determining the success of the application of this technique. This does not necessarily involve the collection of airborne data. Simulation data sets can be obtained as well as data sets from moving platforms which are mechanically controlled allowing for precise measurements of the antenna motion.
- (2) The electrical characteristics of the antenna of different receiver types should be measured and classified as to their capabilities for measuring accurate accelerations.
- (3) An investigation should be conducted into the type of low-pass filter which should be used to separate the high frequency measurement noise from the low frequency acceleration signal of the receiver. This filter should not distort the characteristics of the low frequency acceleration signal as was experienced in this research.
- (4) More research is needed in order to determine the effect of selective availability on the determination of accelerations using the second time derivative of the carrier phase. A modification of the technique used in this thesis should be investigated. This modification would be to difference between receivers first and then perform the time differencing to get relative velocities and accelerations. This may prove to be less sensitive to Selective Availability.

## REFERENCES

- Abidin, H.Z. (1989). "The link between the fourier spectrum and covariance matrix." Unpublished paper prepared for PhD requirements, Department of Surveying Engineering, University of New Brunswick, Fredericton, N.B. Canada.
- Allison, T., R. Eschenbach, R. Hyatt and B. Westfall (1988). "C/A code dual frequency surveying receiver, architecture and performance." *Proceedings of the IEEE Position Location and Navigation Symposium.*, Orlando, Florida, U.S.A., pp. 434-441.
- Ashjaee, J. (1988). "Differential GPS with Ashtech XII." *Proceedings of the IEEE Position Location and Navigation Symposium*, Orlando, Florida, U.S.A., pp., 318 - 322.
- Ashjaee, J.M., D.R. Bourn, R.J. Helkey, R.G. Lorenz, J.B. Minazio, B.W. Remondi, and R.R. Sutherland (1988). "Ashtech XII GPS receiver, the all-in-one all-in-view." *Proceedings of the Satellite Division's International Technical Meeting*, The Institute of Navigation, Colorado Springs, Colorado, U.S.A. Sept., pp. 403-410.
- Bell, R., J. LaBrecque, C. Raymond, D. Chayes and J. Brozena (1986). "GPS vertical velocities: A source of vertical accelerations for airborne gravity surveys." Paper presented at the AGU Fall Meeting San Francisco, Dec. 8-12 (Abstract: EOS 67, p. 911).
- Bell, R. E., J. M. Brozena, W. F. Haxby and J. L. LaBrecque (1989). "Gravity field of the western Weddell Sea: Comparison of airborne gravimetry and Geosat derived gravity." Paper presented at the Chapman Conference on Progress of the Determination of the Earth's Gravity Field, Florida.
- Beutler, G., I. Bauersima, W. Gurtner, M. Rothacher, T. Schildknecht and A. Geiger (1987). "Atmospheric refraction and other important biases in GPS carrier phase observations." Paper presented at General Assembly of I.A.G., Vancouver, August, 1987.
- Bloomfield, P. (1976). *Fourier Analysis of Time Series: An Introduction*. John Wiley and Sons, New York, U.S.A.
- Bomford, G. (1971). *Geodesy*. 3rd rev. ed., Oxford University Press, Walton Street, Oxford, Great Britain.
- Bower, D.R. and J.F. Halpenny (1987). " On the technical feasibility of airborne gravity measurements." Internal Report, Geophysics Division, Geological Survey of Canada, EMR, Ottawa, Ont., Canada.
- Bower, D.R., J. Kouba and R.J. Beach (1989). " A note on the accuracy of airborne gravity measurements." Internal Report, Geophysics Division, Geological Survey of Canada, EMR, Ottawa, Ont., Canada.
- Brozena, J. (1988). "A preliminary analysis of the NRL airborne gravimetry system." *Geophysics*, Vol. 49, No. 7, pp 1060-1069

- Brozena, J.M., G.L. Mader and M.F. Peters (1988). "Interferometric GPS: A 3-D positioning source for Airborne gravimetry." *Journal of Geophysical Research*, Vol. 94, No. B9, pp. 12,153-12,162.
- Brozena, J.M., J.G. Eskinzes and J.D. Clamons (1986). "Hardware design for a fixed-wing airborne gravity measurement system." Naval Research Laboratory Report 9000, Washington, D.C.
- Brozena, J. and M. Peters (1988). "An airborne gravity study of eastern North Carolina." *Geophysics*, Vol. 53, No. 2, pp 245-253
- Cannon, M.E., Schwarz, K.P. and R.V.C. Wong (1986). "Kinematic positioning with GPS: An analysis of road tests." *Proceeding of the Fourth International Geodetic Symposium on Satellite Positioning*, April, University of Austin, Austin, Texas, U.S.A., Vol II, pp. 1251-1267.
- Evans, A. G. (1983). "The effect of a global positioning system (GPS) receiver measurement error on gravity anomaly survey accuracy." Naval Service Weapons Center Technical Report No. 83-401, Dahgren, Virginia, U.S.A.
- Evans, A. G. (1986). "Comparison of GPS pseudo-range and biased doppler range measurements to demonstrate signal multipath effects." *Proceeding of the Fourth International Geodetic Symposium on Satellite Positioning*, April, University of Austin, Austin, Texas, U.S.A., Vol I, pp. 573-588.
- Evans, E., D. Coco and J. Clynych (1985). "Collocation tests of an advanced geodetic Global Positioning receiver." *Proceeding of the First International Symposium on Precise Positioning with the Global Positioning System*, April, Rockville, Maryland, U.S.A., Vol. I, pp. 245-254.
- Georgiadou, Y. and A. Kleusberg (1988). "On carrier signal multipath effects in relative GPS positioning." *Manuscripta Geodaetica*, Vol. 13, pp.172 - 179.
- Gilman, D., J. Lovell, A. Stavros, J. Tang, L. Weber (1988). "Design considerations for a self-contained GPS receiver." *Proceedings of the Satellite Division's International Technical Meeting*, The Institute of Navigation, Colorado Springs, Colorado, U.S.A. Sept., pp. 397-402.
- Goad, C.C. (1985). "Precise positioning with the Global Positioning System." *Proceedings of the Third International Symposium on Inertial Technology for Surveying and Geodesy*, Banff, Alberta, Sept., Vol. 2, pp. 745 - 756.
- Goodacre, A.K. (1987). "Some order-of-magnitude estimates of vertical positioning requirements for airborne gravity." Internal Report, Geophysics Division, Geological Survey of Canada, EMR, Ottawa, Ont., Canada.
- Green, G.B., P.D. Massatt and N.W. Rhodus (1988). "The GPS 21 primary satellite constellation." *Proceedings of the Satellite Division's International Technical Meeting*, The Institute of Navigation, Colorado Springs, Colorado, U.S.A. Sept., pp. 27-40.

- Gumert, W.R., G.F. Wertz and R.M. Iverson (1985). "An application study for using differential GPS in airborne gravity surveying." *Proceedings of the First International Symposium on Precise Positioning with the Global Positioning System*, Rockville, Maryland, U.S.A., April, Vol. II, pp. 829 - 832.
- Heroux, P. (1988). "GPS and the ionosphere in Auroral Regions." Unpublished paper presented as a Graduate Seminar, Department of Surveying Engineering, University of New Brunswick, Fredericton, N.B., Canada. October, 25 pp.
- Hopfield, H. S. (1971). "Tropospheric effect on electromagnetically measured range: Prediction from surface weather data." *Radio Science*, Vol. 6, No. 3, pp 357-367.
- King, R.W., E.G. Masters, C. Rizos, A. Stolz and J. Collins (1985). "Surveying with GPS." School of Surveying Monograph 9, University of New South Wales, Kensington, N.S.W. Australia
- Kleusberg, A. (1986). "Ionospheric propagation effects in geodetic relative GPS positioning." *Manuscripta Geodaetica*, Vol. 11, pp.256 - 261.
- Kleusberg, A. (1987). Personnel Communications. SE 5042: Course Material. Department of Surveying Engineering, University of New Brunswick, Fredericton, N.B., Canada.
- Kleusberg, A. (1988). "Integration of INS and GPS measurements." *High Precision Navigation: Proceedings of an International Workshop on the Integration of Navigational and Geodetic Methods*. Organized by the Sonderforschungsberiech 228 of the Deutsche Forschungsgemeinschaft, Springer-Verlag, May, pp. 137-146.
- Kleusberg, A. (1989a). Personal communication. Professor, Department of Surveying Engineering, University of New Brunswick, Fredericton, N.B., Canada.
- Kleusberg, A. (1989b). "Separation of inertia and gravitation in airborne gravimetry with GPS." Paper presented at the Ron Mather Symposium on four-dimensional geodesy, University of New South Wales, Kensington, NSW, Australia, March.
- Kleusberg, A., A. Goodacre and R. G. Beach (1989). "On the use of GPS for airborne gravimetry." *Fifth International Geodetic Symposium on Satellite Positioning*, New Mexico State University, Las Cruces, New Mexico, March, pp. 977-986.
- Kleusberg, A., S. H. Quek, D. E. Wells and J. Hagglund (1985). "Comparison of INS and GPS ship velocity determination." *Proceedings of the Third International Symposium on Inertial Technology for Surveying and Geodesy*, Banff, Alberta, Sept., Vol. 2, pp. 791 - 805.
- Krakiwsky, E.J. and D.B. Thomson (1974). "Geodetic position computations." Department of Surveying Engineering Lecture Notes No. 39, University of New Brunswick, Fredericton, N.B. Canada.
- Krakiwsky, E.J., D.B. Thomson and R.R. Steeves (1977). "A manual for geodetic coordinate transformations in the maritimes." Department of Surveying Engineering Technical Report No.48, University of New Brunswick, Fredericton N.B., Canada.

- Krakiwsky, E.J., and D.E. Wells (1971). "Coordinate systems in geodesy." Department of Surveying Engineering Lecture Notes No. 16, University of New Brunswick, Fredericton, N.B. Canada.
- Kremer, G. T., R. M. Kalafus, P. Loomis and J. C. Reynolds (1989). "The effect of selective availability on differential GPS corrections." Paper presented at the Satellite Division's International Technical Meeting, The Institute of Navigation, Colorado Springs, Colorado, U.S.A. September.
- Lachapelle, G., M. Casey, R.M. Eaton, A. Kleusberg, J. Tranquilla and D. Wells (1987). "GPS marine kinematic positioning accuracy and reliability." *The Canadian Surveyor*, Vol. 41, No. 2, pp.143 - 172.
- Langley, R. (1986). Personnel Communications, Technical Memorandum, November 17, 1986. Professor, Department of Surveying Engineering, University of New Brunswick, Fredericton, N.B., Canada.
- Mader, G.L. (1986). "Dynamic positioning using GPS carrier phase measurements." *Manuscripta Geodaetica*, Vol. 11, pp.272 - 277.
- Mader, G. L., and J. R. Lucas (1989). "Verification of airborne positioning using Global Positioning System carrier phase measurements." *Journal of Geophysical Research*, Vol. 94, No. B8, pp.10,175-10,181.
- Maher, R. (1986). "A comparison of multichannel, sequential and multiplex GPS receivers for air navigation." *Navigation, Journal of the Institute of Navigation*, Global Positioning System, Papers published in Navigation, Vol. III, pp. 3-18.
- McDonald, K.D. (1988). "GPS receiver trends in technology, equipment and performance." *Proceedings of the Satellite Division's International Technical Meeting*, The Institute of Navigation, Colorado Springs, Colorado, U.S.A. Sept., pp. 357-360.
- Milliken, R. J. and C. J. Zoller (1980). "Principle of operation of NAVSTAR and system characteristics." *Navigation, Journal of the Institute of Navigation*, Global Positioning System, Papers published in Navigation, Vol. I, pp. 3-14.
- Otnes, R. K., and L. Enochson (1978). *Applied Time Series Analysis*. John Wiley and Sons, New York, U.S.A.
- Press, W.H., B.P. Flannery, S.A. Teukolsky and W.T. Vetterling (1986). *Numerical Recipes: The Art of Scientific Computing*. Cambridge University Press, Cambridge.
- Quek, See Hean (1988). "Decoding of Texas Instruments TI 4100 NAVSTAR and GESAR Data." DIPOP 2.0 User's Guide, Texas Instruments TI 4100, Department of Surveying Engineering, University of New Brunswick, Fredericton, New Brunswick.
- Remondi, B. W., and B. Hofmann-Wellenhof (1989). "GPS broadcast orbits versus precise orbits: A comparison study." Paper presented at the IAG General Meeting, August, Edinburgh, Scotland.

- Remondi, B.W., and J.M. Ashjaee (1988). "Precision survey with the Ashtech XII GPS receiver." *Proceedings of the Satellite Division's International Technical Meeting*, The Institute of Navigation, Colorado Springs, Colorado, U.S.A. September, pp. 159-166.
- Robinson, G.L. (1989). "Review of the Various Sources of GPS Orbital Data (Including a Discussion of the Canadian Active Control System)." Unpublished paper presented as a Graduate Seminar, Department of Surveying Engineering, University of New Brunswick, Fredericton, April, 29 pp.
- Schwarz, K.P. (1977). "Airborne inertial systems for gravity determination in ocean areas." Paper presented at the First International Symposium on Inertial Technology for Surveying and Geodesy, Ottawa, October.
- Schwarz, K.P., M.E. Cannon and R.V.C. Wong (1987). "The use of GPS in exploration geophysics - A comparison of kinematic models." Paper presented at IAG Section II Scientific Meeting, XIX General Assembly of IUGG, Vancouver, B.C., Canada. August, 20 pp.
- Smit, J. H. M. (1988). "Sea Gravimetry and Eotvos Correction." Faculty of Geodesy Report No 88.3, Delft University of Technology, Delft, The Netherlands.
- Spilker, J. (1980). "GPS signal structure and performance characteristics." *Navigation, Journal of the Institute of Navigation*, Global Positioning System, Papers published in Navigation, Vol. I, pp. 29-54.
- Srinivasan, J.M., T.K. Meehan and L.E. Young (1989). "Code and codeless ionospheric measurements with NASA's Rogue GPS Receiver." Paper presented at the Satellite Division's International Technical Meeting, The Institute of Navigation, Colorado Springs, Colorado, U.S.A. September.
- Tapley, B. D. (1985). *Geodesy: A Look to the Future*. National Academy Press, Washington, D.C., U.S.A. pp. 26 - 144.
- Telford, W. M., L. P. Geldart, R. E. Sheriff and D. A. Keys (1976). *Applied Geophysics*. Cambridge University Press, London, Great Britain.
- Texas Instruments, (1984). "TI4100 NAVSTAR Navigator, Owner's Manual." GPS Navigation Systems, Lewisville, Texas, U.S.A.
- Tranquilla, J. M. (1986). "Multipath and imaging problems in GPS receiver antennas." *Proceeding of the Fourth International Geodetic Symposium on Satellite Positioning*, April, University of Austin, Austin, Texas, U.S.A., Vol I, pp. 557-572.
- Tranquilla, J. M. (1989). Personal communication. Professor, Department of Electrical Engineering, University of New Brunswick, Fredericton, N.B., Canada.
- Van Dierendonck, A. J., S.S. Russel, E.R. Kopitzke and M. Birnbaum (1980). "The GPS navigation message." *Navigation, Journal of the Institute of Navigation*, Global Positioning System, Papers published in Navigation, Vol. I, pp. 55-73.

- Vanicek, P. (1974). "Introduction to adjustment calculus." Department of Surveying Engineering Lecture Notes No. 35, University of New Brunswick, Fredericton, N.B. Canada.
- Vanicek, P., A. Kleusberg, R. G. Chang, H. Fashir, N. Christou, M. Hofman, T. King and T. Arsenault (1986). "The Canadian Geoid." Contract Report No. 86-001, Geodetic Surveys of Canada, Department of Energy, Mines, and Resources, Ottawa, February, pp. 117.
- Vanicek, P. and E.J. Krakiwsky (1986). *Geodesy: The Concepts*. 2nd rev. ed., North-Holland, Amsterdam, The Netherlands.
- Ward, P. (1984). "An advanced single-channel NAVSTAR GPS multiplex receiver with up to eight pseudochannels." *Navigation, Journal of the Institute of Navigation*, Global Positioning System, Papers published in Navigation, Vol. II, pp. 78-94.
- Wells, D.E. (1985). "Recommended GPS Terminology." *Proceedings of the First International Symposium on Precise Positioning with the Global Positioning System*, Rockville, Md., U.S.A., April, Vol.II, pp. 903 - 932.
- Wells, D. (1988). "Notes on Airborne Gravity Workshop" held in Ottawa, Ontario, Canada. March 10, 6 pages.
- Wells, D. (1989). Personal communication. Professor, Department of Surveying Engineering, University of New Brunswick, Fredericton, N.B., Canada.
- Wells, D.E., N. Beck, D. Delikaraoglou, A. Kleusberg, E.J. Krakiwsky, G. Lachapelle, R.B. Langley, M. Nakiboglu, K.P. Schwarz, J.M. Tranquilla, and P. Vanicek (1986). *Guide to GPS Positioning*. Canadian GPS Associates, Fredericton, N.B., Canada.
- Wells, D.E., and A. Kleusberg (1989). "Kinematic differential Global Positioning System." Contract report for the U.S. Army Engineer Topographic Laboratories, Fort Belvoir, Virginia, March, 36 pp.
- Wells, D.E. and E.J. Krakiwsky (1971). "The method of least squares." Department of Surveying Engineering Lecture Notes No. 18, University of New Brunswick, Fredericton, N.B. Canada.
- Young, L. E., R. E. Neilan and F. R. Bletzacker (1985). "GPS satellite multipath: An experimental investigation." *Proceeding of the First International Symposium on Precise Positioning with the Global Positioning System*, April, Rockville, Maryland, U.S.A., Vol. I, pp. 423-422.
- Zachmann, G.W. (1989). "GPS accuracy for civil marine navigation." *Points and Positions*. Magnavox, Vol.VI, No.1, Torrance, Calif., U.S.A., pp. 2 - 8.



## APPENDIX I

### Sensitivity of Phase Acceleration to Errors in Position and Velocity using Propagation of Errors

The equation for the second time derivative of the phase in the direction of the satellite is given from equation (5.2) as follows:

$$\begin{aligned}
 \delta\delta\phi = \frac{\partial^2\phi}{\partial t^2} = \frac{1}{\rho_j^k} & \left[ \{ (X^k - X_j)(\ddot{X}^k - \ddot{X}_j) + (\dot{X}^k - \dot{X}_j)^2 \} + \{ (Y^k - Y_j)(\ddot{Y}^k - \ddot{Y}_j) + (\dot{Y}^k - \dot{Y}_j)^2 \} + \dots \right. \\
 & \left. \dots + \{ (Z^k - Z_j)(\ddot{Z}^k - \ddot{Z}_j) + (\dot{Z}^k - \dot{Z}_j)^2 \} \right] - \dots \\
 & \dots - \frac{1}{(\rho_j^k)^3} \left[ (X^k - X_j)(\dot{X}^k - \dot{X}_j) + (Y^k - Y_j)(\dot{Y}^k - \dot{Y}_j) + (Z^k - Z_j)(\dot{Z}^k - \dot{Z}_j) \right]^2 + \dots \\
 & \dots + c(\ddot{t}^k + \ddot{t}_j) - \ddot{d}_{ion} + \ddot{d}_{trop} + \ddot{\varepsilon}
 \end{aligned} \tag{I.1}$$

where,  $\rho_j^k = \sqrt{(X^k - X_j)^2 + (Y^k - Y_j)^2 + (Z^k - Z_j)^2}$

The sensitivity of the phase acceleration to an error on position can be determined by error propagation. Assuming all other variables of equation (I.1) are known, the error in the phase acceleration due to the error in position is given from equation (5.3) as follows:

$$\sigma_{\delta\delta\phi}^2 = \left(\frac{\partial\delta\delta\phi}{\partial X_j}\right)^2 \sigma_{X_j}^2 + \left(\frac{\partial\delta\delta\phi}{\partial Y_j}\right)^2 \sigma_{Y_j}^2 + \left(\frac{\partial\delta\delta\phi}{\partial Z_j}\right)^2 \sigma_{Z_j}^2 \quad (I.2)$$

The expression  $\left(\frac{\partial\delta\delta\phi}{\partial X_j}\right)$  is evaluated as follows:

$$\frac{\partial\delta\delta\phi}{\partial X_j} = \frac{1}{\rho_j^k} (\ddot{X}_j - \ddot{X}^k) - \frac{1}{(\rho_j^k)^3} (\text{TOP}_A (X_j - X^k)) - \frac{2}{(\rho_j^k)^3} \text{TOP}_B^{1/2} (\dot{X}_j - \dot{X}^k) + \frac{3}{(\rho_j^k)^5} \text{TOP}_B (X_j - X^k) \quad (I.3)$$

where from equation (5.2),

$$\text{TOP}_A = \{ (X^k - X_j)(\ddot{X}^k - \ddot{X}_j) + (\dot{X}^k - \dot{X}_j)^2 \} + \{ (Y^k - Y_j)(\ddot{Y}^k - \ddot{Y}_j) + (\dot{Y}^k - \dot{Y}_j)^2 \} + \dots$$

$$\dots + \{ (Z^k - Z_j)(\ddot{Z}^k - \ddot{Z}_j) + (\dot{Z}^k - \dot{Z}_j)^2 \}$$

$$\text{TOP}_B = \{ (X^k - X_j)(\dot{X}^k - \dot{X}_j) + (Y^k - Y_j)(\dot{Y}^k - \dot{Y}_j) + (Z^k - Z_j)(\dot{Z}^k - \dot{Z}_j) \}^2$$

The expressions for  $\left(\frac{\partial\delta\delta\phi}{\partial Y_j}\right)$ , and  $\left(\frac{\partial\delta\delta\phi}{\partial Z_j}\right)$  are solved for by substituting the corresponding coordinates into equation (I.3) and then substituting back into equation (I.2).

The sensitivity of the phase acceleration to an error on velocity can also be determined by error propagation. Assuming all other variables of equation (I.1) are known, the error in the phase acceleration due to an error in velocity is given as follows:

$$\sigma_{\delta\delta\phi}^2 = \left(\frac{\partial\delta\delta\phi}{\partial\dot{X}_j}\right)^2 \sigma_{\dot{X}_j}^2 + \left(\frac{\partial\delta\delta\phi}{\partial\dot{Y}_j}\right)^2 \sigma_{\dot{Y}_j}^2 + \left(\frac{\partial\delta\delta\phi}{\partial\dot{Z}_j}\right)^2 \sigma_{\dot{Z}_j}^2 \quad (I.4)$$

The expression  $\left(\frac{\partial\delta\delta\phi}{\partial\dot{X}_j}\right)^2$  is evaluated as follows:

$$\left(\frac{\partial\delta\delta\phi}{\partial\dot{X}_j}\right)^2 = \frac{2}{\rho_j^k} (\dot{X}_j - \dot{X}^k) - \frac{2}{(\rho_j^k)^3} 2\text{TOP}_B^{1/2} (X_j - X^k)$$

The expressions for  $\left(\frac{\partial\delta\delta\phi}{\partial\dot{Y}_j}\right)^2$  and  $\left(\frac{\partial\delta\delta\phi}{\partial\dot{Z}_j}\right)^2$  are solved by substituting the corresponding coordinates into equation (I.5) and then substituting back into equation (I.4).

### Worked Example:

Equation (I.3) shows that the error in the phase acceleration depends on the spatial relationship between the satellite and receiver at the time of observation. Noting that this spatial relationship is constantly changing, it would not be feasible to solve all the acceleration phase errors for an observing session. Instead, a worked example is performed in order to provide some insight to the sensitivity of the phase acceleration to receiver position.

The data for the following example was taken from the TI 4100 data set used in this thesis. The velocity and acceleration of the receiver were taken as being zero for this particular example. The satellite and receiver position, velocity, and acceleration parameters are provided as follows:

Variable	Receiver Parameters	Satellite Parameters
X	1 082 330 m	-7 350 072 m
Y	-4 378 230 m	-15 951 690 m

Z	4 495 070	m	20 299 553	m
$\dot{X}$	0	m/sec	2130	m/sec
$\dot{Y}$	0	m/sec	1333	m/sec
$\dot{Z}$	0	m/sec	1789	m/sec
$\ddot{X}$	0	m/sec <sup>2</sup>	0.31	m/sec <sup>2</sup>
$\ddot{Y}$	0	m/sec <sup>2</sup>	-0.07	m/sec <sup>2</sup>
$\ddot{Z}$	0	m/sec <sup>2</sup>	0.42	m/sec <sup>2</sup>
$\rho_j^k$	= 21 326 792 m			

Assuming an error in the XYZ position of the receiver to be 200 metres and substituting this, along with the above parameters, into equation (I.2) gives a phase acceleration error of approximately  $10^{-4}$  mm/sec<sup>2</sup>. This value is well below the expected accuracy of the acceleration obtainable in this thesis. Consequently, the pseudo-range observation can be used to determine the receiver position when computing the acceleration using the second time derivative of the second time derivative of the phase measurement.

Assuming a noise level of approximately 1 m/sec for the velocity estimate using only the pseudo-range observation, then the resultant error in the carrier phase acceleration will be in the magnitude of  $10^{-1}$  mm/sec<sup>2</sup>. This equates to several mGals which is not acceptable for reconnaissance airborne gravimetry. Consequently, the carrier phase observation is preferred when determining velocity estimates in the acceleration model because of its low noise level characteristics.

## APPENDIX II

### Phase Velocity and Acceleration Over Three Epochs

In many instances the time interval between phase observations may not be equal. In the case of determining accelerations this becomes critical, since the change in phase over two subsequent epochs gives the acceleration. If the time interval for the phase observations are not the same, then it is recommended that, when dealing with a three epoch observation scheme, a higher weight be placed on the shorter time interval. This is because the phase information collected over the shorter time interval will give a better representation of the receiver movement than the phase information obtained over the longer time interval. Kleusberg [1989] gives a method of determining the phase velocity and acceleration using this weighting technique. The equations for this method are developed below.

Let the phase observations at time  $t_1$ ,  $t_2$ , and  $t_3$  be represented by  $\phi_1$ ,  $\phi_2$ , and  $\phi_3$  respectively. Also, let the velocity and acceleration at epoch  $t_2$  be represented by  $\dot{\phi}$  and  $\ddot{\phi}$  respectively. The phase observations at each of the three epochs can be expressed using the following equations for acceleration.

$$\phi_1 = \phi_2 + \dot{\phi}(t_1-t_2) + \frac{1}{2} \ddot{\phi} (t_1-t_2)^2 \quad (\text{II.1})$$

$$\phi_2 = \phi_2 \quad (\text{II.2})$$

$$\phi_3 = \phi_2 + \dot{\phi}(t_3-t_2) + \frac{1}{2} \ddot{\phi} (t_3-t_2)^2 \quad (\text{II.3})$$

Subtracting equation (II.2) from equations (II.1) and (II.3) gives,

$$\phi_1 - \phi_2 = \dot{\phi}(t_1-t_2) + \frac{1}{2} \ddot{\phi} (t_1-t_2)^2 \quad (\text{II.4})$$

$$\phi_3 - \phi_2 = \dot{\phi}(t_3 - t_2) + \frac{1}{2} \ddot{\phi} (t_3 - t_2)^2 \quad (\text{II.5})$$

Equations (II.4) and (II.5) can be expressed in matrix form as follows:

$$\begin{bmatrix} \phi_1 - \phi_2 \\ \phi_3 - \phi_2 \end{bmatrix} = \begin{bmatrix} (t_1 - t_2) & \left(\frac{t_1 - t_2}{2}\right)^2 \\ (t_3 - t_2) & \left(\frac{t_3 - t_2}{2}\right)^2 \end{bmatrix} \begin{bmatrix} \dot{\phi} \\ \ddot{\phi} \end{bmatrix}$$

Solving for the velocity and acceleration values gives,

$$\dot{\phi} = \frac{\phi_1 - \phi_2}{(t_1 - t_2) \left(1 - \frac{t_1 - t_2}{t_3 - t_2}\right)} + \frac{\phi_3 - \phi_2}{(t_3 - t_2) \left(1 - \frac{t_3 - t_2}{t_1 - t_2}\right)} \quad (\text{II.6})$$

$$\ddot{\phi} = \frac{\phi_3 - \phi_2}{(t_3 - t_2) \left(\frac{t_3 - t_1}{2}\right)} + \frac{\phi_1 - \phi_2}{(t_1 - t_2) \left(\frac{t_1 - t_3}{2}\right)} \quad (\text{II.7})$$

For cases where the epoch interval is a constant (ie.  $(t_3 - t_2) = (t_2 - t_1) = \Delta t$ ), then the above velocity and acceleration equations simplify as follows:

$$\dot{\phi} = \frac{1}{2\Delta t} (\phi_3 - \phi_1) \quad (\text{II.8})$$

$$\ddot{\phi} = \frac{1}{(\Delta t)^2} (\phi_3 - 2\phi_2 + \phi_1) \quad (\text{II.9})$$

## APPENDIX III

### Satellite Orbital Accelerations

#### 1.0 Introduction

The determination of the satellite orbital accelerations are derived by taking the second time derivatives of the orbital parameters given in the broadcast ephemeris, and the subsequent second time derivatives of the transformation equations which express the accelerations of the satellite in the Earth Centred Earth Fixed coordinate system. The following abbreviations are used in order to simplify the formula given below. The abbreviations are with respect to satellite  $k$  at time  $t_k$  unless otherwise specified.

$a, b$	= semi-major and semi-minor axis of the reference ellipsoid (WGS 84)
$e$	= the first eccentricity of the ellipsoid ( $e^2 = (a^2 - b^2)/a^2$ )
$\omega_e$	= mean earth rotation ( $7.292115147 \times 10^{-5}$ rad/sec)
$\omega$	= the argument of perigee (rad)
$t_k$	= time since reference epoch ( $t - t_{0e}$ )
$c$	= speed of light in a vacuum
$E_k$	= the eccentric anomaly
$\dot{E}_k$	= the first time derivative of the eccentric anomaly
$M_k$	= the mean anomaly of the satellite at time $t_k$
$\dot{M}_k$	= the first time derivative of the mean anomaly at time $t_k$ (available from the broadcast ephemeris)
$f_k$	= the true anomaly
$\dot{f}_k$	= the first time derivative of the true anomaly
$\ddot{f}_k$	= the second time derivative of the true anomaly

$C_{uc}$	= coefficient of the cosine correction term to the argument of latitude (rad)
$C_{us}$	= coefficient of the sine correction term to the argument of latitude (rad)
$u_k$	= the argument of latitude (rad)
$\dot{u}_k$	= the first time derivative of the argument of latitude
$\ddot{u}_k$	= the second time derivative of the argument of latitude
$C_{rc}$	= coefficient of the cosine correction term to the orbital radius (rad)
$C_{rs}$	= coefficient of the sine correction term to the orbital radius (rad)
$r_k$	= the orbital radius
$\dot{r}_k$	= the first time derivative of the orbital radius
$\ddot{r}_k$	= the second time derivative of the orbital radius
$C_{ic}$	= coefficient of the cosine correction term to the orbital plane inclination (rad)
$C_{is}$	= coefficient of the sine correction term to the orbital plane inclination (rad)
$i_0$	= the orbital inclination at time $t_{oe}$
$i_k$	= the orbital inclination
$\dot{i}_k$	= the first time derivative of the orbital inclination
$\ddot{i}_k$	= the second time derivative of the orbital inclination
$\Omega_0$	= the right ascension parameter in the broadcast ephemeris
$\dot{\Omega}$	= the rate of change of the right ascension
$\lambda_k$	= the longitude of the ascending node
$\dot{\lambda}_k$	= the first time derivative of the longitude of the ascending node
$\ddot{\lambda}_k$	= the second time derivative of the longitude of the ascending node
$XYZ_{ORB}$	= orbital coordinates
$\dot{X}\dot{Y}\dot{Z}_{ORB}$	= orbital velocities
$\ddot{X}\ddot{Y}\ddot{Z}_{ORB}$	= orbital accelerations
$\rho$	= the range from the satellite to the receiver in the ECEF (or CT) system



$\dot{\rho}$  = the range rate from the satellite to the receiver in the ECEF (or CT) system

$$= \frac{\Delta XYZ}{\rho}$$

$\ddot{\rho}$  = the change in range rate from the satellite to the receiver in the ECEF (or CT) system

$$= \frac{\Delta \Delta XYZ}{\rho} - \frac{(\Delta XYZ)^2}{\rho^3}$$

$XYZ_{ECSF}$  = satellite coordinates in Earth Centred Space Fixed coordinate system

$\dot{X}\dot{Y}\dot{Z}_{ECSF}$  = satellite velocities in Earth Centred Space Fixed coordinate system

$\ddot{X}\ddot{Y}\ddot{Z}_{ECSF}$  = satellite accelerations in Earth Centred Space Fixed coordinate system

$XYZ_{ECEF}$  = satellite coordinates in Earth Centred Earth Fixed (or CT) coordinate system

$\dot{X}\dot{Y}\dot{Z}_{ECEF}$  = satellite velocities in Earth Centred Earth Fixed (or CT) coordinate system

$\ddot{X}\ddot{Y}\ddot{Z}_{ECEF}$  = satellite accelerations in Earth Centred Earth Fixed (or CT) coordinate system

## 1.1 Time Derivative of Eccentric Anomaly

$$M_k = E_k - e \sin(E_k)$$

$$\frac{\partial M_k}{\partial t} = \frac{\partial E_k}{\partial t} - e \frac{\partial E_k}{\partial t} \cos(E_k)$$

$$\dot{E}_k = \frac{\dot{M}_k}{(1 - e \cos(E_k))}$$

## 1.2 Time Derivative of True Anomaly

$$f_k = \text{Tan}^{-1} \left\{ \frac{(1-e^2)^{\frac{1}{2}} \text{Sin}(E_k)}{\text{Cos}(E_k) - e} \right\}$$

$$\dot{f}_k = \frac{(1-e^2)^{\frac{1}{2}} \dot{E}_k}{\{1 - e \text{Cos}(E_k)\}^2}$$

$$\ddot{f}_k = \frac{-2e (1-e^2)^{\frac{1}{2}} \dot{E}_k^2 \text{Sin}(E_k)}{\{1 - e \text{Cos}(E_k)\}^4}$$

### 1.3 Time Derivative of Argument of Latitude

$$u_k = \omega + f_k + C_{uc} \text{Cos}2(\omega + f_k) + C_{us} \text{Sin}2(\omega + f_k)$$

$$\dot{u}_k = \dot{f}_k + 2\dot{f}_k \{ C_{us} \text{Cos}2(\omega + f_k) - C_{uc} \text{Sin}2(\omega + f_k) \}$$

$$\begin{aligned} \ddot{u}_k = \ddot{f}_k + 2\ddot{f}_k \{ C_{us} \text{Cos}2(\omega + f_k) - C_{uc} \text{Sin}2(\omega + f_k) \} - \dots \\ \dots - 4(\dot{f}_k)^2 \{ C_{us} \text{Sin}2(\omega + f_k) + C_{uc} \text{Cos}2(\omega + f_k) \} \end{aligned}$$

### 1.4 Time Derivative of Orbital Radius

$$r_A = a(1 - e \text{Cos}(E_k))$$

$$r_B = C_{rc} \text{Cos}2(\omega + f_k) + C_{rs} \text{Sin}2(\omega + f_k)$$

$$r_k = r_A + r_B$$

$$\dot{r}_A = \frac{ae\dot{E}_k \text{Sin}(E_k)}{1-e\text{Cos}(E_k)}$$

$$\dot{r}_B = 2\dot{f}_k \{ C_{rs}\text{Cos}2(\omega+f_k) - C_{rc}\text{Sin}2(\omega+f_k) \}$$

$$\dot{r}_k = \dot{r}_A + \dot{r}_B$$

$$\ddot{r}_A = \frac{-ae\dot{E}_k^2}{\{1-e\text{Cos}(E_k)\}^3} \{e-\text{Cos}(E_k)\}$$

$$\ddot{r}_B = 2\ddot{f}_k \{ C_{rs}\text{Cos}2(\omega+f_k) - C_{rc}\text{Sin}2(\omega+f_k) - \dots \\ \dots - 4(\dot{f}_k)^2 \{ C_{rs}\text{Sin}2(\omega+f_k) + C_{rc}\text{Cos}2(\omega+f_k) \}$$

$$\ddot{r}_k = \ddot{r}_A + \ddot{r}_B$$

## 1.5 Time Derivative of Orbital Plane Inclination

$$i_k = i_0 + \dot{i}(t_k) + C_{ic}\text{Cos}2(\omega+f_k) + C_{is}\text{Sin}2(\omega+f_k)$$

$$\dot{i}_k = \dot{i} + 2\dot{f}_k \{ C_{is}\text{Cos}2(\omega+f_k) - C_{ic}\text{Sin}2(\omega+f_k) \}$$

$$\ddot{i}_k = 2\ddot{f}_k \{ C_{is}\text{Cos}2(\omega+f_k) - C_{ic}\text{Sin}2(\omega+f_k) \} - \dots \\ \dots - 4(\dot{f}_k)^2 \{ C_{is}\text{Sin}2(\omega+f_k) + C_{ic}\text{Cos}2(\omega+f_k) \}$$

## 1.6 Time Derivative of Longitude of Ascending Node

$$\lambda_k = \Omega_0 + (\dot{\Omega} - \omega_e)t_k - \omega_e t_{oe}$$

$$\dot{\lambda}_k = \dot{\Omega} - \omega_e$$

$$\ddot{\lambda}_k = 0$$

## 1.7 Time Derivative of the Orbital Coordinate System

$$X_{\text{ORB}} = r_k \text{Cos}(u_k)$$

$$Y_{\text{ORB}} = r_k \text{Sin}(u_k)$$

$$Z_{\text{ORB}} = 0$$

$$\dot{X}_{\text{ORB}} = \dot{r}_k \text{Cos}(u_k) - r_k \dot{u}_k \text{Sin}(u_k)$$

$$\dot{Y}_{\text{ORB}} = \dot{r}_k \text{Sin}(u_k) + r_k \dot{u}_k \text{Cos}(u_k)$$

$$\dot{Z}_{\text{ORB}} = 0$$

$$\ddot{X}_{\text{ORB}} = \{ \ddot{r}_k - r_k (\dot{u}_k)^2 \} \text{Cos}(u_k) - \{ 2\dot{r}_k \dot{u}_k + r_k \ddot{u}_k \} \text{Sin}(u_k)$$

$$\ddot{Y}_{\text{ORB}} = \{ \ddot{r}_k - r_k (\dot{u}_k)^2 \} \text{Sin}(u_k) + \{ 2\dot{r}_k \dot{u}_k + r_k \ddot{u}_k \} \text{Cos}(u_k)$$

$$\ddot{Z}_k = 0$$

## 1.8 Time Derivative of the ECSF Coordinate System

$$X_{\text{ECSF}} = X_{\text{ORB}} \text{Cos}(\lambda_k) - Y_{\text{ORB}} \text{Sin}(\lambda_k) \text{Cos}(i_k)$$

$$Y_{\text{ECSF}} = X_{\text{ORB}} \text{Sin}(\lambda_k) + Y_{\text{ORB}} \text{Cos}(\lambda_k) \text{Cos}(i_k)$$

$$Z_{\text{ECSF}} = Y_{\text{ORB}} \text{Sin}(i_k)$$

$$\begin{aligned} \dot{X}_{\text{ECSF}} = & \{ \dot{X}_{\text{ORB}} \text{Cos}(\lambda_k) - X_{\text{ORB}} \dot{\lambda}_k \text{Sin}(\lambda_k) \} - \dots \\ & \dots - \{ Y_{\text{ORB}} [ \dot{\lambda}_k \text{Cos}(\lambda_k) \text{Cos}(i_k) - \dot{i}_k \text{Sin}(\lambda_k) \text{Sin}(i_k) ] + \dot{Y}_{\text{ORB}} \text{Sin}(\lambda_k) \text{Cos}(i_k) \} \end{aligned}$$

$$\begin{aligned} \dot{Y}_{\text{ECSF}} = & \{ \dot{X}_{\text{ORB}} \text{Sin}(\lambda_k) - X_{\text{ORB}} \dot{\lambda}_k \text{Cos}(\lambda_k) \} + \dots \\ & \dots + \{ \dot{Y}_{\text{ORB}} \text{Cos}(\lambda_k) \text{Cos}(i_k) - Y_{\text{ORB}} [ \dot{i}_k \text{Cos}(\lambda_k) \text{Sin}(i_k) + \dot{\lambda}_k \text{Sin}(\lambda_k) \text{Cos}(i_k) ] \} \end{aligned}$$

$$\dot{Z}_{ECSF} = \dot{Y}_{ORB} \sin(i_k) + Y_{ORB} \dot{i}_k \cos(i_k)$$

$$\begin{aligned} \ddot{X}_{ECSF} = & \cos(\lambda_k) \{ \ddot{X}_{ORB} - \dot{X}_{ORB}(\dot{\lambda}_k)^2 \\ & - 2\dot{X}_{ORB}\dot{\lambda}_k\dot{\sin}(\lambda_k) \\ & - 2\dot{Y}_{ORB}\dot{\lambda}_k\cos(\lambda_k)\cos(i_k) \\ & + \sin(\lambda_k)\sin(i_k) \{ 2\dot{Y}_{ORB}\dot{i}_k + Y_{ORB}\ddot{i}_k \} \\ & + 2Y_{ORB}\dot{\lambda}_k\dot{i}_k\cos(\lambda_k)\sin(i_k) \\ & + \sin(\lambda_k)\cos(i_k) \{ Y_{ORB}(\dot{\lambda}_k)^2 + Y_{ORB}(\dot{i}_k)^2 - \ddot{Y}_{ORB} \} \end{aligned}$$

$$\begin{aligned} \ddot{Y}_{ECSF} = & \sin(\lambda_k) \{ \ddot{X}_{ORB} - \dot{X}_{ORB}(\dot{\lambda}_k)^2 \\ & + 2\dot{X}_{ORB}\dot{\lambda}_k\cos(\lambda_k) \\ & + 2Y_{ORB}\dot{\lambda}_k\dot{i}_k\sin(\lambda_k)\sin(i_k) \\ & - \cos(\lambda_k)\sin(i_k) \{ 2Y_{ORB}\ddot{i}_k + \dot{Y}_{ORB}\dot{i}_k \} \\ & - 2\dot{Y}_{ORB}\dot{\lambda}_k\sin(\lambda_k)\cos(i_k) \\ & + \cos(\lambda_k)\cos(i_k) \{ \ddot{Y}_{ORB} - Y_{ORB}(\dot{\lambda}_k)^2 - Y_{ORB}(\dot{i}_k)^2 \} \end{aligned}$$

$$\ddot{Z}_{ECSF} = \cos(i_k) \{ 2\dot{Y}_{ORB}\dot{i}_k + Y_{ORB}\ddot{i}_k \} + \sin(i_k) \{ \ddot{Y}_{ORB} - Y_{ORB}(\dot{i}_k)^2 \}$$

## 1.9 Time Derivative of the ECEF (or CT) Coordinate System

$$\rho = \left\{ (X^s - X_p)^2 + (Y^s - Y_p)^2 + (Z^s - Z_p)^2 \right\}^{\frac{1}{2}}$$

$$\Delta XYZ = \{ (X^s - X_p)(\dot{X}^s - \dot{X}_p) + (Y^s - Y_p)(\dot{Y}^s - \dot{Y}_p) + (Z^s - Z_p)(\dot{Z}^s - \dot{Z}_p) \}$$

$$\begin{aligned} \Delta\Delta XYZ = & \{ [ (X^s - X_p)(\ddot{X}^s - \ddot{X}_p) + (\dot{X}^s - \dot{X}_p) ] + \dots \\ & \dots + [ (Y^s - Y_p)(\ddot{Y}^s - \ddot{Y}_p) + (\dot{Y}^s - \dot{Y}_p) ] + \dots \\ & \dots + [ (Z^s - Z_p)(\ddot{Z}^s - \ddot{Z}_p) + (\dot{Z}^s - \dot{Z}_p) ] \end{aligned}$$

$$X_{ECEF} = X_{ECSF} \cos\left(\frac{\rho}{c}\omega\right) + Y_{ECSF} \sin\left(\frac{\rho}{c}\omega\right)$$

$$Y_{ECEF} = -X_{ECSF} \sin\left(\frac{\rho}{c}\omega\right) + Y_{ECSF} \cos\left(\frac{\rho}{c}\omega\right)$$

$$Z_{ECEF} = Z_{ECSF}$$

$$\dot{X}_{ECEF} = \cos\left(\frac{\rho}{c}\omega\right) \left\{ \dot{X}_{ECSF} + Y_{ECSF} \frac{\omega}{c\rho} \Delta XYZ \right\} + \sin\left(\frac{\rho}{c}\omega\right) \left\{ \dot{Y}_{ECSF} - X_{ECSF} \frac{\omega}{c\rho} \Delta XYZ \right\}$$

$$\dot{Y}_{ECEF} = \cos\left(\frac{\rho}{c}\omega\right) \left\{ \dot{Y}_{ECSF} - X_{ECSF} \frac{\omega}{c\rho} \Delta XYZ \right\} - \sin\left(\frac{\rho}{c}\omega\right) \left\{ \dot{X}_{ECSF} + Y_{ECSF} \frac{\omega}{c\rho} \Delta XYZ \right\}$$

$$\dot{Z}_{ECEF} = \dot{Z}_{ECSF}$$

$$\begin{aligned} \ddot{X}_{ECEF} = & \cos\left(\frac{\rho}{c}\omega\right) \left\{ \ddot{X}_{ECSF} + \dots \right. \\ & \dots + \frac{\omega}{c\rho} \left[ \Delta XYZ (2\dot{Y}_{ECSF} - \frac{\omega}{c\rho} (\Delta XYZ) X_{ECSF}) + Y_{ECSF} (\Delta\Delta XYZ - \frac{\Delta XYZ}{3\rho}) \right] \left. \right\} + \dots \\ & \dots + \sin\left(\frac{\rho}{c}\omega\right) \left\{ \ddot{Y}_{ECSF} - \dots \right. \\ & \dots - \frac{\omega}{c\rho} \left[ \Delta XYZ (2\dot{X}_{ECSF} + \frac{\omega}{c\rho} (\Delta XYZ) Y_{ECSF}) + X_{ECSF} (\Delta\Delta XYZ - \frac{\Delta XYZ}{3\rho}) \right] \left. \right\} \end{aligned}$$

$$\begin{aligned}
\ddot{Y}_{ECEF} = & \cos\left(\frac{\rho}{c}\omega\right) \left\{ \ddot{Y}_{ECSF} - \dots \right. \\
& \dots - \frac{\omega}{c\rho} \left[ \Delta XYZ (2\dot{X}_{ECSF} + \frac{\omega}{c\rho} (\Delta XYZ) Y_{ECSF}) + X_{ECSF} \left( \Delta \Delta XYZ - \frac{\Delta XYZ}{3} \right) \right] \dots \\
& \dots - \sin\left(\frac{\rho}{c}\omega\right) \left\{ \ddot{X}_{ECSF} + \dots \right. \\
& \dots + \frac{\omega}{c\rho} \left[ \Delta XYZ (2\dot{Y}_{ECSF} - \frac{\omega}{c\rho} (\Delta XYZ) X_{ECSF}) + Y_{ECSF} \left( \Delta \Delta XYZ - \frac{\Delta XYZ}{3} \right) \right] \left. \right\}
\end{aligned}$$

$$\ddot{Z}_{ECEF} = \ddot{Z}_{ECSF}$$

## APPENDIX IV

### Transformation of Position, Velocity, and Acceleration from the CT-System to the Geodetic Coordinate Systems

The transformation of the receiver geodetic  $\phi\lambda h$  coordinates to the CT coordinates is given as follows [Krakiwsky et al 1977]:

$$X = (N+h) \text{Cos}(\phi) \text{Cos}(\lambda) \quad (\text{IV.1})$$

$$Y = (N+h) \text{Cos}(\phi) \text{Sin}(\lambda) \quad (\text{IV.2})$$

$$Z = \{N(1-e^2) + h\} \text{Sin}(\phi) \quad (\text{IV.3})$$

The error propagation for this three dimensional transformation, and the reverse transformation, is given as follows [Krakiwsky et al 1977]:

$$C_{XYZ} = J C_{\phi\lambda h} J^T \quad (\text{IV.4})$$

$$C_{\phi\lambda h} = J^{-1} C_{XYZ} (J^{-1})^T \quad (\text{IV.5})$$

where in both of the above equations, J represents the Jacobian of the transformation from the CT coordinate system to the geodetic coordinate system. The Jacobian matrix for the above transformation is given as [Krakiwsky et al 1977]:



$$J = \begin{bmatrix} \frac{-\sin(\phi) \cos(\lambda)}{M+h} & \frac{-\sin(\phi) \sin(\lambda)}{M+h} & \frac{\cos(\phi)}{M+h} \\ \frac{-\sin(\lambda)}{(N+h) \cos(\phi)} & \frac{\cos(\lambda)}{(N+h) \cos(\phi)} & 0 \\ \cos(\phi) \cos(\lambda) & \cos(\phi) \sin(\lambda) & \sin(\phi) \end{bmatrix} \quad (\text{IV.6})$$

In this thesis it becomes necessary to transform the velocities and accelerations from the cartesian CT- coordinate system to the geodetic coordinate system. Letting X represent the XYZ coordinate of the receiver, and U represent the  $\phi\lambda h$  coordinate of the same point, then the transformation from X to U is given by:

$$U = J^{-1} X \quad (\text{IV.7})$$

Thus the propagation of errors from X to U can be represented by:

$$\Sigma_U = J^{-1} \Sigma_X (J^{-1})^T \quad (\text{IV.8})$$

The transformation of the receiver velocities from the CT-system to the geodetic coordinate system is obtained by taking the time derivatives of equations (IV.1), (IV.2), and (IV.3). This exercise shows that the Jacobian matrix for the velocity transformation is equivalent to the Jacobian matrix of equation (IV.6). Thus, the reverse transformation of the velocities is represented as follows:

$$\dot{U} = J^{-1} \dot{X} \quad (\text{IV.9})$$

The corresponding propagation of velocity errors from the CT-system to the geodetic coordinate system is then given as follows:

$$\Sigma_{\dot{U}} = J^{-1} \Sigma_{\dot{X}} (J^{-1})^T \quad (\text{IV.10})$$

The change in  $\dot{U}$ , in equation (IV.9), with respect to a change in time, represents the receiver acceleration in the geodetic coordinate system. Consequently, the time derivative of equation (IV.9) is given as follows:

$$\frac{\partial \dot{U}}{\partial t} = J^{-1} \frac{\partial \dot{X}}{\partial t} + \dot{J}^{-1} \dot{X} \quad (\text{IV.11})$$

Denoting  $\frac{d\dot{U}}{dt}$  as  $\ddot{U}$ , the receiver accelerations in the geodetic system, and  $\frac{\partial \dot{X}}{\partial t}$  as  $\ddot{X}$ , the receiver acceleration in the CT-system, then equation (IV.11) can be written as:

$$\ddot{U} = J^{-1} \ddot{X} + \dot{J}^{-1} \dot{X} \quad (\text{IV.12})$$

The  $\dot{J}$  term of equation (IV.12) is the time derivative of the Jacobian matrix expressed in equation (IV.6). The corresponding propagation of acceleration errors from the CT coordinate system to the geodetic coordinate system is then given as follows:

$$\Sigma_{\ddot{U}} = J^{-1} \Sigma_{\ddot{X}} (J^{-1})^T + \dot{J}^{-1} \Sigma_{\dot{X}} (\dot{J}^{-1})^T + \dot{J}^{-1} \Sigma_{\ddot{X}\dot{X}} (J^{-1})^T + J^{-1} \Sigma_{\dot{X}\ddot{X}} (\dot{J}^{-1})^T \quad (\text{IV.13})$$

The last two terms of equation (IV.13) represents the correlations between the velocities and accelerations.

## APPENDIX V

### **Power Spectral Density Plots of Undifferenced Accelerations**

The following pages contain plots of the power spectral density values of the undifferenced accelerations of each of the data sets obtained for this thesis. The plots of the PSD accelerations from both receivers within each data set are given. A polar plot giving the satellite sky distribution of each data set is provided as well.

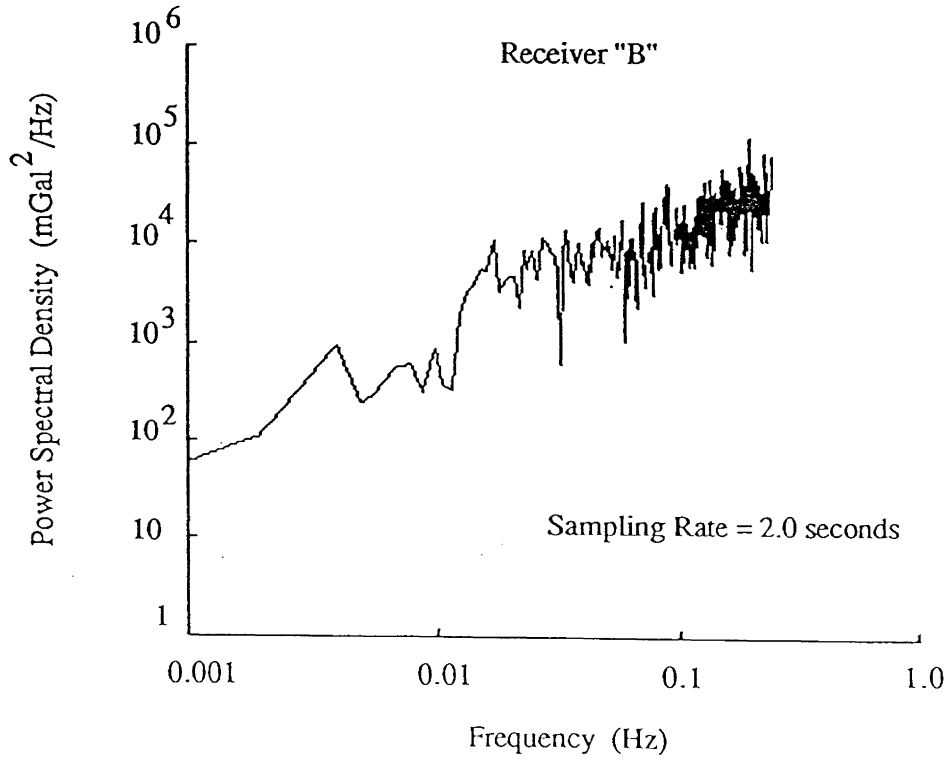
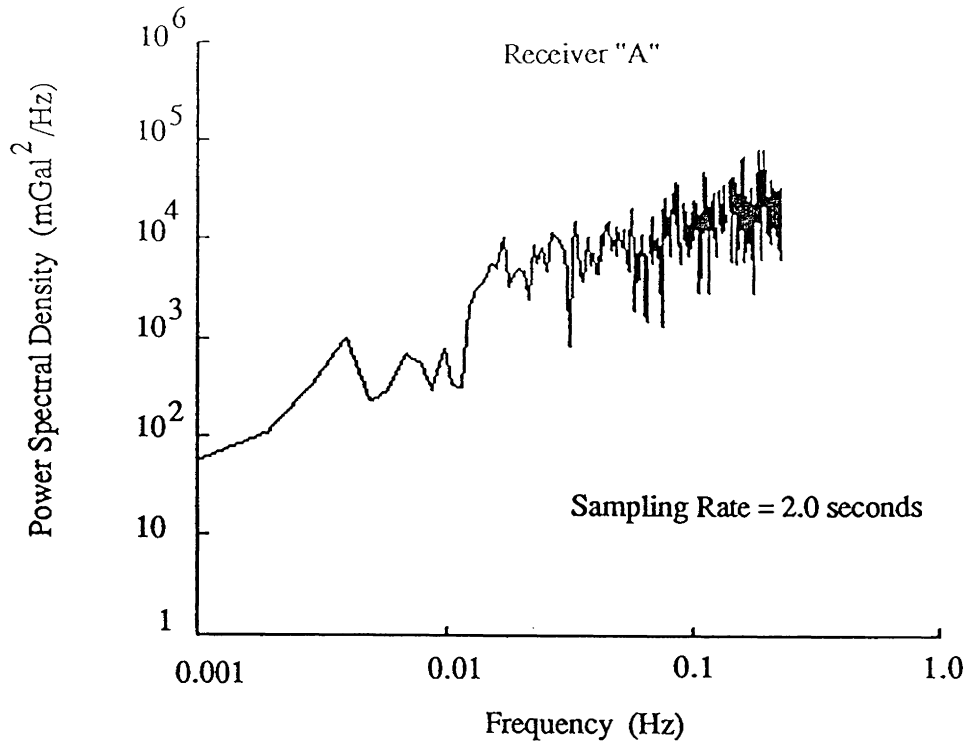


Figure V.1

Power Spectral Density of TI 4100 Undifferenced Vertical Accelerations

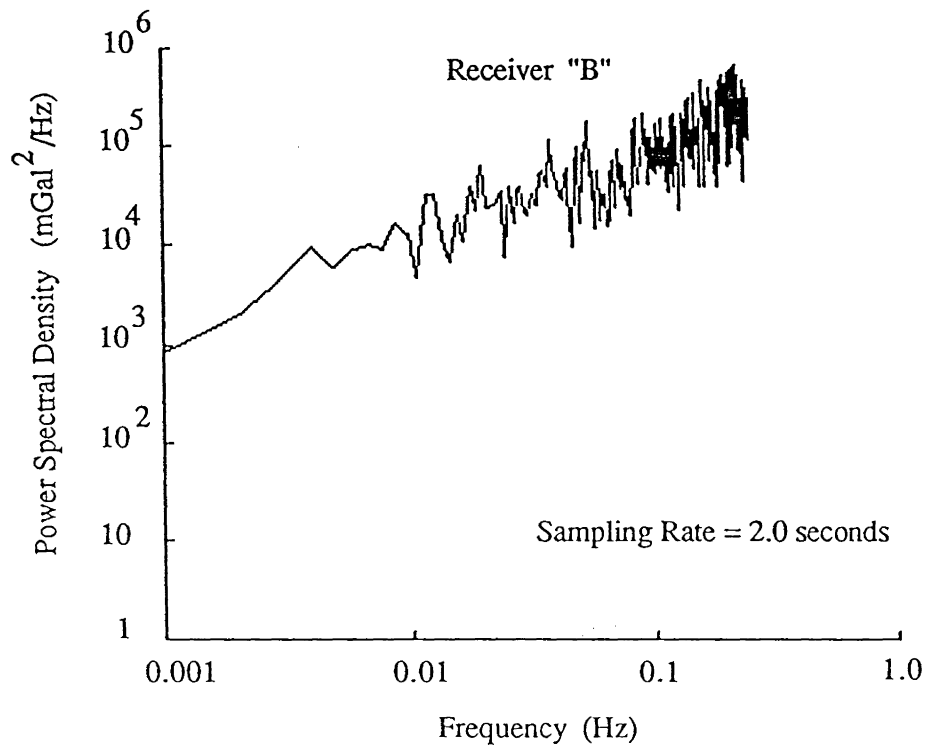
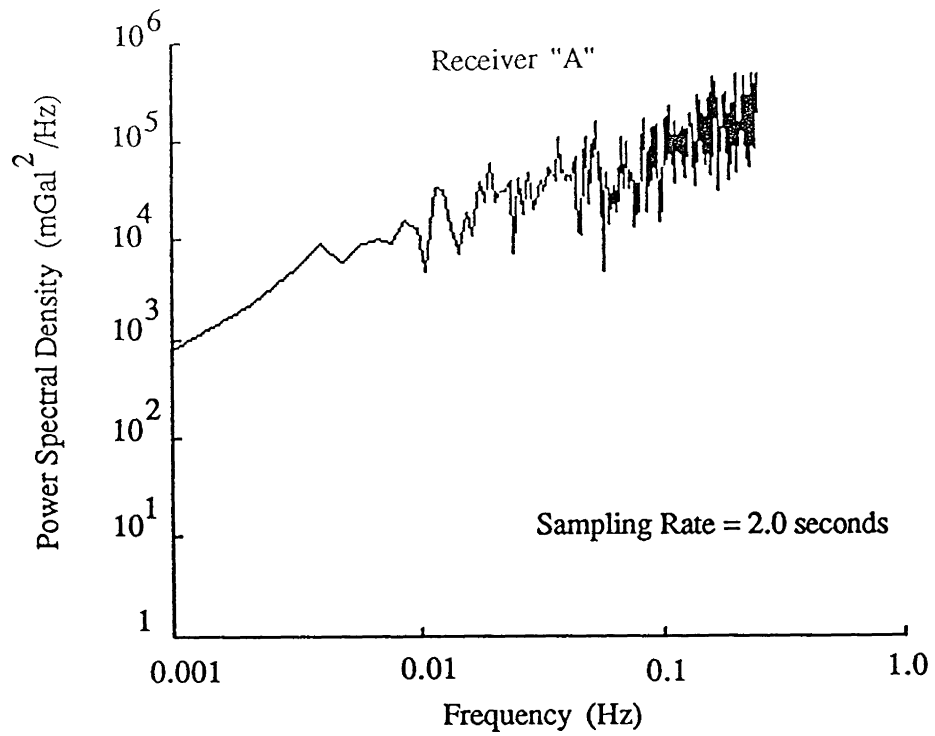


Figure V.2

Power Spectral Density of TI 4100 Undifferenced Accelerations in Latitude

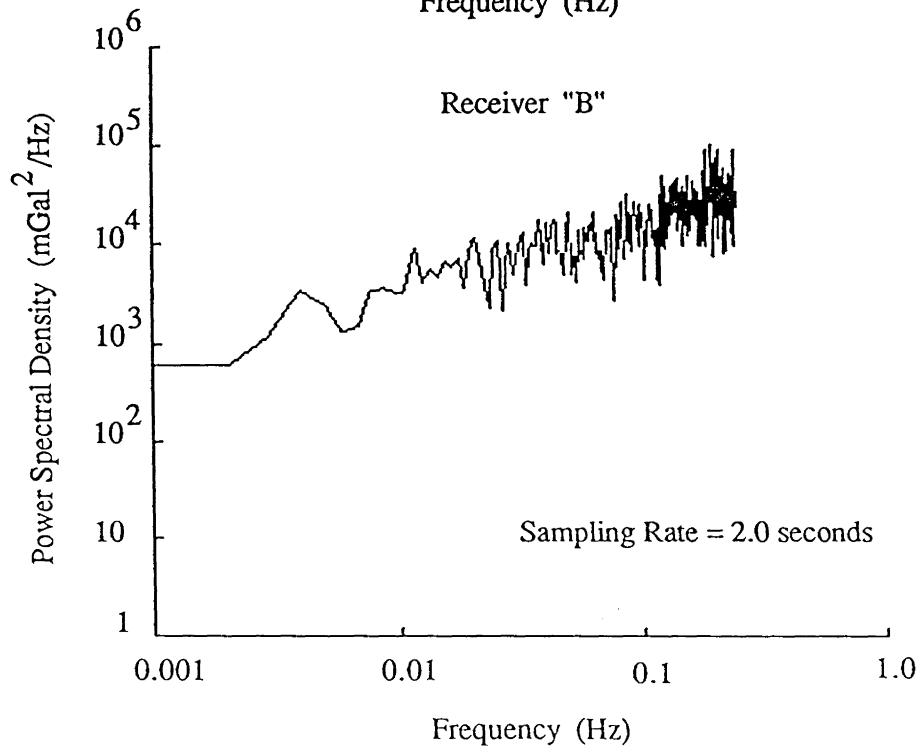
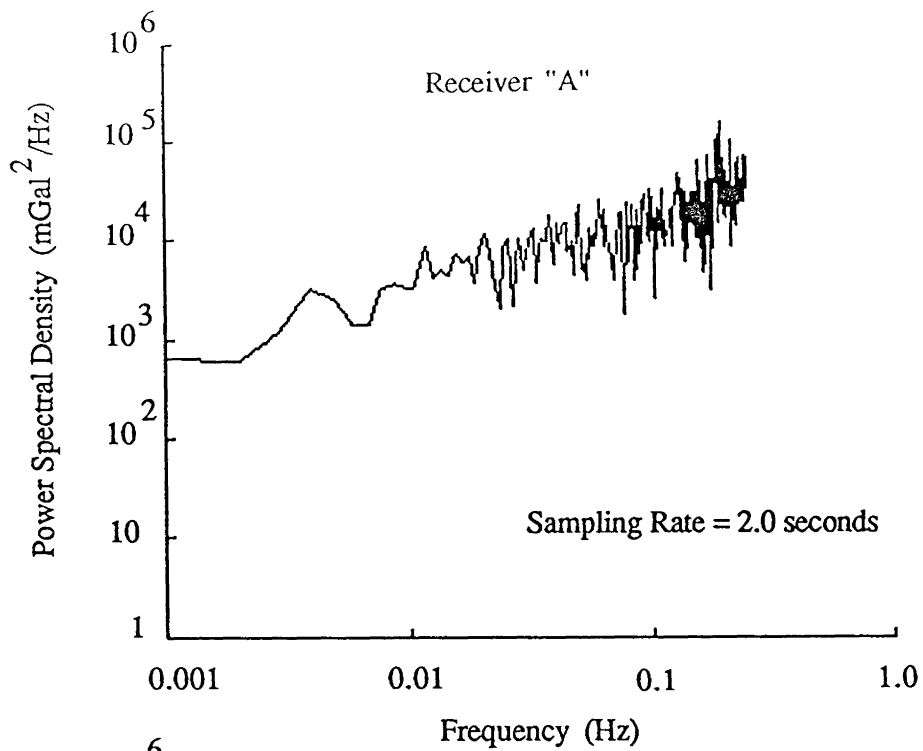


Figure V.3

Power Spectral Density of TI 4100 Undifferenced Accelerations in Longitude

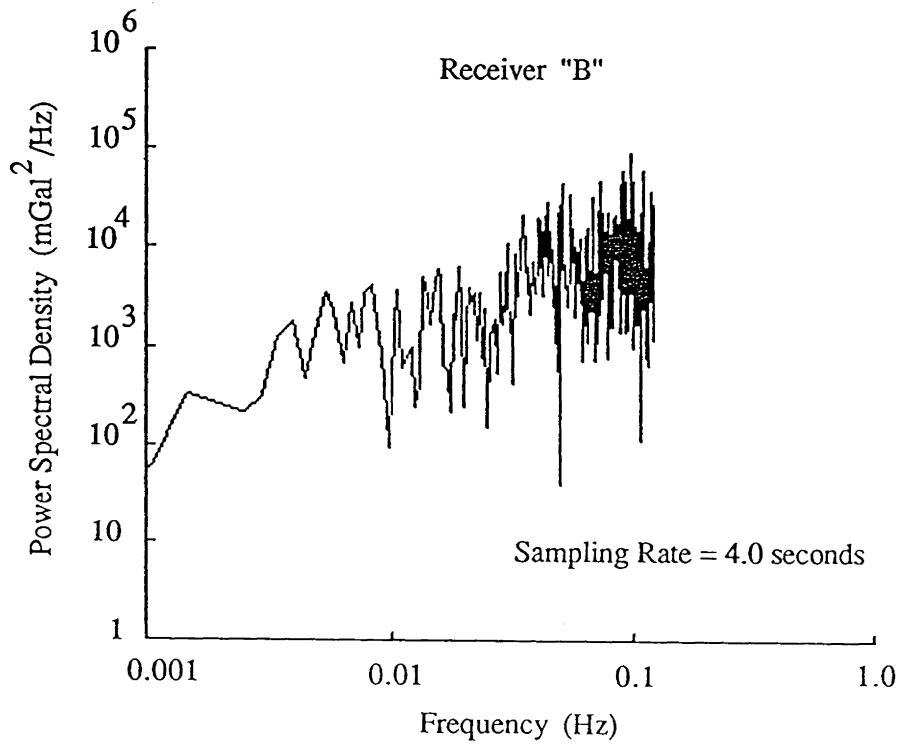
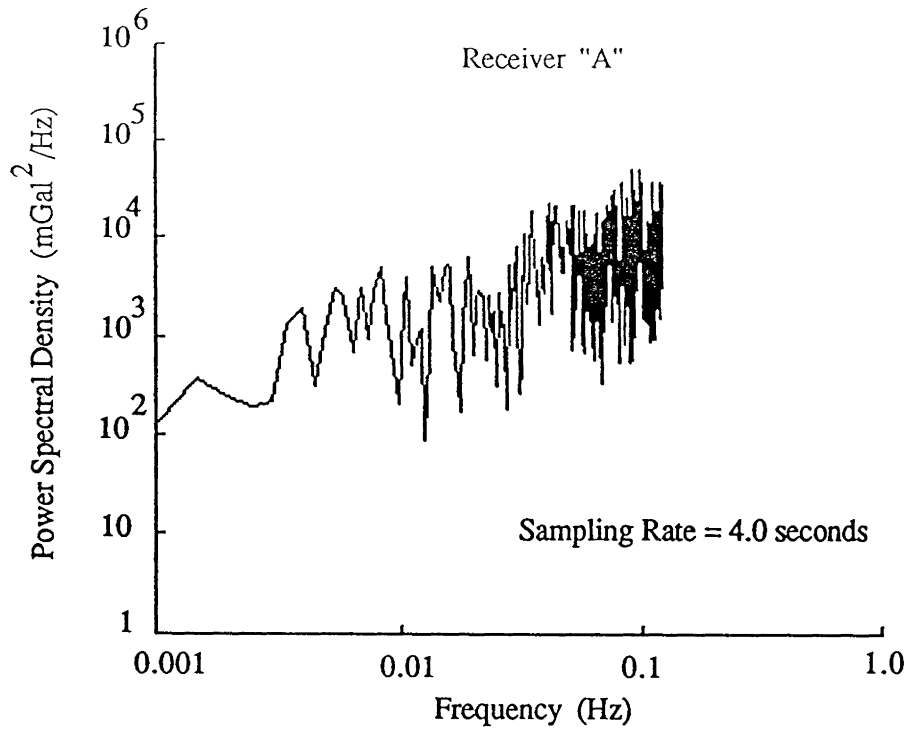


Figure V.4

Power Spectral Density of Trimble 4000 SLD Undifferenced Vertical Accelerations

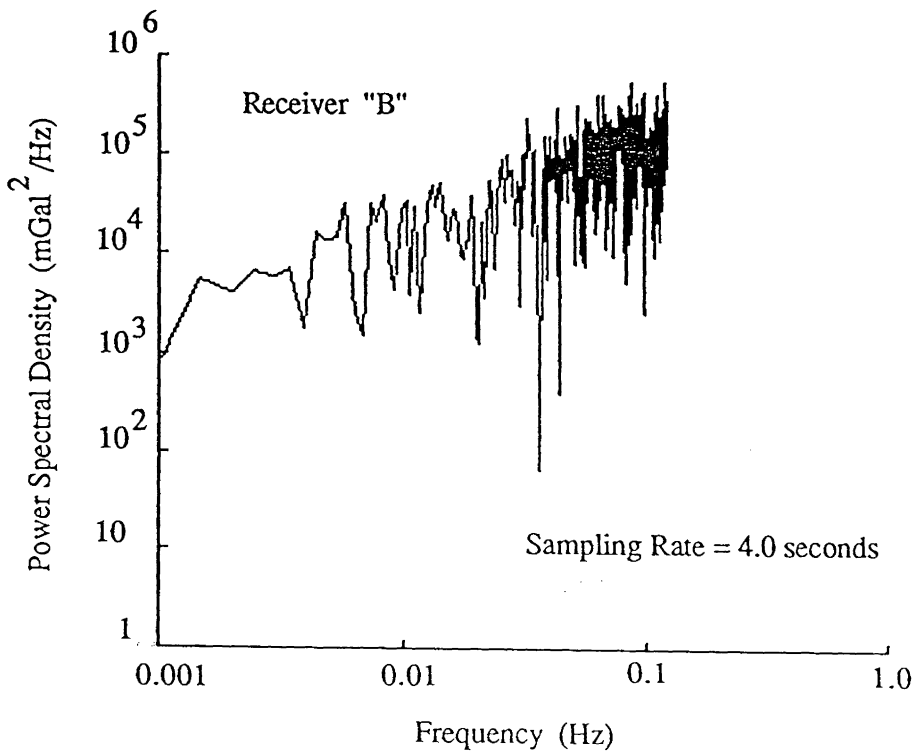
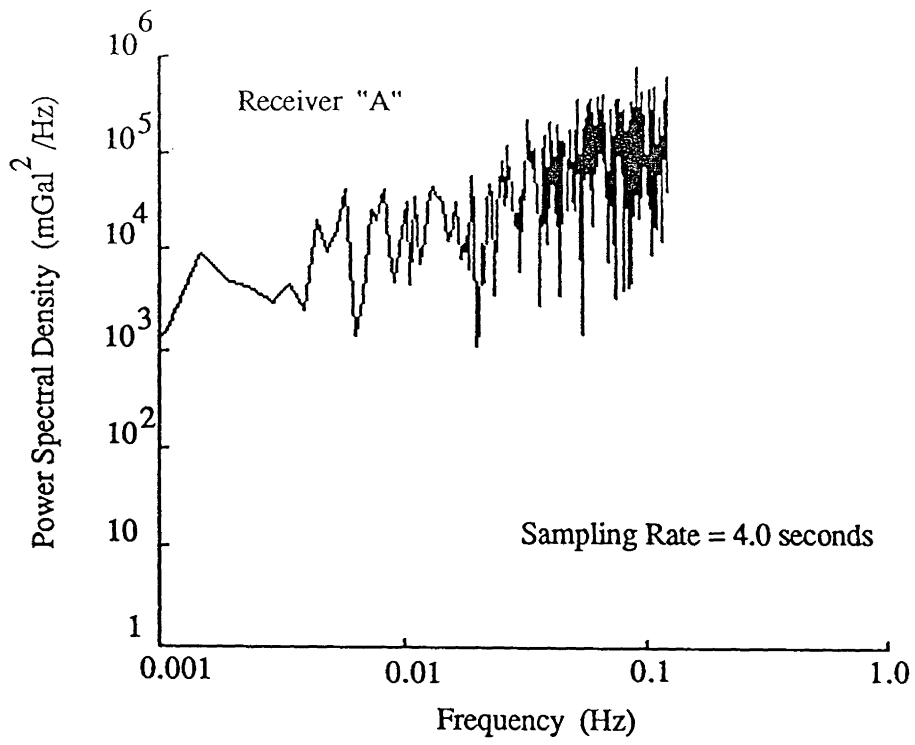


Figure V.5

Power Spectral Density of Trimble 4000 SLD Undifferenced Accelerations in Latitude



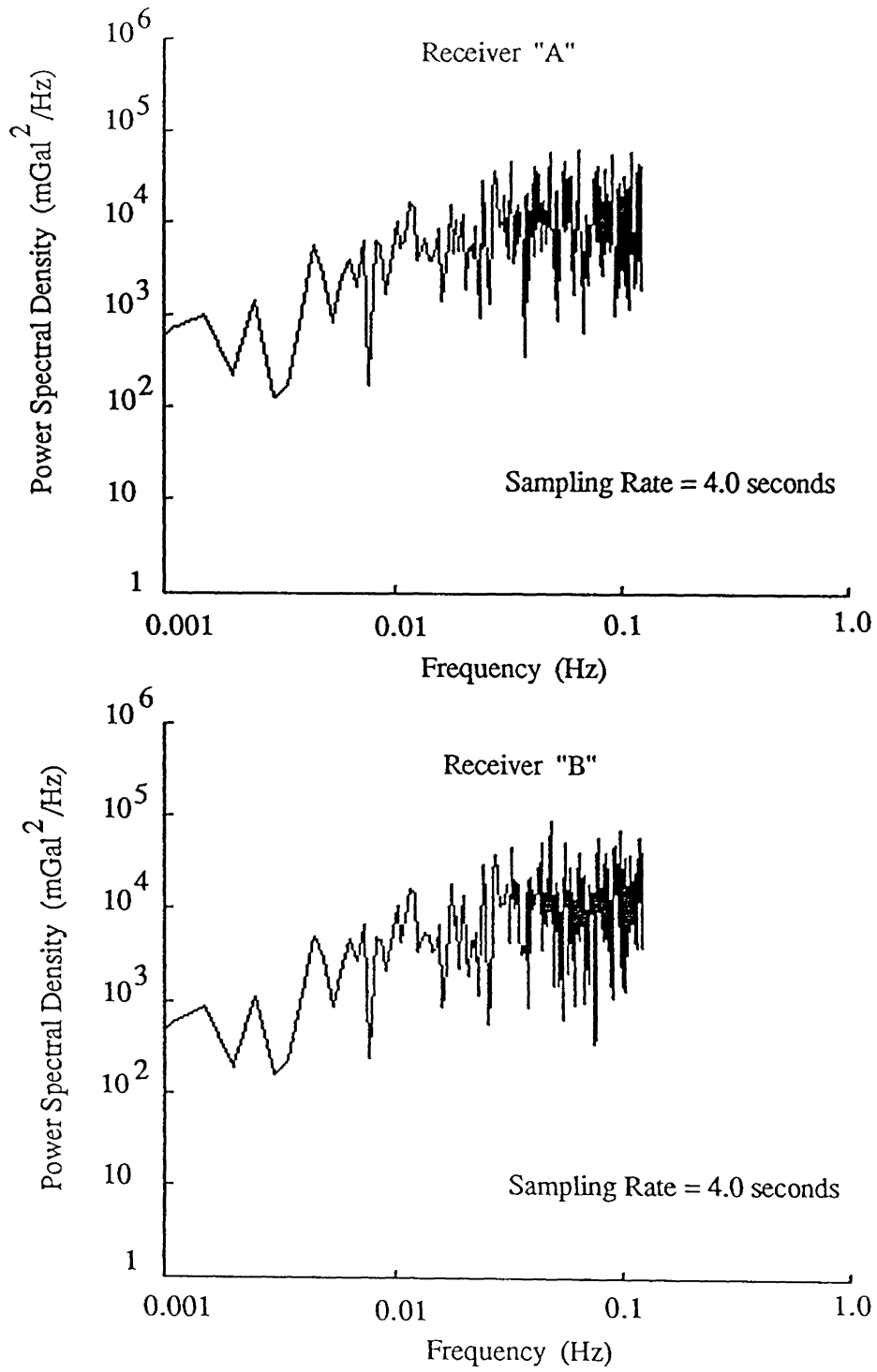


Figure V.6

Power Spectral Density of Trimble 4000 SLD Undifferenced Accelerations in Longitude

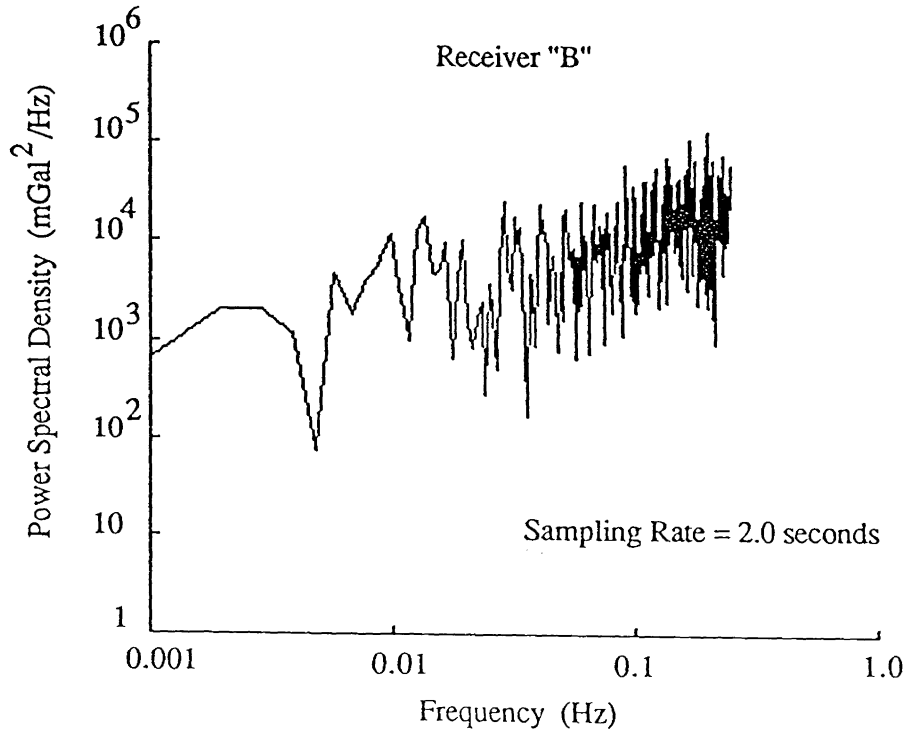
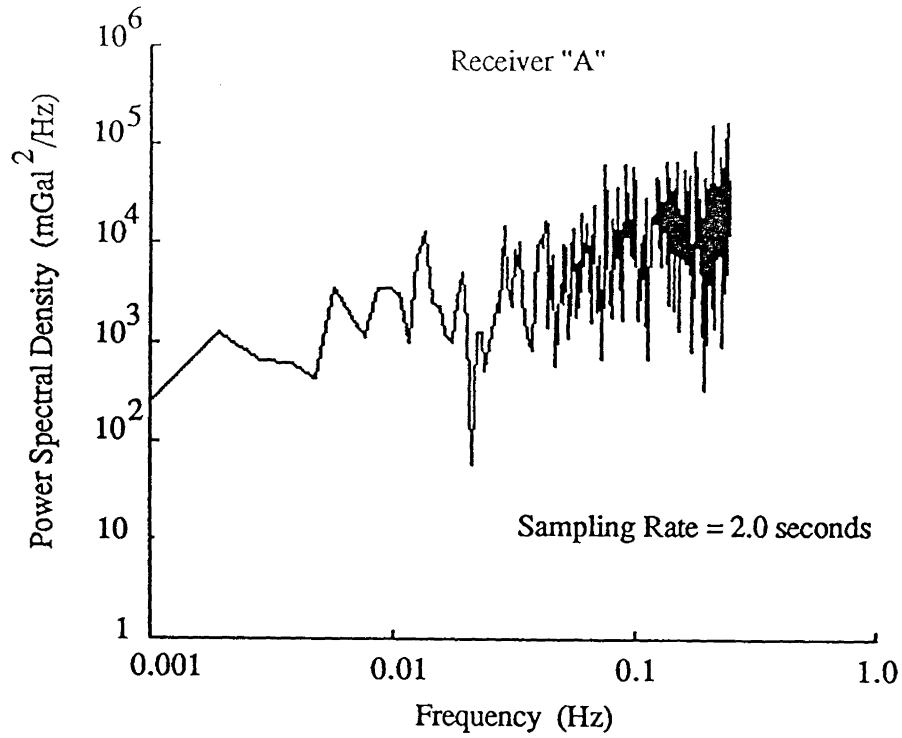


Figure V.7

Power Spectral Density of Ashtech XII Undifferenced Vertical Accelerations

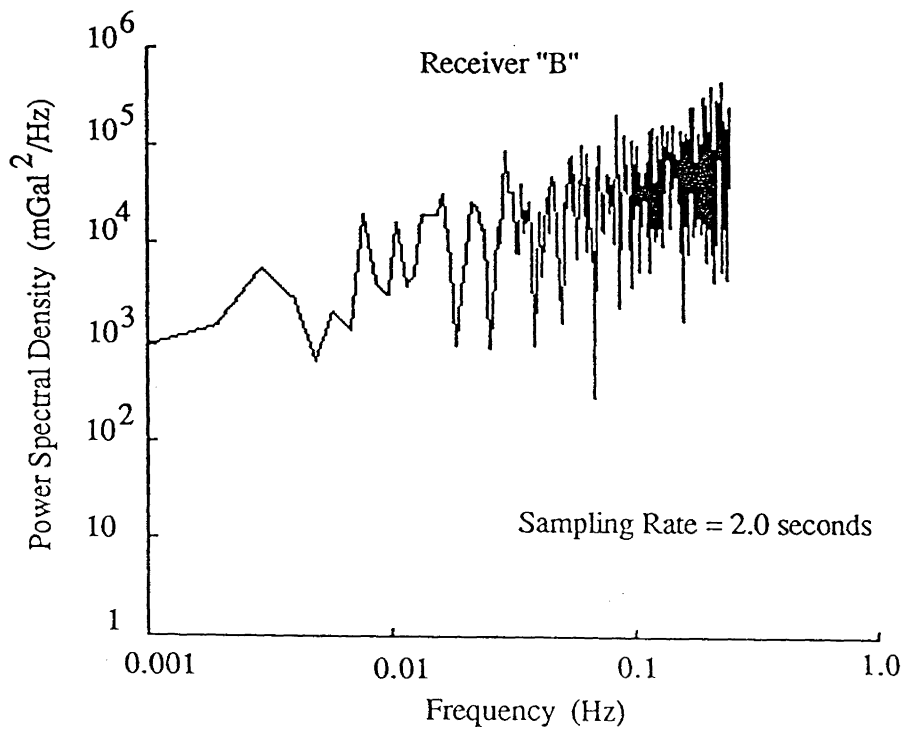
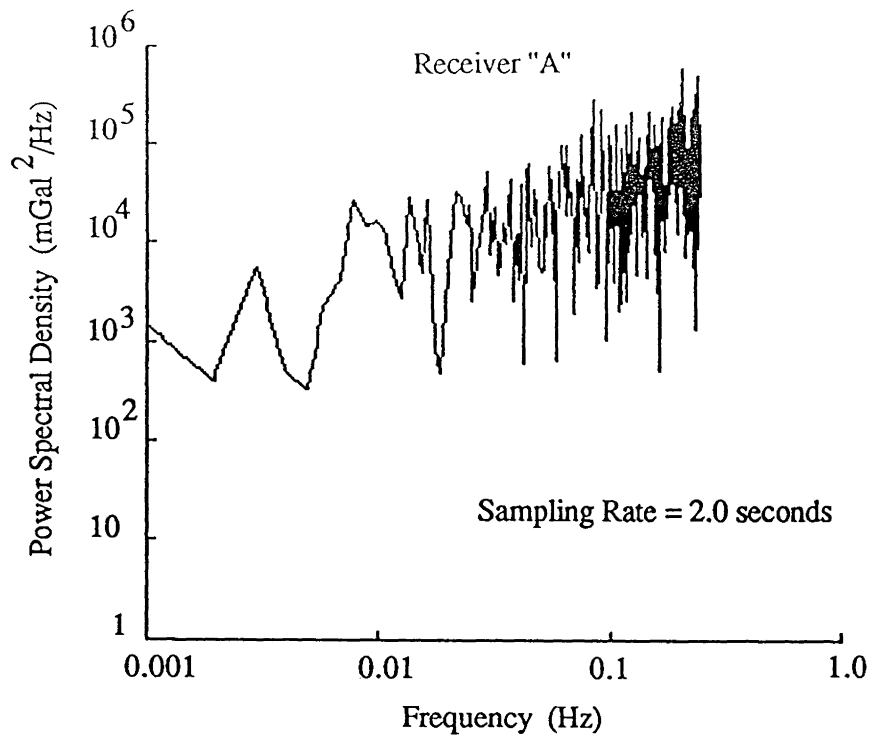


Figure V.8

Power Spectral Density of Ashtech XII Undifferenced Accelerations in Latitude

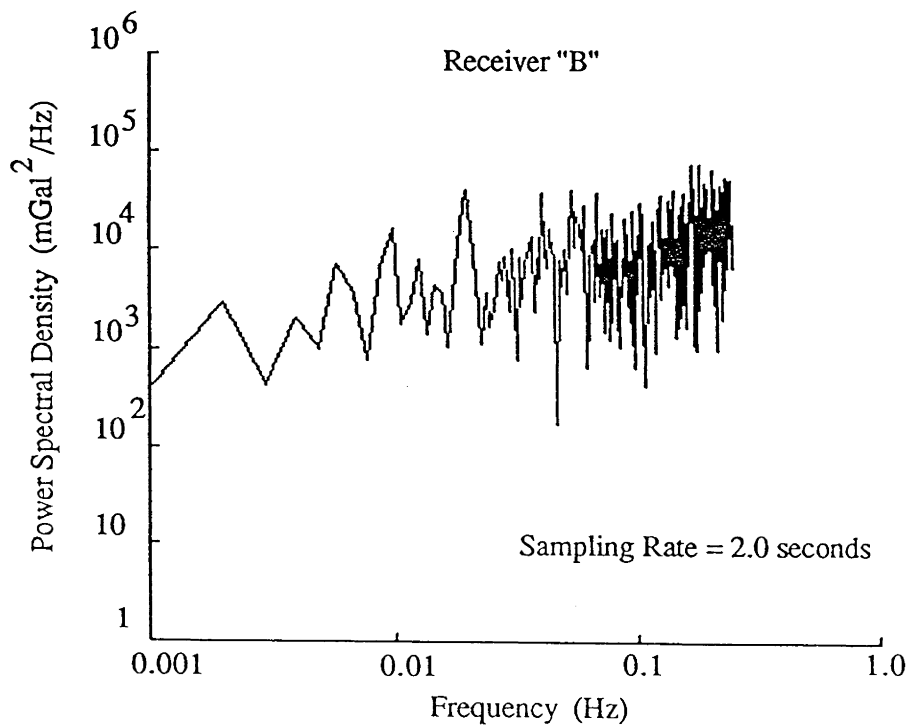
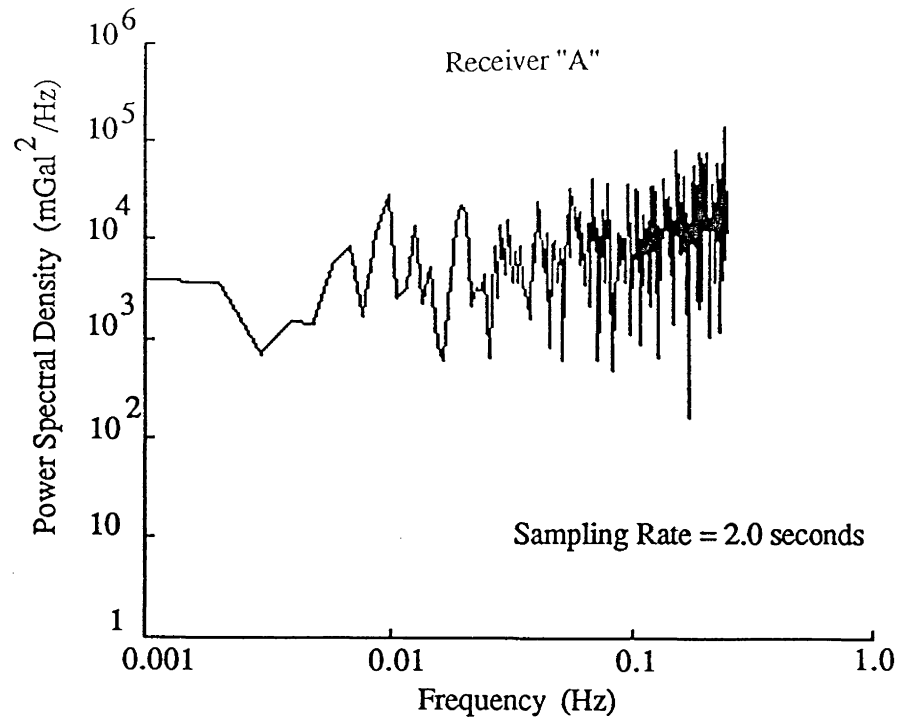


Figure V.9

Power Spectral Density of Ashtech XII Undifferenced Accelerations in Longitude

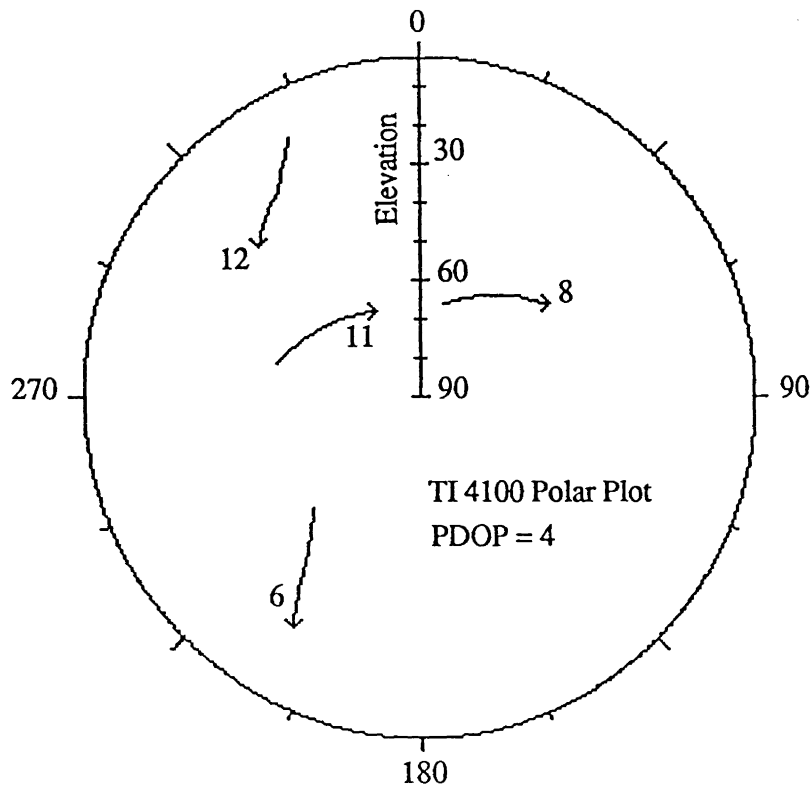


Figure V.10

Polar Plot of Satellite Sky Distribution for TI 4100 Data

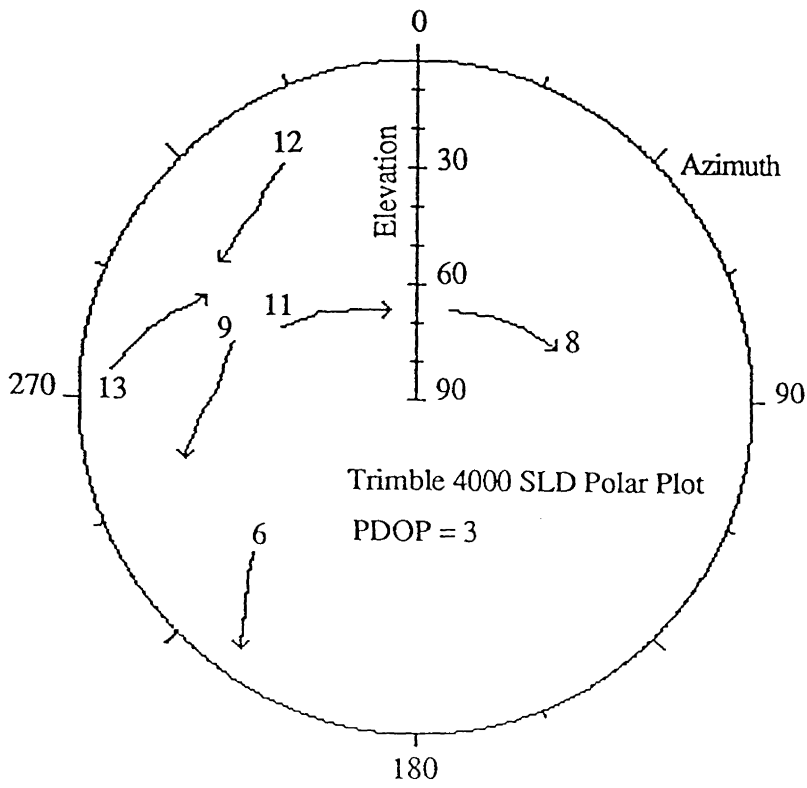
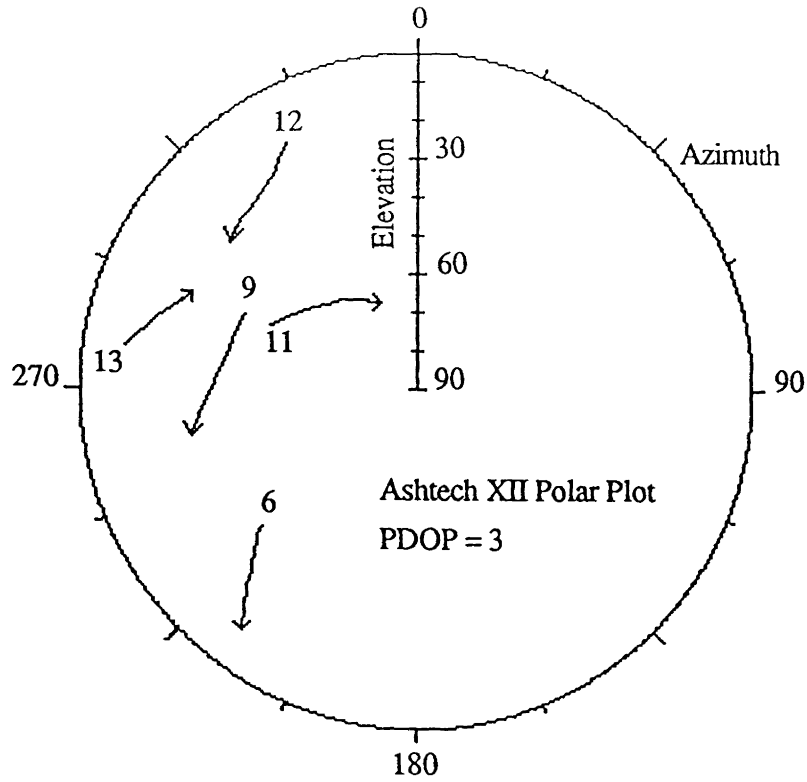


Figure V.11

Polar Plot of Satellite Sky Distribution for Trimble 4000 SLD and Ashtech XII Data

## APPENDIX VI

### Power Spectral Density Plots of Differenced Accelerations

The following pages contain plots of the power spectral density values of the differenced accelerations of each of the data sets obtained for this thesis

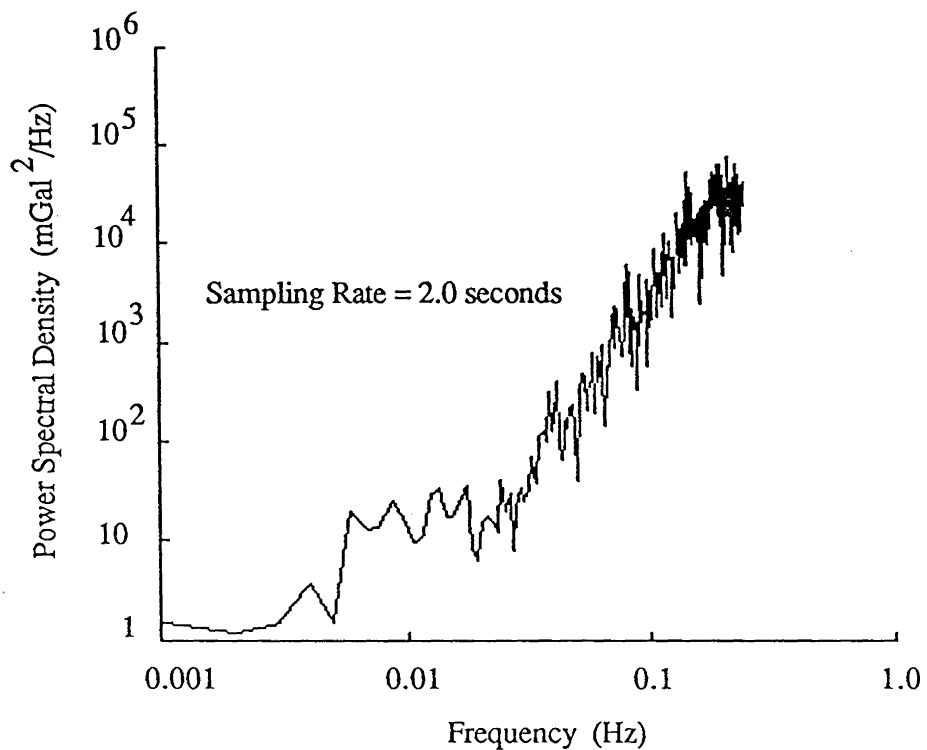


Figure VL1

Power Spectral Density of TI 4100 Differenced Vertical Accelerations

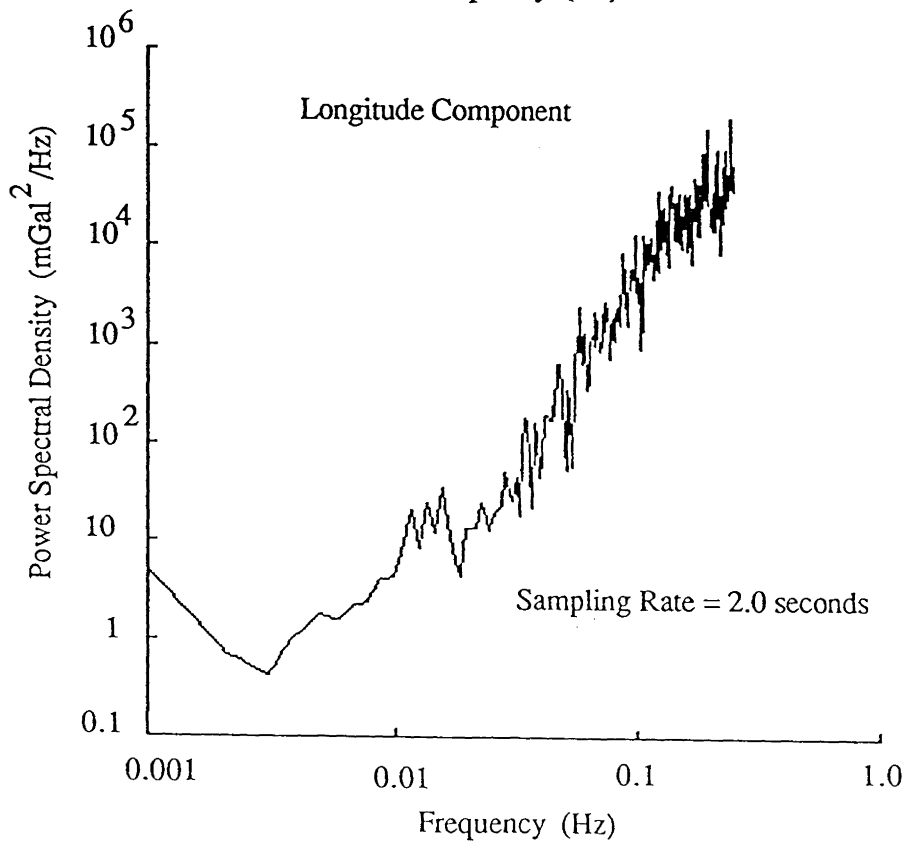
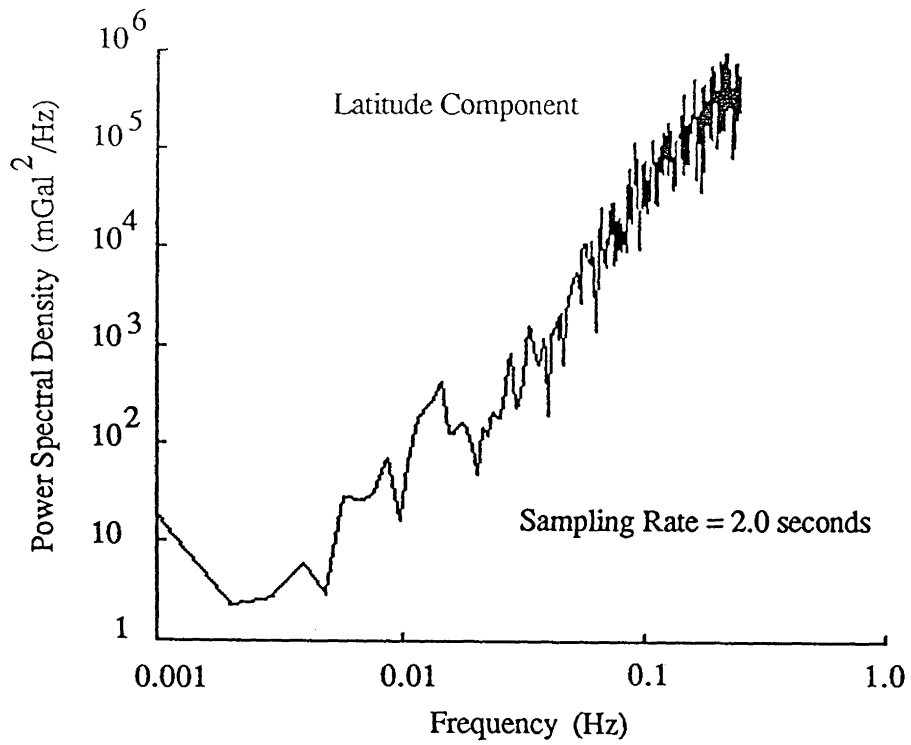


Figure VI.2

Power Spectral Density of TI 4100 Differenced Horizontal Accelerations



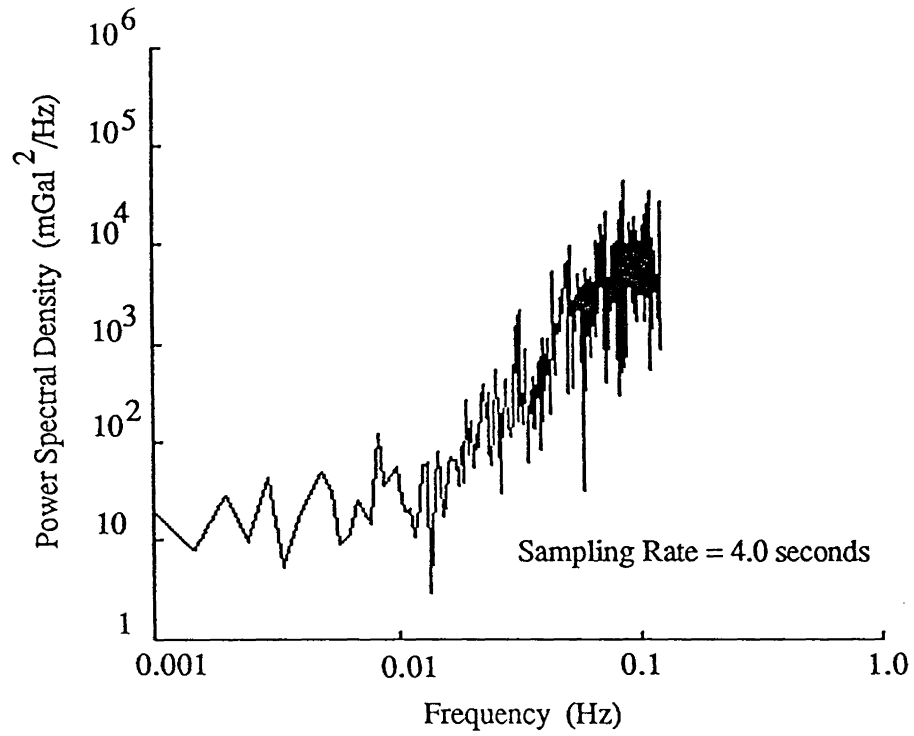


Figure VI.3

Power Spectral Density of Trimble 4000 SLD Differenced Vertical Accelerations

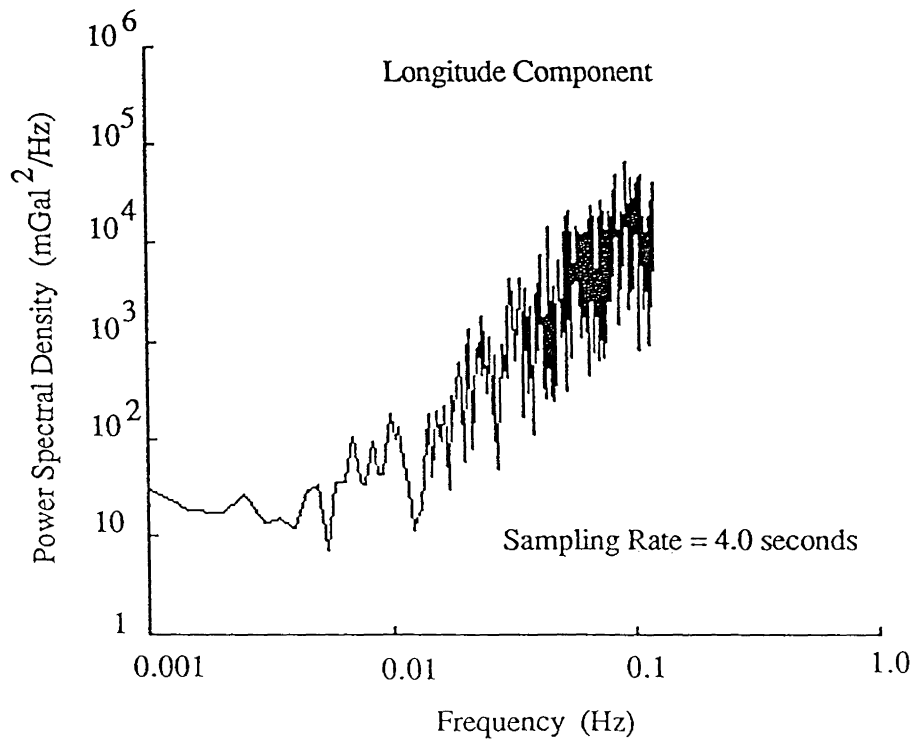
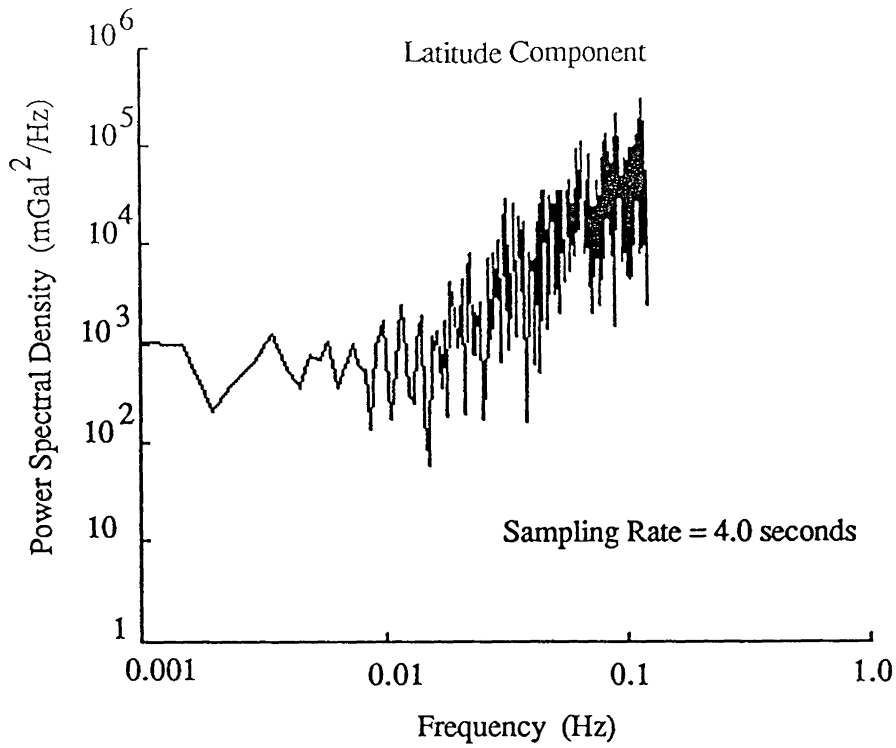


Figure VI.4

Power Spectral Density of Trimble 4000 SLD Differenced Horizontal Accelerations

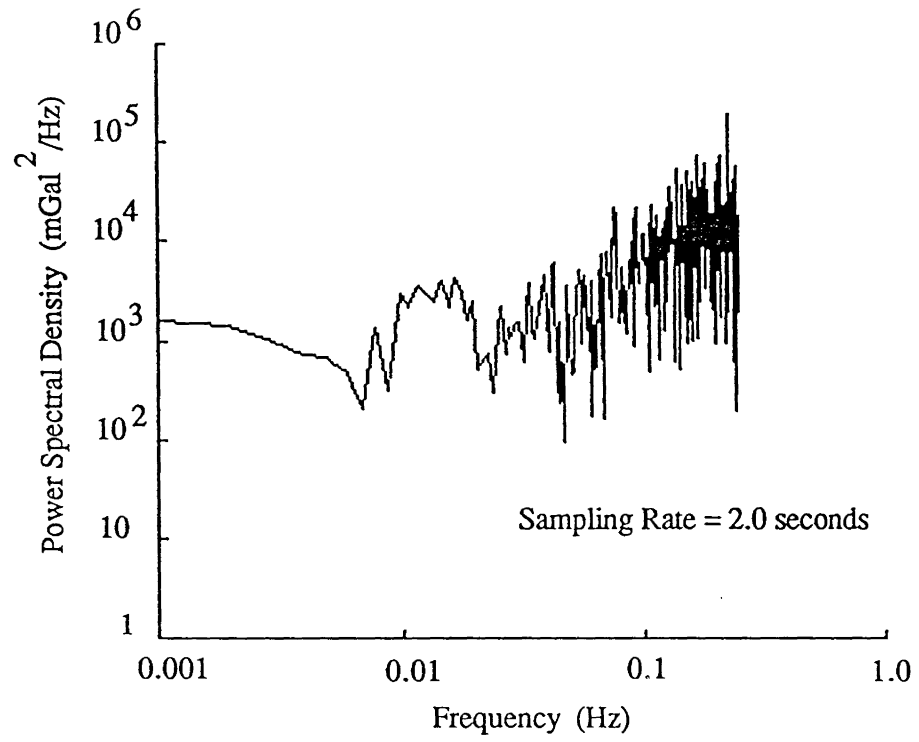


Figure VI.5

Power Spectral Density of Ashtech XII Differenced Vertical Accelerations

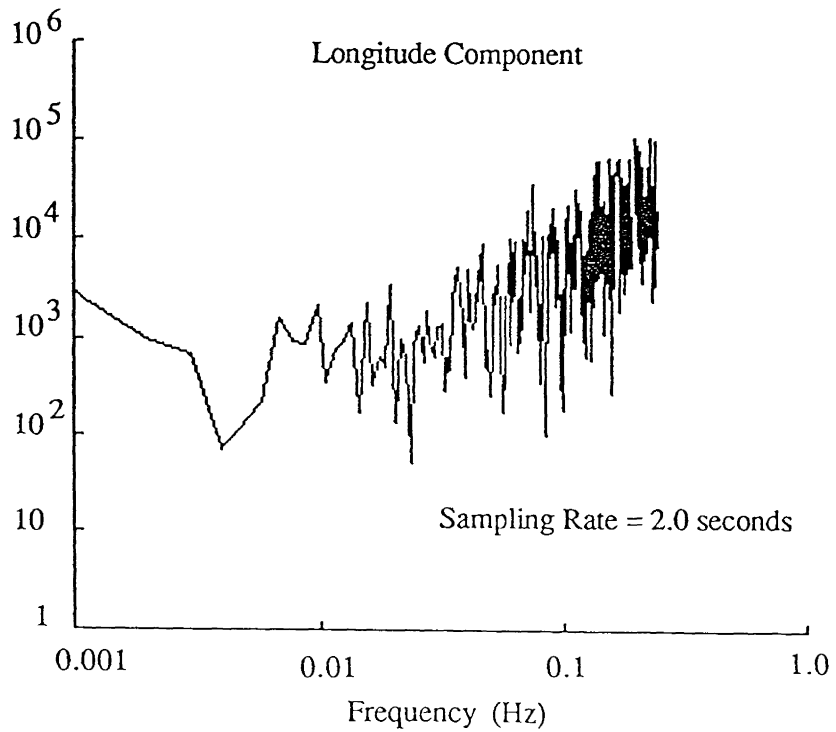
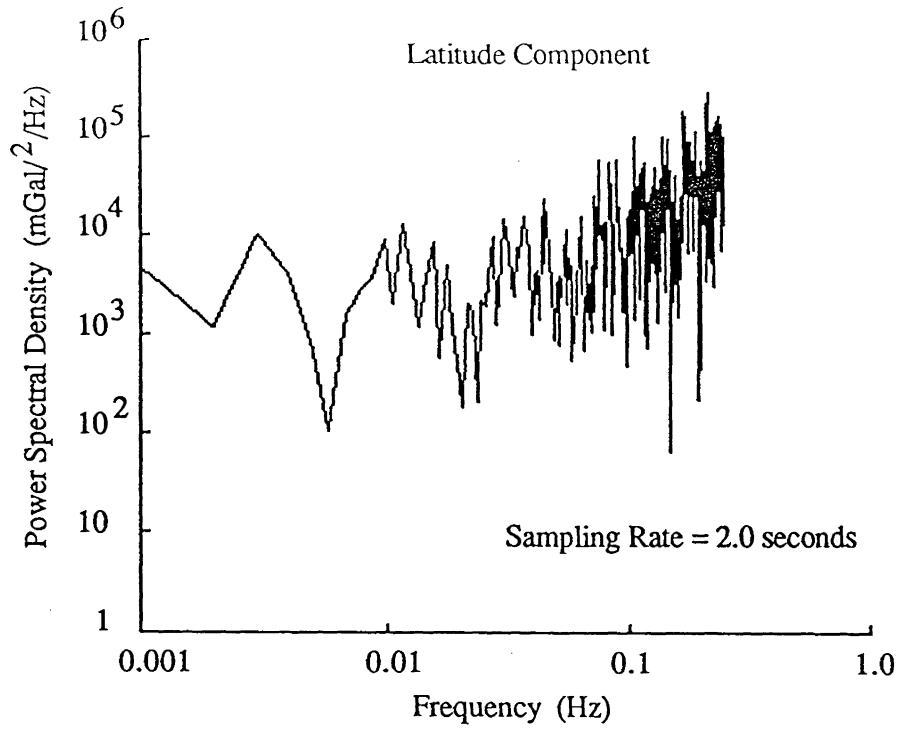


Figure VI.6

Power Spectral Density of Ashtech XII Differenced Horizontal Accelerations

APPENDIX VII

Power Spectral Density Plots  
of  
Unfiltered and Filtered Accelerations

The following pages contain plots of the power spectral density values of the unfiltered and filtered accelerations as computed using the differenced data sets of the TI 4100 receiver.

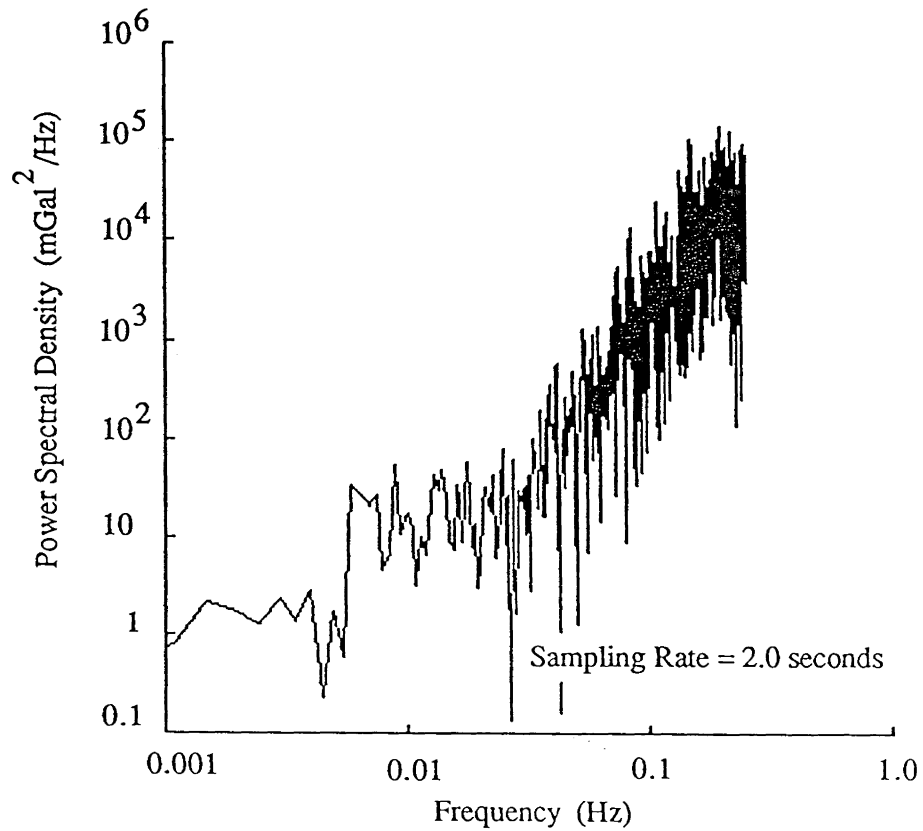


Figure VII.1  
Power Spectral Density of Unfiltered Differenced  
TI 4100 Vertical Acceleration Data

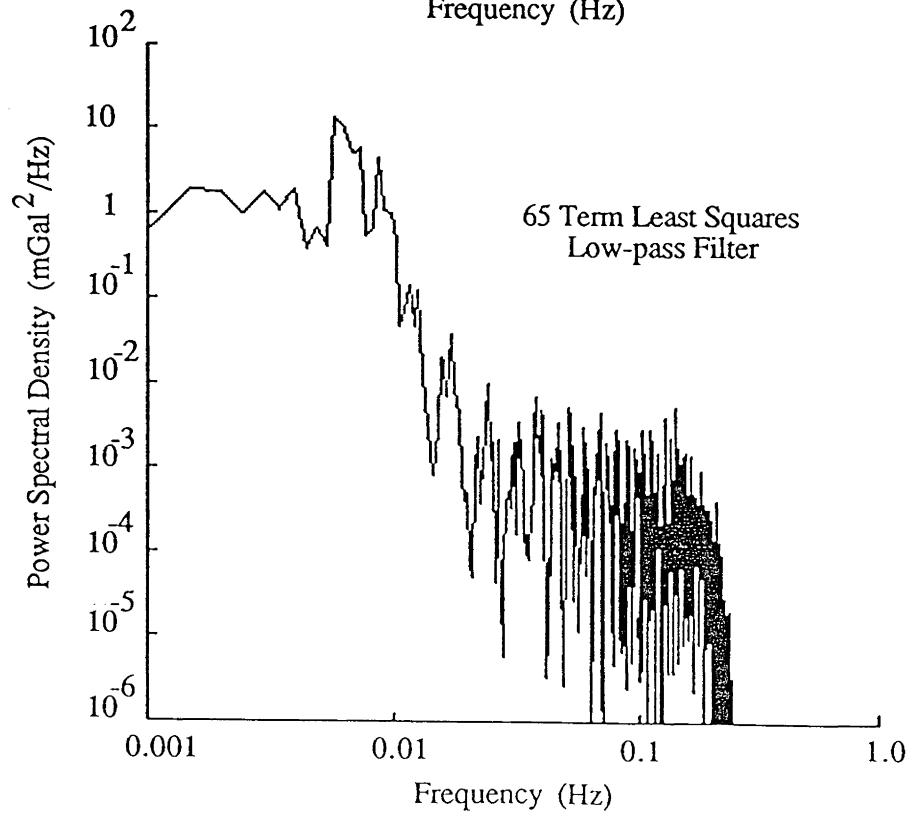
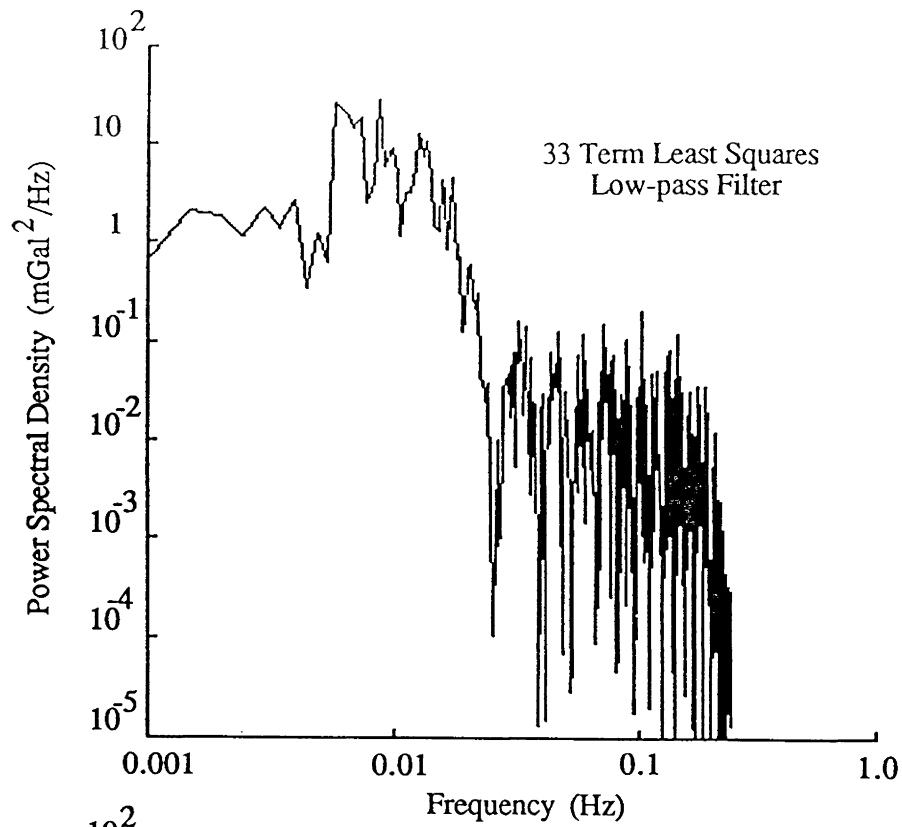


Figure VII.2

Power Spectral Density of Filtered Differenced TI 4100 Vertical Acceleration Data

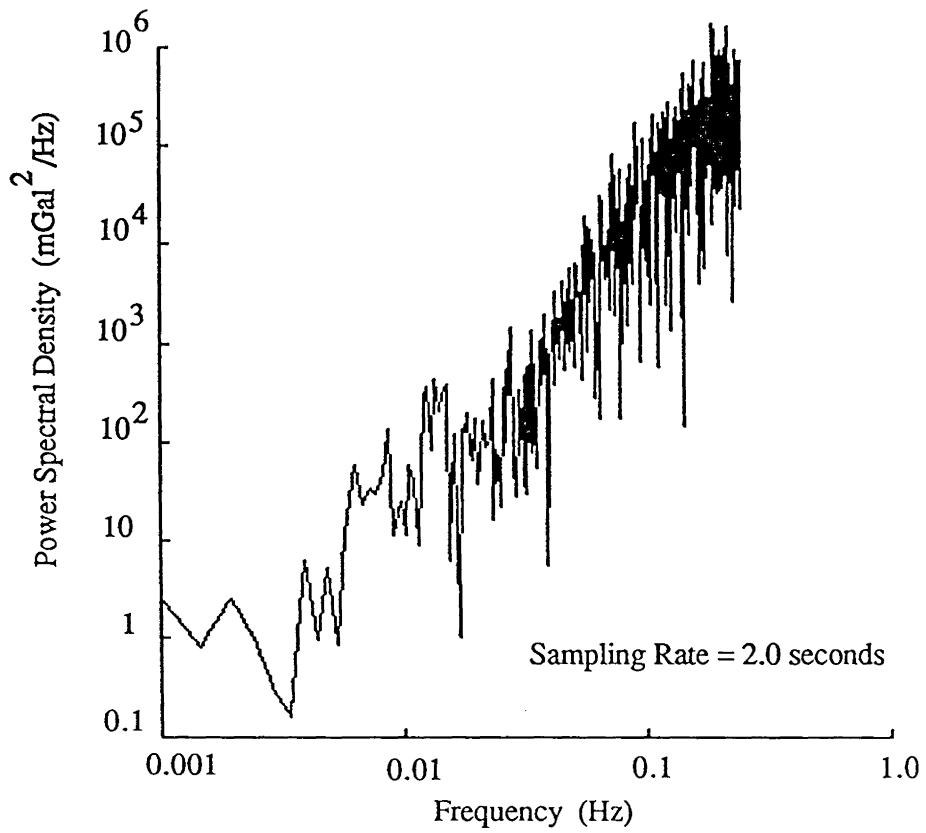


Figure VII.3

Power Spectral Density of Unfiltered Differenced  
TI 4100 Accelerations in Latitude

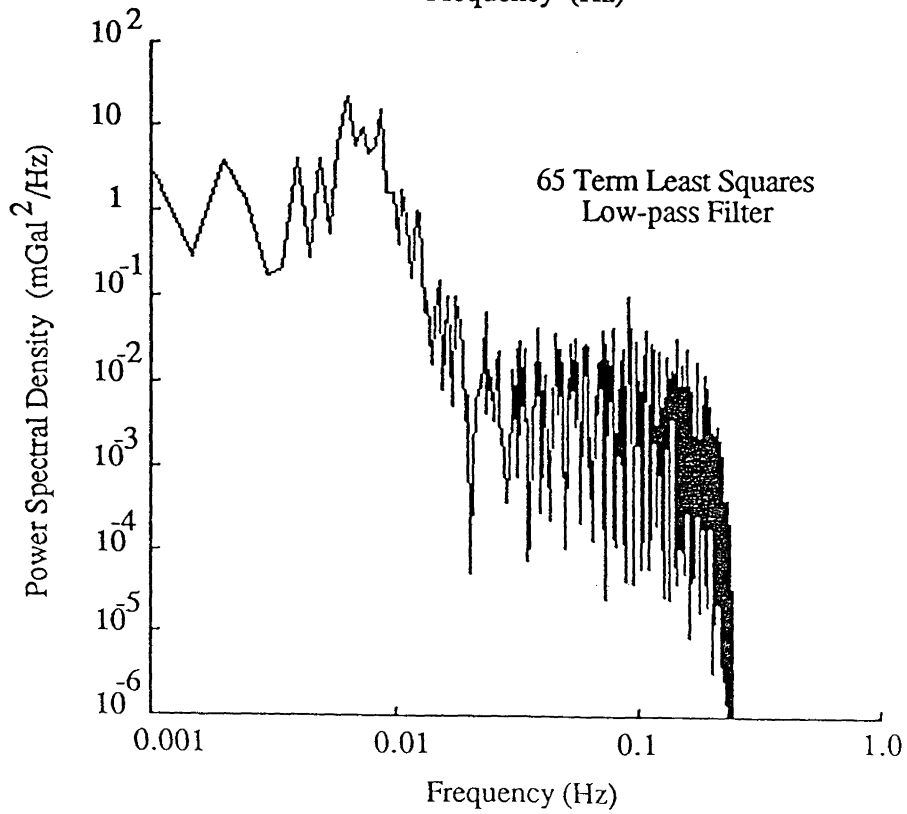
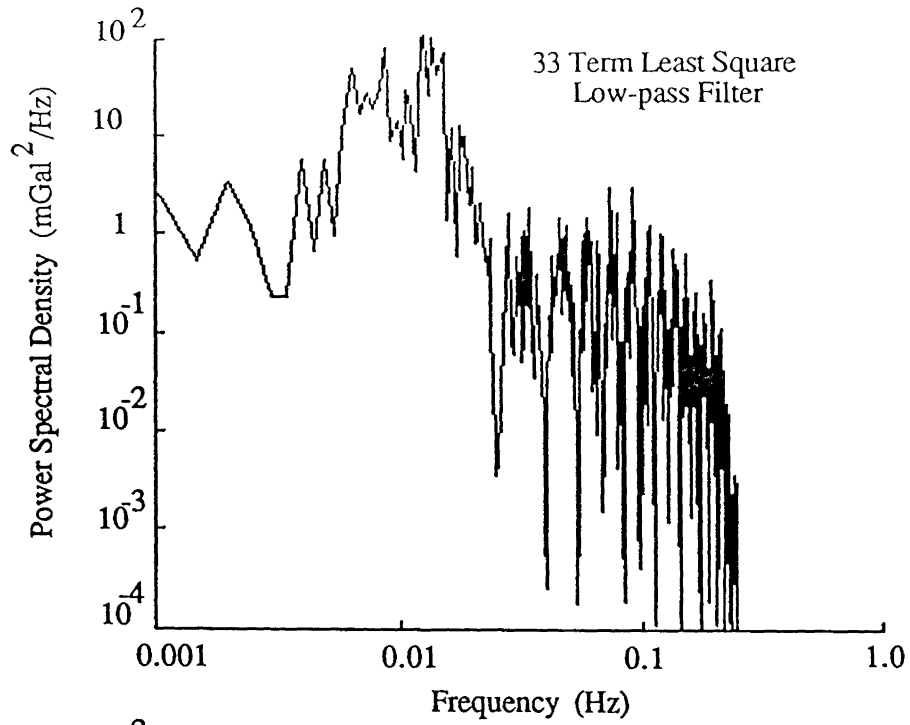


Figure VII.4

Power Spectral Density of Filtered Differenced  
TI 4100 Accelerations in Latitude



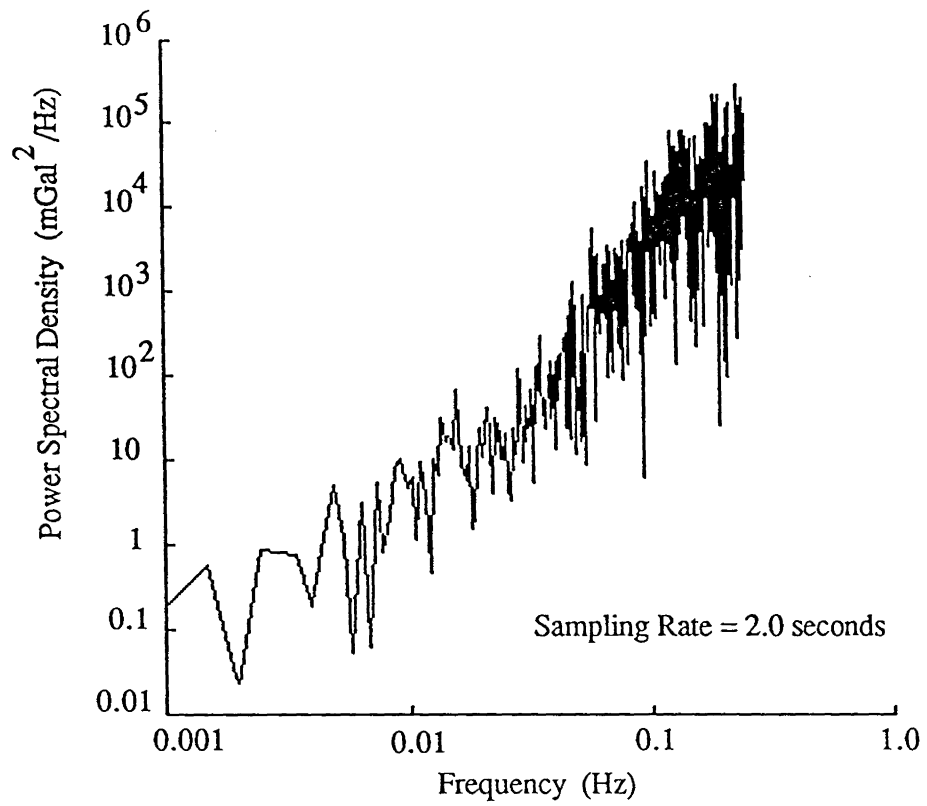


Figure VII.5

Power Spectral Density of Unfiltered Differenced  
TI 4100 Acceleration in Longitude

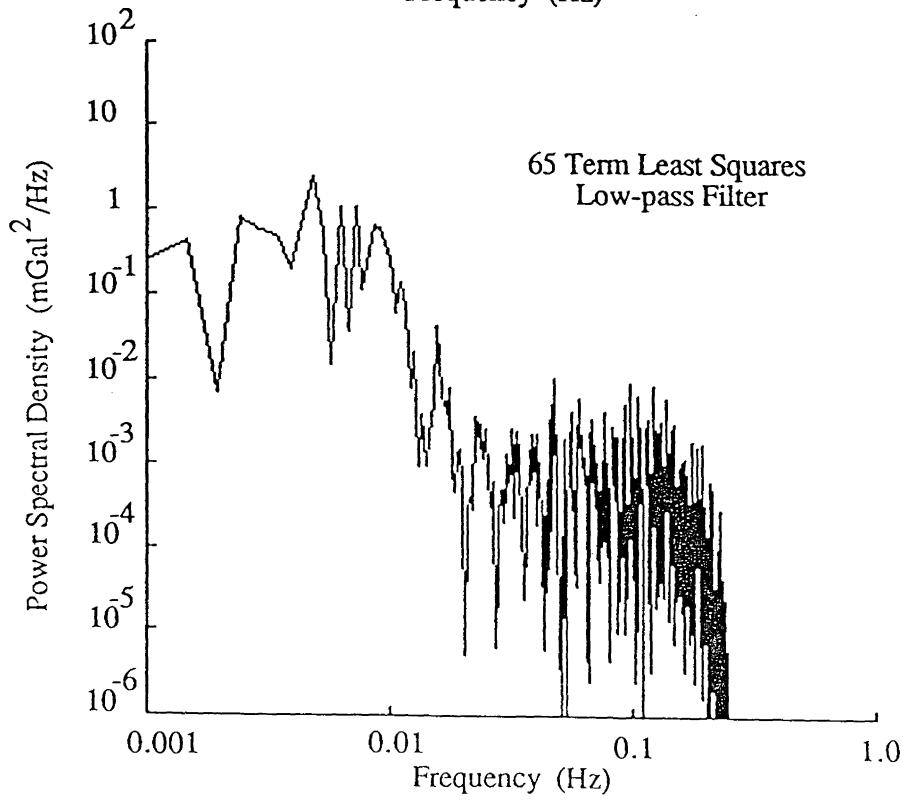
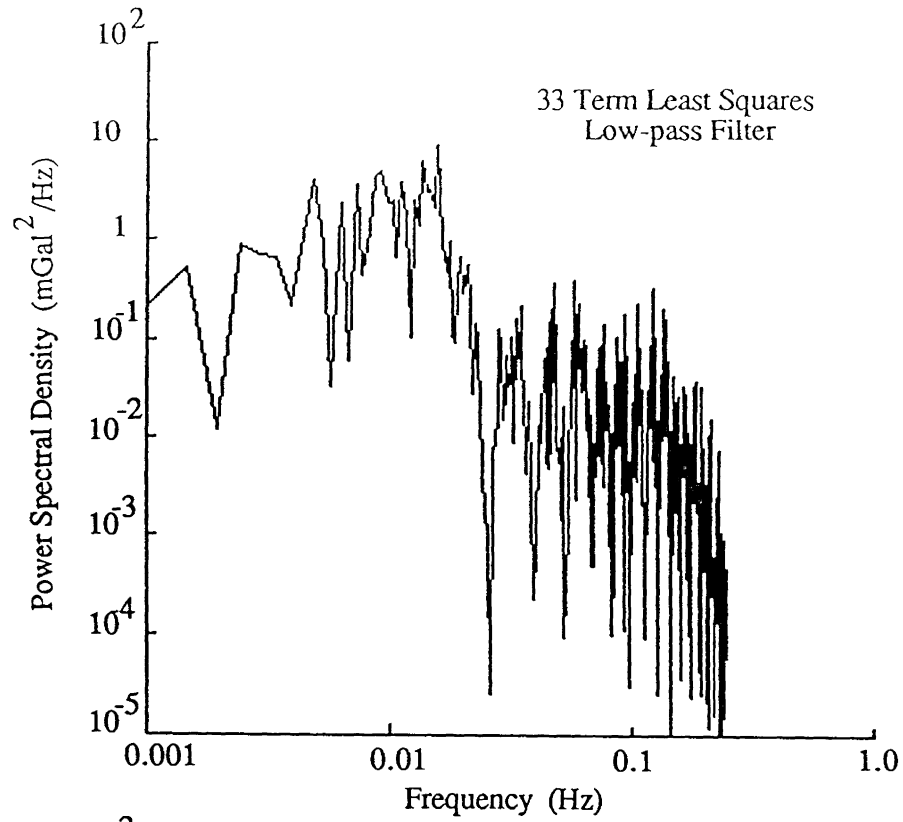


Figure VII.6

Power Spectral Density of Filtered Differenced  
TI 4100 Accelerations in Longitude

## APPENDIX VIII

### **Power Spectral Density Plots of Undifferenced Accelerations Influenced by Selective Availability**

The following pages contain plots of the power spectral density values of the differenced and undifferenced accelerations which have been contaminated by selective availability. The data set used was from the Trimble 4000 SLD receiver. A polar plot giving the satellite sky distribution for the data set is provided as well.

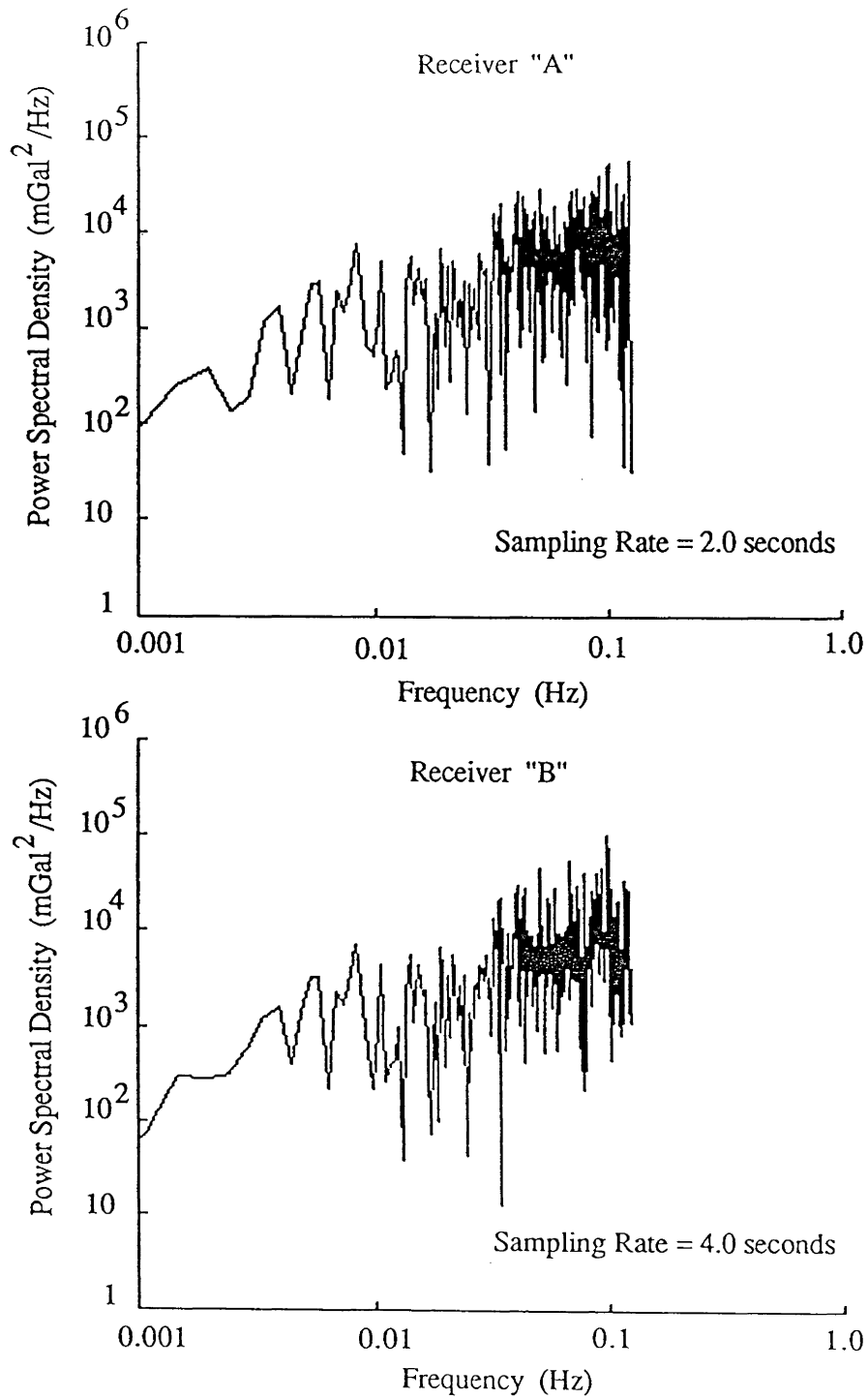


Figure VIII.1

Power Spectral Density of Undifferenced Vertical Accelerations  
Influenced by Selective Availability

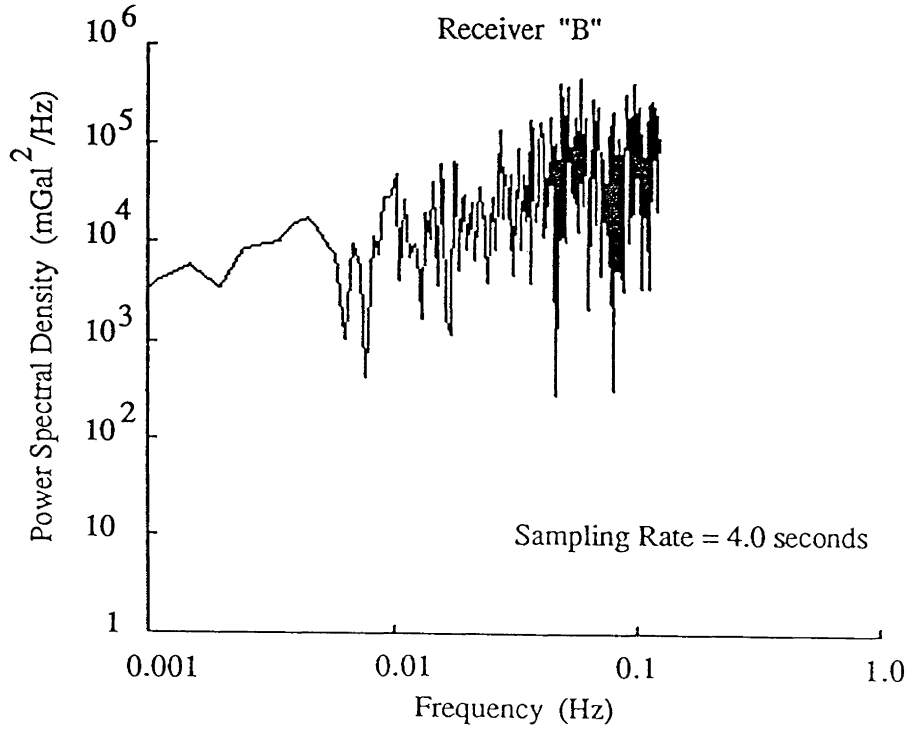
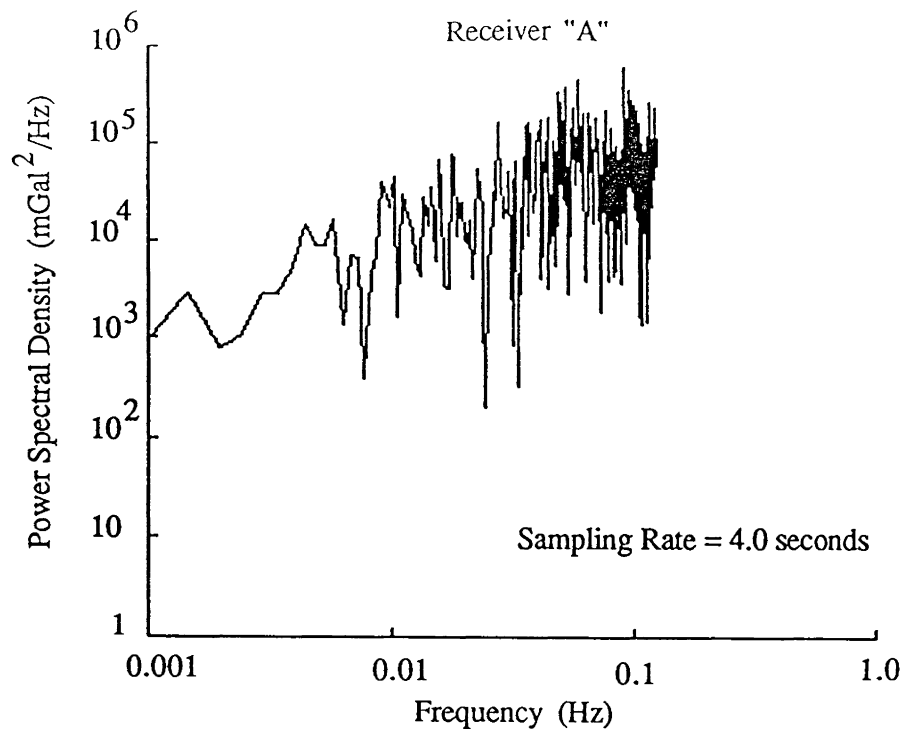


Figure VIII.2

Power Spectral Density of Undifferenced Accelerations in Latitude  
 Influenced by Selective Availability  
 136

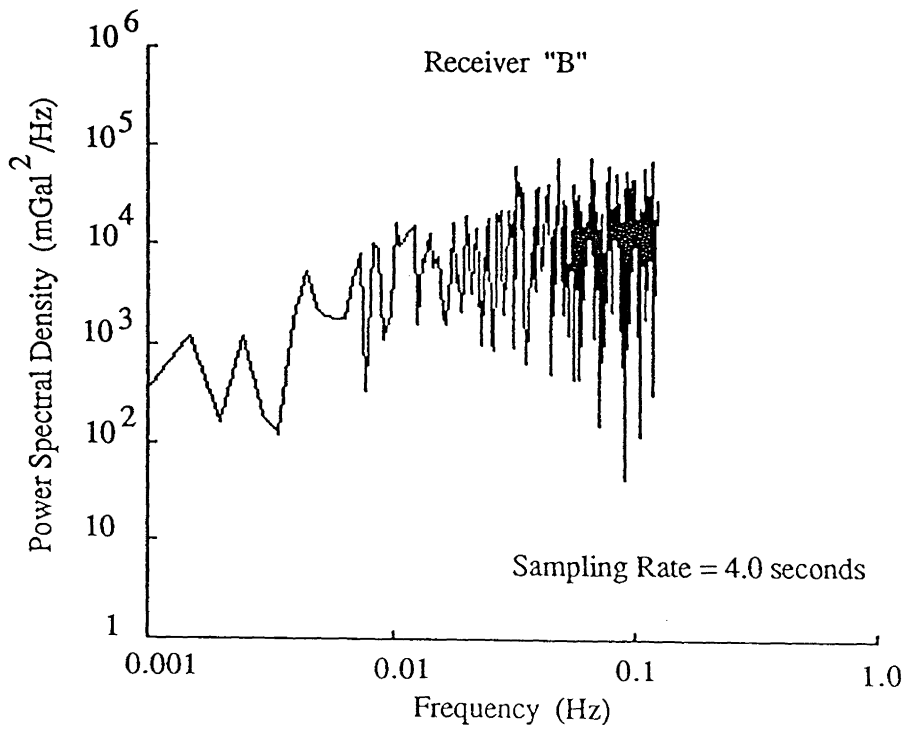
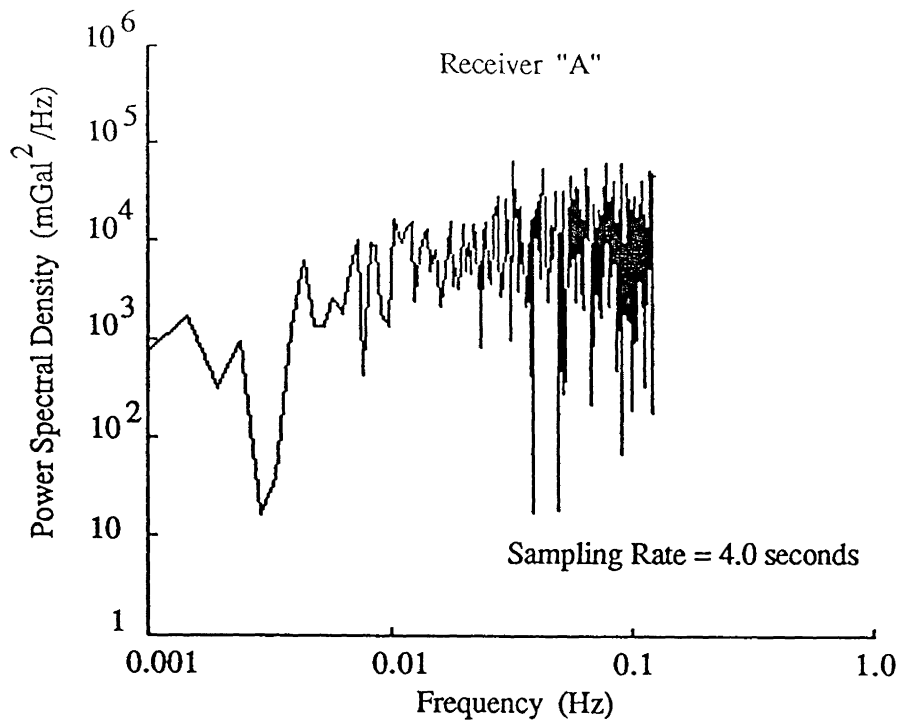


Figure VIII.3

Power Spectral Density of Undifferenced Accelerations in Longitude  
Influenced by Selective Availability

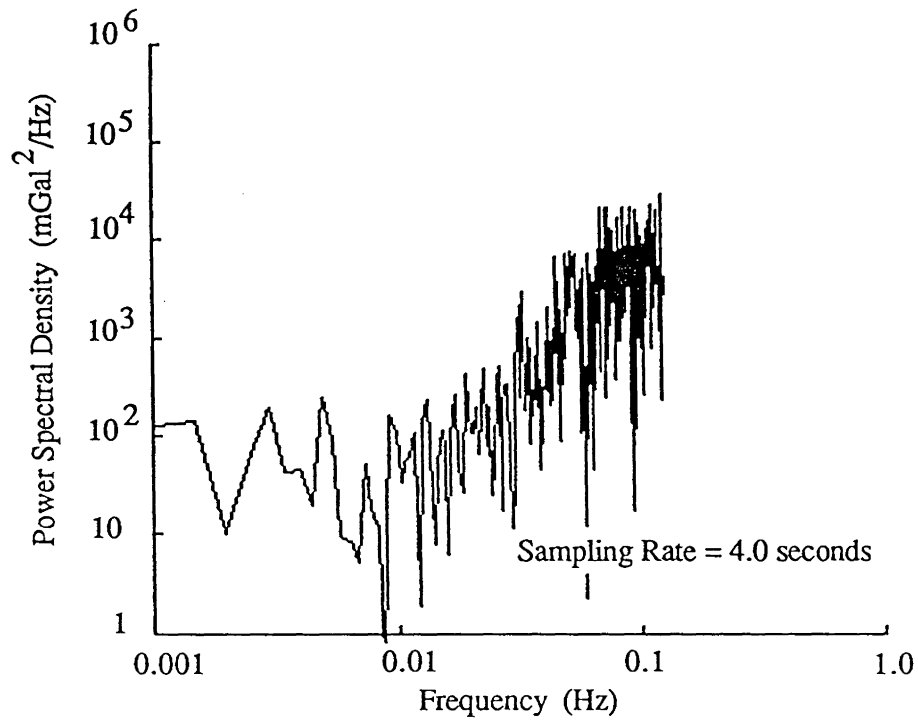


Figure VIII.4

Power Spectral Density of Differenced Vertical Accelerations  
Influenced by Selective Availability

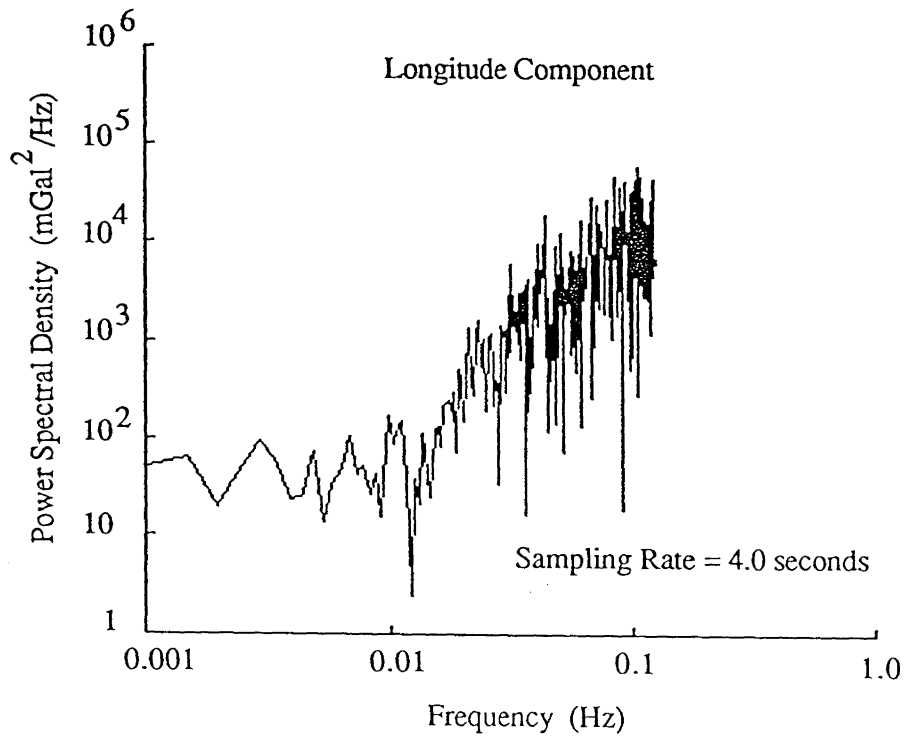
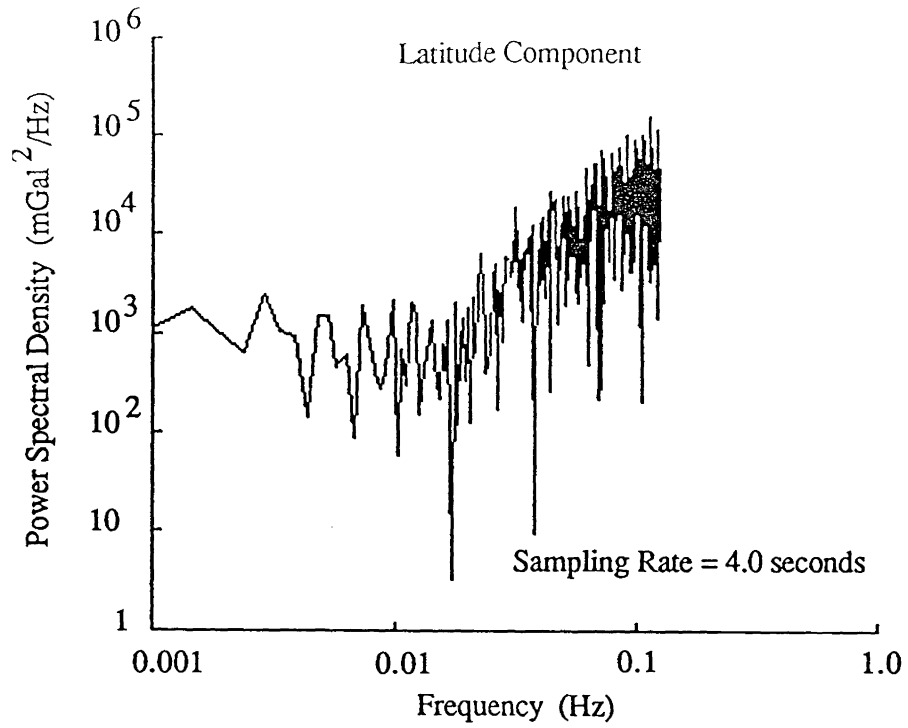


Figure VIII.5

Power Spectral Density of Differenced Horizontal Accelerations  
Influenced by Selective Availability



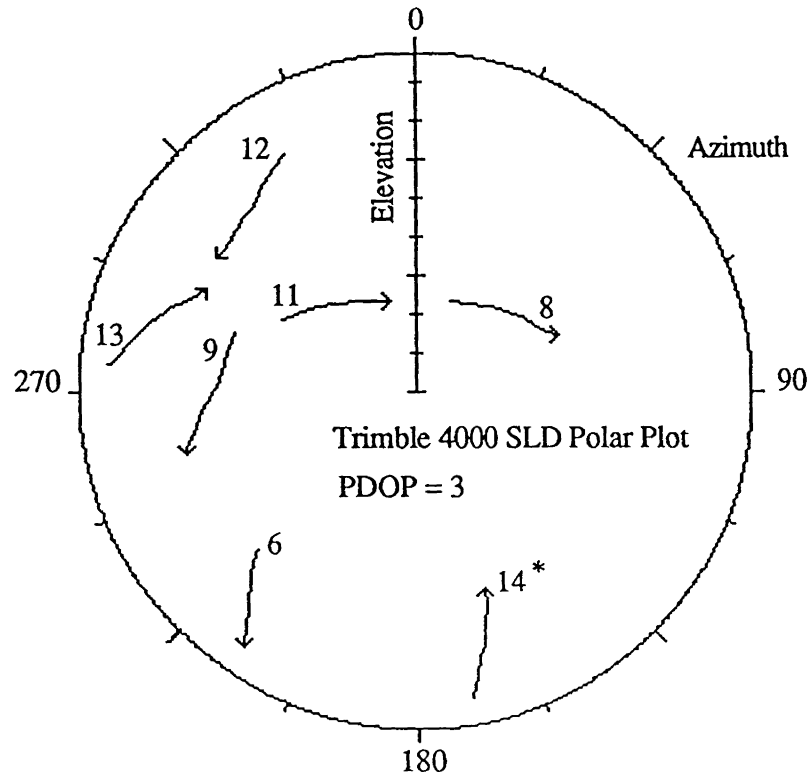


Figure VIII.6

Polar Plot of Satellite Sky Distribution for Trimble 4000 SLD Data Set

\* Satellite #14 is Influenced by Selective Availability

## VITA

Candidate's full name: Derrick Ross Peyton

Place and date of birth: Botwood, Newfoundland, Canada  
December 4, 1958

Permanent address: P.O. Box 568  
Botwood, Newfoundland, Canada  
A0H 1E0

Schools attended: Botwood Senior High School  
Botwood, Newfoundland  
1973-1975

Grand Falls District Vocational School  
Grand Fall, Newfoundland  
Drafting  
1975-1976

College of Trades and Technology  
St. John's, Newfoundland  
Surveying Technology  
1976-1978

Universities attended: University of New Brunswick  
Fredericton, New Brunswick  
Surveying Engineering  
1978-1982

Publications: Kleusberg, A., D.R. Peyton, and D.E. Wells (1990).  
"Airborne gravimetry and the Global Positioning System"  
*Proceedings of the IEEE Position Location and Navigation  
Symposium, PLANS'90*, Las Vegas, Nev., March 20-23, pp.  
273-278.